University of Alberta

Development of a Low Emissions, Lean Premixed, Natural Gas Burner

by

MATTHEW RONALD JOHNSON

A thesis submitted to the Faculty of Graduate Studies and Research in partial fulfillment of the requirements for the degree of Master of Science

Department of Mechanical Engineering

Edmonton, Alberta

Fall 1995

Canada

University of Alberta

Library Release Form

Name of Author: Matthew Ronald Johnson

Title of Thesis: Development of a Low Emissions, Lean Premixed, Natural Gas Burner

Degree: Master of Science

Year this Degree Granted: 1995

9 Wedgewood Drive

Antigonish, Nova Scotia

Canada   B2G 1J1
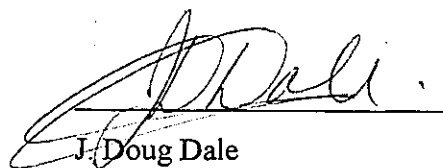
Date: SEPTEMBER 25, 1995

University of Alberta

Faculty of Graduate Studies and Research

The undersigned certify that they have read, and recommend to the Faculty of Graduate Studies and Research for acceptance, a thesis entitled Development of a Low Emissions, Lean Premixed, Natural Gas Burner submitted by Matthew Ronald Johnson in partial fulfillment of the requirements for the degree of Master of Science.

Larry W. Kostiuk

J. Doug Dale

Alan E. Mather

Mark Y. Ackerman

Date: SEPTEMBER 22, 1995

ABSTRACT

A novel method of aerodynamically stabilizing lean premixed natural gas flames on a conventional burner was investigated. Flames were anchored in the wake behind a small ring placed in the exit plane of a conventional burner. The overall stability regime of the burner was significantly increased, permitting stable lean premixed combustion down to equivalence ratios of 0.55. The lower flame temperatures associated with lean premixed combustion resulted in significantly reduced emissions, particularly NOx emissions which could be virtually eliminated. CO emissions were reduced at equivalence ratios down to approximately 0.75 due primarily to the excess air available for combustion. At equivalence ratios below 0.75, temperatures in the exhaust gas dropped to the point where the conversion of CO to CO_2 was inhibited and CO concentrations increased. Unburned hydrocarbon emissions were found to increase at very low equivalence ratios as the flame becomes more upright and reactant leakage around the edge of the ring is more apparent. Simultaneous measurements of NOx, CO, and hydrocarbon emissions suggests that a combustion equivalence ratio near 0.8 is optimum. At this optimum, measured pollutant emissions met and surpassed the most stringent standards in North America.

ACKNOWLEDEGEMENTS

TABLE OF CONTENTS

LIST OF TABLES

LIST OF FIGURES

NOMENCLATURE

D	burner diameter
FFID	fast flame ionization detector
H	flame height
$H°$	adjusted flame height, corrected for flow blockage and ring diameter
HC	unburned hydrocarbon
Hz	Hertz (1/s)
M	unspecified molecule in a chemical reaction which accepts energy from bonding of free radicals
$h\nu$	light energy (Joules)
NOx	nitrogen oxides: nitric oxide (NO) and nitrogen dioxide (NO_2) combined
R	burner radius
R_{RING}	outer radius of stabilizer ring
Re_D	Reynolds number of reactant flow based on burner diameter
Re_R	Reynolds number of reactant flow based on width of the ring stabilizer (width is outer radius minus the inner radius of the ring)
SCAQMD	South Coast Air Quality Management District
S_L	local laminar burning velocity
$S_L°$	laminar burning velocity of the main flow
T	absolute temperature (Kelvin)
T_{RECIRC}	absolute temperature of recirculation zone in the wake of a bluff body stabilizer
T_F	adiabatic temperature of the flame
T_∞	absolute temperature of uniform reactant stream
t	time (seconds)
U_{AVG}	average axial reactant flow velocity
U_L	laminar reactant gas velocity

U_∞	velocity of uniform reactant stream
W_{RING}	width of ring stabilizer (outer radius of ring minus the inner radius of the ring)
α	flame angle
β	ring stabilizer blockage, ring planform area divided by burner exit area
δ	gap size between inner edge of burner rim and outer edge of ring stabilizer
$\mu_{REACTANTS}$	dynamic viscosity of reactants
$\rho_{REACTANTS}$	bulk density of reactants
ϕ	equivalence ratio
$[i]$	concentration of species i

"Our doubts are our traitors

Which make us lose the good we might win

By fearing the attempt"

Measure for Measure, Shakespeare

"Fire hot. No touch."

Matt Johnson at 3 years of age

"Damn! I burned myself!"

Matt Johnson at 23, 24, and 25 years of age

1. INTRODUCTION

1.1 Environmental Concerns

The combustion of fossil fuels is the predominant energy source in the world. In 1980, 91% of the energy consumed in the United States was obtained through combustion processes [1]. As much as we are dependent on fossil fuels as an energy source, we can not overlook the fact that they are responsible for the majority of pollutants in the atmosphere. Since it is unrealistic to expect society to wean itself completely from fossil fuels (at least in the near future), much research has been focused on trying to reduce the amount of pollution generated in various combustion processes to reduce environmental damage

In Canada, natural gas consumption is increasing as consumers move to cheaper and cleaner sources of energy [2]. Compared to coal and heavier hydrocarbons, natural gas produces much cleaner burning flames with virtually no soot or sulfur dioxide emissions. However emissions of NOx (nitric oxide -- NO -- and nitrogen dioxide -- NO_2 -- combined), CO (carbon monoxide), HC (unburned hydrocarbons), and CO_2 (carbon dioxide) remain as problems. CO_2 emissions are an inevitable product of all hydrocarbon combustion processes and, although CO_2 is responsible for the greenhouse effect, it is highly unlikely that it will ever be eliminated as a primary combustion product [1].

NOx is probably the most serious pollutant from natural gas flames. In the lower atmosphere, NO_2, NO, and sunlight combine to form ground level ozone via Equations 1.1 [3].

$$NO_2 + hv \rightarrow NO + O$$
$$O + O_2 + M \rightarrow O_3 + M$$
$$O_3 + NO \Leftrightarrow NO_2 + O_2$$
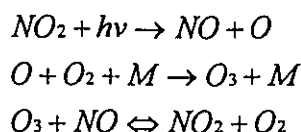
Equations 1.1: Photochemical Reactions to Produce Ground Level Ozone

1

Once ground level ozone is created it can enter a series of very complex reactions with atmospheric hydrocarbons to produce smog and PAN (peroxyacetyl nitrate, an eye irritant) [3]. NO and NO_2 can also react with HO_2 and OH radicals to produce HNO_3 (nitric acid) which precipitates out of the atmosphere as acid rain. Moreover, NOx is responsible for approximately half of the ozone depletion in the stratosphere [4].

Carbon monoxide, a toxic gas, is also a harmful pollutant in hydrocarbon combustion systems. A product of incomplete combustion, CO produces carboxy-hemoglobin in humans, which significantly decreases the oxygen carrying capacity of the blood. In concentrations as low as 100 PPM CO can cause headaches and reduced mental acuity and at concentrations of 600 PPM CO can be fatal [3]. CO also reacts in the atmosphere with excited OH^* radicals to produce excited HO_2^* radicals, an intermediate step in the reactions leading to acid rain [3].

Unburned hydrocarbons are a third relevant pollutant in natural gas systems. The principle constituent of natural gas is methane, which is a greenhouse gas. Hydrocarbons in general are necessary components in the NOx and sunlight system leading to the production of photochemical smog [3].

The purpose of this research was to try to develop a technologically simple natural gas burner that produces very low levels of NOx emissions without adversely affecting CO and HC emissions. This burner would be suitable for home and industrial heating in a variety of processes.

1.2 Emissions Legislation

As worldwide concern for the environment increases, governments are under increasing pressure to introduce new and more stringent emissions standards. In the United States, the US Clean Air Act has recently come into effect and promises to have a significant impact on existing pollution guidelines. At the forefront of emissions legislation is the South Coast Air Quality Management District (SCAQMD) in California. Local emissions standards in this district are some of the most restrictive in the world.

NOx emission limits taken from rules 1111 and 1121 of SCAQMD read, 'Natural-gas-fired, fan-type central furnaces shall not emit more than 40 nanograms of oxides of nitrogen (calculated as NO_2) per joule of useful heat delivered..." [5]. For CO emissions from gas-fired central furnaces, the current legislated limits are found in the joint ANSI/CGA standard. Here, it is specified that "A furnace shall not produce a concentration of carbon monoxide in excess of 0.04 percent in an air-free sample of the flue gases..." [6]. While unburned hydrocarbon emission restrictions for automobiles are numerous, as of yet none exist for gas fired furnaces. However, controlling HC emissions is synonymous with the goal of improved combustion efficiency [1].

While in many combustion systems it would be easy to meet any one of these standards, the difficulty lies in meeting all guidelines simultaneously. An exception would be the SCAQMD's NOx standard which is the most strict. Many existing appliances are unable to meet this limit.

1.3 Formation of Pollutants During Combustion

1.3.1 NOx Production Mechanisms

NOx is produced via three different mechanisms: thermal NOx, 'prompt" NOx, and fuel NOx. Fuel NOx involves a set of reactions that take place when nitrogen atoms are chemically bound within the fuel molecules. This is not relevant in natural gas systems.

In natural gas burners, the predominant mode of NOx production is thermal NOx [4]. This mechanism is so named because of the exponential temperature dependence of the rate of NOx formation. Reactions responsible for the formation of thermal NOx are known as the Zeldovich mechanism given by Equations 1.2 [7].

$$O + N_2 \Leftrightarrow NO + N$$
$$N + O_2 \Leftrightarrow NO + O$$

Equations 1.2: Zeldovich Mechanism for Thermal NOx Production

Since the concentration of NO is generally measured in parts per million, it is valid to assume the concentrations of N_2 and O_2 remain constant. Furthermore, since N radicals appear as products and reactants in the equations, the concentration is assumed to remain constant. With these simplifications and after some mathematical manipulation, the following equation for the rate of formation of NO can be produced (refer to appendix A for details).

$$\frac{d[NO]}{dt} = 1.214 * 10^{15} \exp\left(\frac{-68280.8}{T}\right)[O_2]^{0.5}[N_2]$$

where [i] represents concentration of species i
and T is absolute temperature in Kelvin

Equation 1.3: Simplified Kinetic Equation for Zeldovich NO Formation

Obviously the rate of formation has an extremely strong dependence on temperature. Thus, the most direct approach to reducing NOx emissions would be to reduce the temperatures at which combustion takes place, slowing the reactions so that NO does not have time to form in significant quantities. Once the gases in the post-flame zone have transferred energy via a heat exchanger or mixed with cool ambient air, the temperatures are low enough so that the NO reactions are quenched completely. While equilibrium calculations would suggest that any NO produced during combustion would return to molecular nitrogen and oxygen at atmospheric conditions, according to kinetic theory the rate of decomposition is so slow that this does not happen.

A third reaction is sometimes included in the formation process for thermal NO, Equation 1.4, which forms the extended Zeldovich Mechanism. However, since the

reactant species are radicals this reaction will be dominated by the previous two [7-9], and is generally only important in fuel-rich mixtures [10-11].

$$N + OH \Leftrightarrow NO + H$$
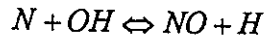
Equation 1.4: Reaction for Extended Zeldovich Mechanism

While the Zeldovich mechanism is the dominant source of NOx production in flames, "prompt NOx" first reported by Fenimore [12], can also be relevant. Fenimore proposed that there is a series of reactions that form NO for a very short time in the flame zone that is not covered by the Zeldovich mechanism. While it is difficult to know exactly what reactions are involved, the following two are relevant components [12-14,7].

$$CH + N_2 \Leftrightarrow HCN + N$$
$$C_2 + N_2 \Leftrightarrow 2CN$$
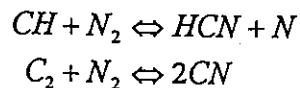
Equations 1.5: Partial "Prompt NOx" Reactions

The CN and N then probably react to form NO according to some version of the following reactions [14].

$$HCN + OH \Leftrightarrow CN + H_2O$$
$$N + OH \Leftrightarrow NO + H$$
$$CN + O_2 \Leftrightarrow CO + NO$$
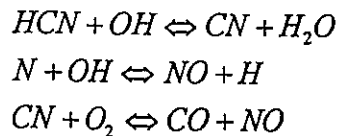
Equations 1.6: Probable "Prompt NO" Formation Equations

Although the prompt NOx mechanism exists in all hydrocarbon flames, the amount of NO produced also seems to decrease in leaner flames [14,12]. In any case since the dominant mode of NOx production in a natural gas burner flame is thermal or Zeldovich NOx, a logical approach to reducing emissions would be to lower the combustion temperature. The rate of formation of NO by the Zeldovich mechanism (Equations 1.3) is

also affected by the concentration of O_2 and N_2. Controlling these species concentrations is an alternative strategy to reducing NOx emissions but the formation rate dependence is only square root and linear respectively.

1.3.2 CO Production Mechanisms

In most stoichiometric combustion systems, CO emissions are primarily a result of incomplete combustion due to poor mixing. In this situation not every CO molecule comes into contact with an O_2 molecule, preventing total oxidation of CO to CO_2. Although intuitively one would expect no CO emissions in fuel-lean systems (where there is a lot of excess oxygen available to react with the CO), this is not always the case. As will be explained in section 1.4, as the combustion mixture is made more lean the flame temperature is reduced. Initially the increase in oxygen available for reaction leads to a drop in CO emissions. However, below a temperature of about 1270 K, an important CO oxidation reaction (Equation 1.7) can be quenched [15].

$$CO + OH \rightarrow CO_2 + H$$
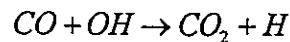
Equation 1.7: CO Oxidation Reaction

Roesler et al. [16] suggest that below a temperature of 1040 K, increasing the O_2 concentration causes a net change in the mechanism responsible for HO_2 consumption, so that the number of OH radicals available for reaction in Equation 1.7 decreases. However, even in lean systems where the combustion temperature is above 1270 K, higher than expected CO emissions have still been observed. Glassman suggests that this is due to an equilibrium shift in the water gas reaction, Equation 1.8 [17].

$$CO + H_2O \Leftrightarrow CO_2 + H_2$$
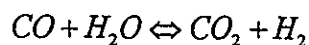
Equation 1.8: Water-Gas Reaction

To prove his theory, using numerical calculations Glassman added extra water to a theoretical combustion system and computed the new species concentrations in the exhaust gases for a range of temperatures from 1100-1500 K. The increase in available moles of water produced an equilibrium shift in the water-gas reaction back towards the products. Conversely an increase in initial H_2 levels, led to a rise in CO concentration.

Thus, although an increase in O_2 concentration from stoichiometric conditions will lead to a decrease in CO emissions there is a limit to this effect. At low temperatures and high O_2 concentrations, CO emissions can actually increase.

1.4 Lean Combustion

1.4.1 Flame Temperature

Fuel lean combustion, or simply lean combustion, occurs when there is an excess of air available for oxidation of the fuel. With equivalence ratio, ϕ, defined as the stoichiometric air to fuel ratio (based on mass) divided by the actual air to fuel ratio, lean combustion occurs in the range where $\phi<1$. Figure 1.1 shows the calculated adiabatic flame temperature for a methane-air flame as determined using the computer program STANJAN [18]. The calculation is based on equilibrium thermodynamics with reactants at 300 K and 1 atm and potential product species being: CO_2, CO, N_2, N, H_2O, H_2, H, O_2, O, OH, NO, NO_2, CH_4, C_3H_8, C, and $i-C_8H_{18}$.

For lean flames ($\phi<1$), as more air is added to the reactants the flame temperature drops due to an increase in the amount of inerts present to absorb the chemical energy released during combustion. As has been shown, NOx production is exponentially dependent on flame temperature. Thus, by burning under fuel-lean conditions, NOx emissions should be reduced. The excess oxygen available should also help ensure complete oxidation of CO to CO_2 as long as the flame temperature is not lowered too

much. This raises the possibility of the existence of an optimum equivalence ratio for low emissions combustion for a given burner configuration.
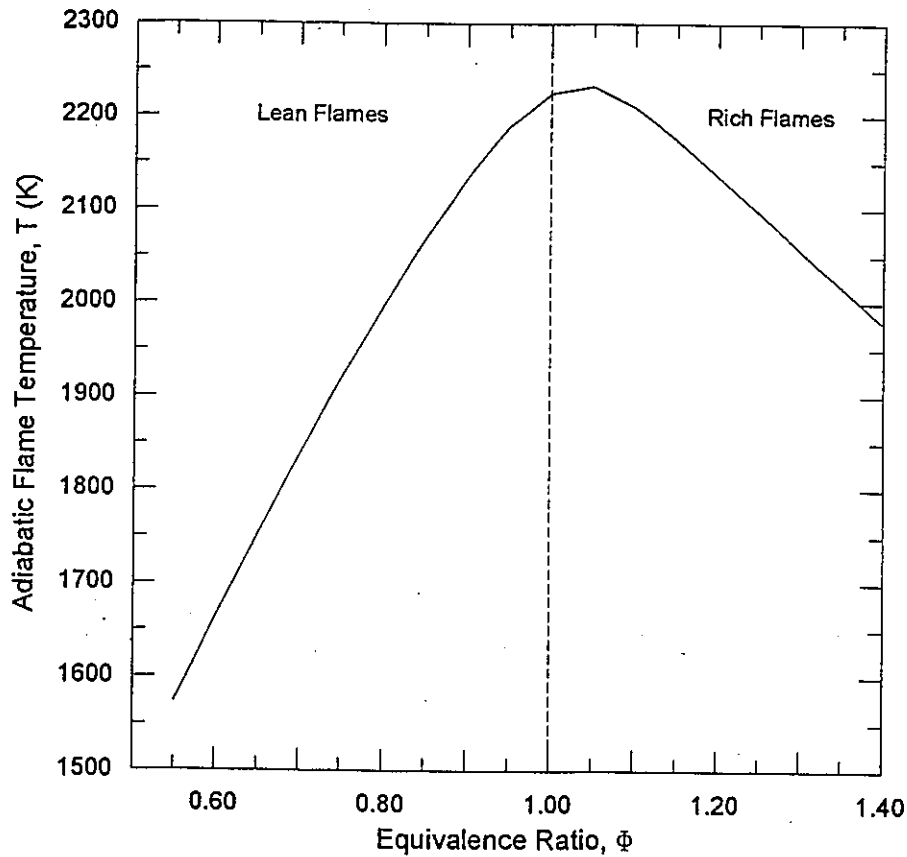
Figure 1.1: Calculated Adiabatic Methane-Air Flame Temperature

1.4.2 Stability Limits: Blowoff and Flashback

Unfortunately while the idea of lean premixed combustion is simple in theory, it has been difficult in practice. On conventional burners lean flames are unstable and prone to blowoff, a condition where the flame destabilizes and separates from the burner. Blowoff occurs when a component of the velocity of the reactants leaving the burner exceeds the burning velocity of the flame so that the flame is pushed away from the burner. The maximum burning velocity occurs where the flame temperature is maximum

and as the equivalence ratio is lowered and the flame temperature is reduced, the burning velocity decreases. Hence, the burning velocity is essentially a function of flame temperature [19]. Figure 1.2 shows the measured burning velocity for a methane and air flame at 1 atm as a function of equivalence ratio as reported by Egolfopoulos et al. [20]. While lowering the equivalence ratio has a positive effect on NOx emissions, the slower burning velocity can have a negative effect on stability, leading to blowoff.
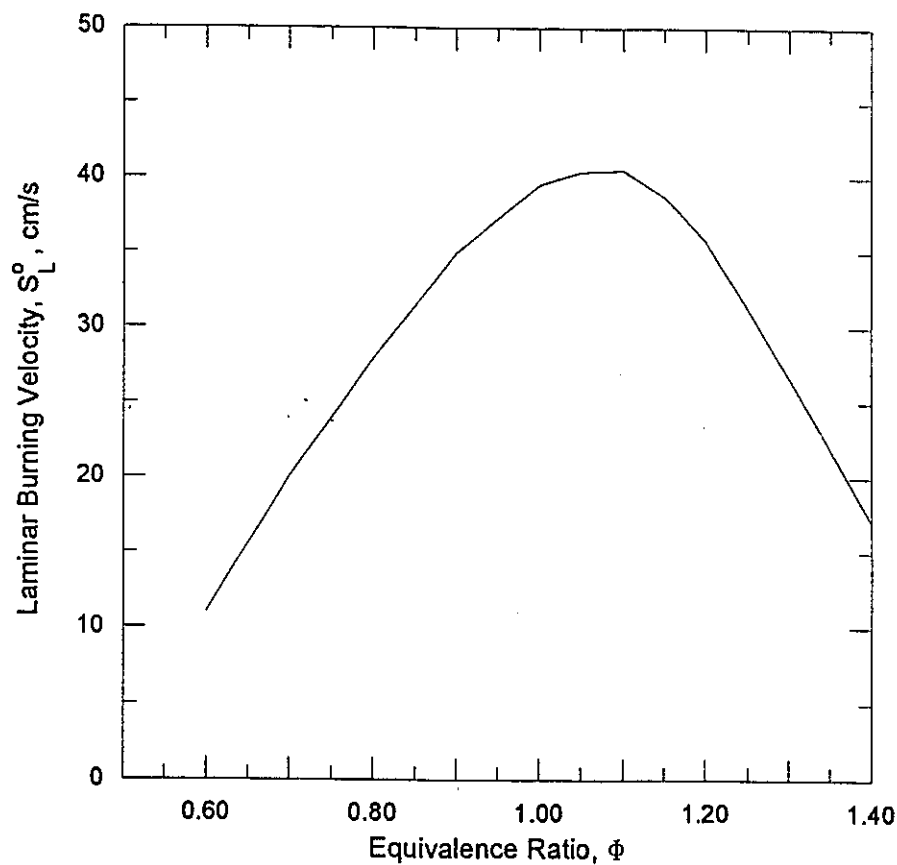
Figure 1.2: Laminar Burning Velocity for a Methane-Air Flame at 1 atm

Flashback introduces a second stability limit in premixed flames. The opposite of blowoff, flashback occurs when the burning velocity exceeds the reactant gas velocity causing the flame to jump inside the burner and propagate back into the reactants. Depending on the volume of premixed gases in the burner, the occurrence of flashback can be potentially dangerous and/or explosive.

A relevant parameter in rating the performance of a burner is the turndown ratio. The turndown ratio is defined as the ratio of the burner's maximum stable input power to its minimum stable input power at a given equivalence ratio (usually unity). These maximum and minimum input powers are limited by the blowoff and flashback limits respectively. A high turndown ratio is desirable in any situation where the required energy output varies. An example would be an industrial steam generating application. Assuming the demand for steam is not always constant, standard practice dictates that the boiler would be sized to produce enough steam for the peak demand. If the turndown ratio is low, when the demand for steam is below the maximum, the boiler will be unable to reduce the output. This necessary oversizing would lead to wasted energy.

1.4.3 Flame Height

As shown in figure 1.3, flame height is directly related to the burning velocity and the reactant gas velocity through the flame angle, α. Thus, if the burning velocity is reduced (presumably by lowering the equivalence ratio), the flame angle will decrease and the height will increase (i.e. the flame angle decreases so that the flow velocity normal to the flame matches the burning velocity). The increased flame height for lean flames could be problematic if a lean flame burner was retrofitted into an existing appliance designed for a stoichiometric burner. The taller flames could impinge on the walls of the appliance leading to a host of pollution and corrosion problems.
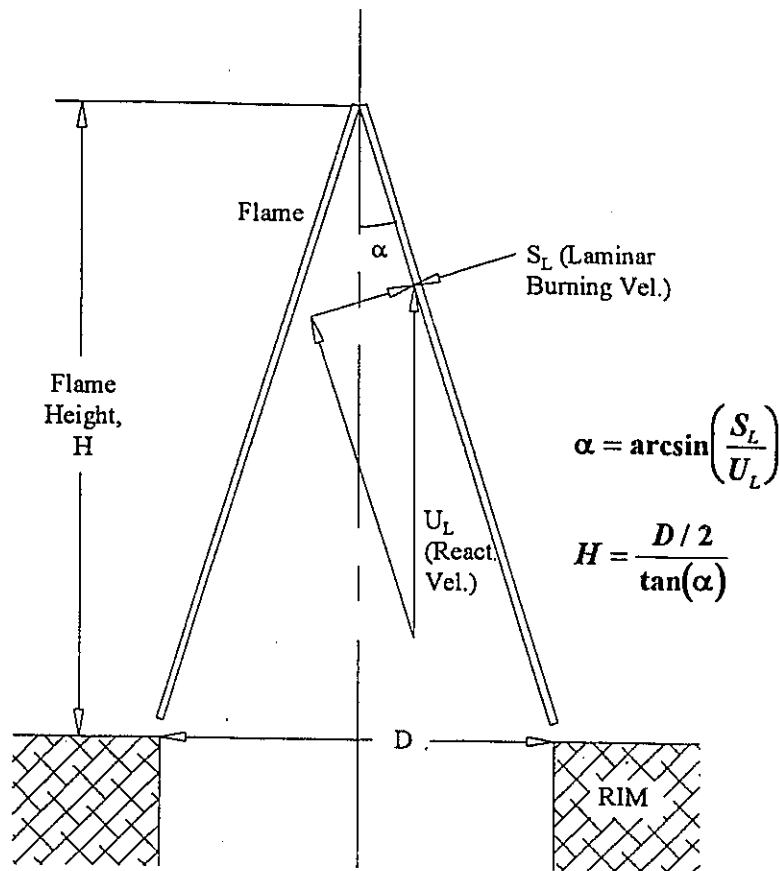
Figure 1.3: Simplified Vector Diagram for a Bunsen Burner Flame

1.5 Other Techniques for Achieving Low Emissions

Fuel lean combustion is just one of a variety of methods for reducing pollutant emissions from burners. Since in general, CO emissions can be easily controlled by burning with a slightly lean mixture, most research has focused on reducing NOx emissions specifically. Methodologies for mitigation of NOx are numerous and varied but most fall under one of two broad categories: combustion control techniques and post-combustion treatment techniques.

1.5.1 Combustion Control Techniques

For systems using natural gas or other non-nitrogen containing fuels, reduction of NOx during combustion is focused primarily on reducing thermal NOx. Emissions control is based on lowering the combustion gas temperature, reducing available oxygen, or reducing residence time of combustion gases at high temperatures or combinations of the above. In all cases NO formation via the Zeldovich mechanism is hindered.

1.5.1.1 Temperature Control

Flue gas recirculation is commonly used in industry to lower peak combustion temperatures. In this process, comparatively cool combustion products are recycled and mixed with the incoming combustion air. The added mass of gas acts as a diluent and absorbs some of the heat generated during combustion [3]. While flue gas recirculation has been successful in reducing NOx emissions by up to 70%, CO emissions have been known to increase as a result [21]. On its own, flue gas recirculation may not provide a significant enough reduction in NOx emissions to meet the South Coast Air Quality Management District's strict standards [4].

Another method of reducing combustion temperatures is humidified combustion or steam addition. Water introduced into either the fuel or the combustion air (usually as steam), again acts as a diluent. In fact steam addition has been found to reduce NO formation independent of its effect of lowering the flame temperature [22]. Although Glassman [17] predicts that steam addition should lower CO emissions, Bowman [4] states the opposite. Regardless, steam addition in gas turbines (where it has been tried in a number of installations) has yet to provide a significant enough reduction in NOx to meet SCAQMD gas turbine guidelines [4]. Furthermore, issues of corrosion in humidified combustion systems have yet to be resolved [21].

A third method of achieving low NOx emissions via lower combustion temperatures is lean premixed combustion which is the focus of this research. As

previously mentioned, the most prevalent problem in lean combustion is one of flame stability. Several methods of stabilizing lean premixed flames have been investigated by a variety of researchers and some of their approaches will be discussed in detail in the next chapter.

1.5.1.2 Control of Oxygen Availability at High Temperatures

Instead of reducing peak combustion temperatures, another approach to reducing NOx emissions is to reduce the amount of oxygen available in locations where the temperatures are maximum. In this fashion the Zeldovich reactions are retarded. The common method for restricting available oxygen is called staged combustion or air staging in which the primary combustion zone is fuel rich and additional combustion air (overfire air) is added downstream. Combined with flue gas recirculation, air staged combustion has achieved NOx emissions of 40-50 PPM (@3% O_2) in natural gas burners [4]. However, CO emissions have been found to increase as a result of this approach [21,4].

A variation on the air staging approach is called fuel staging or reburning. Here the primary combustion zone is fuel-lean and additional fuel is injected further downstream in the reburning zone. The added fuel acts as a reducing agent as CH fragments react with NO [23]. In the final stage, the burnout zone, air is added to provide overall lean conditions and oxidize all remaining fuel. Optimum equivalence ratios in the primary and reburning zones are near 0.9 and 1.15 respectively [23,24]. In full scale natural gas furnaces with reburning, NOx reductions of up to 50 % have been realized [4].

1.5.1.3 Reduction of High Temperature Residence Time

Still another approach to reducing NOx emissions is pulsed combustion or cyclical combustion in which fuel is burnt intermittently in a repeating cycle. This process makes use of the fact that the Zeldovich formation reactions are slow compared to the

hydrocarbon combustion reactions. In essence, the hot combustion products are cooled by mixing with cooler residual products so that the combustion gases exist at high temperatures for only short periods of time -- too short a time for large quantities of NOx to form [25]. Although pulsed combustors generally produce low NOx emissions, further reductions are required to meet stricter government standards [26]. Recently simultaneous emissions of NOx and CO below 5 PPM (@3 % O_2) have been reported for a pulsed combustor operating in lean-premixed mode with enhanced exhaust gas mixing [27]. Pulse combustors offer an additional advantage of increased efficiency due to the increased mass, momentum, and heat transfer associated with pulsating flows, although acoustic noise and moderate cost remain as problems [26,21].

1.5.2 Post-Combustion Treatment

There are a number of post-combustion removal techniques for reducing NOx emissions and the most common ones can be divided into two categories: Selective Non-Catalytic Reduction (SNCR) and Selective Catalytic Reduction (SCR). These processes involve the addition of nitrogen containing additives into the combustion products downstream of the combustion zone which initiate a set of reactions that result in the reduction of NO [4]. The most common additives are ammonia, urea ($[NH_2]_2CO$) and cyanuric acid ($[HOCN]_3$) [4]. In SNCR the reduction reactions occur in the gas phase whereas for SCR the reactions occur on the surface of a catalyst. In the proper temperature range NO will react with nitrogen containing radicals from the additive to form N_2 or N_2O. However, at high temperatures the added nitrogen may react to form additional NO and at low temperatures the NO removal process may not proceed at all [4]. Because of this relatively narrow effective temperature range it is difficult to apply SCR and SNCR to full-scale boilers with spatial variations in temperature and finite mixing rates of additives in flue gas [4].

1.6 Target Applications and Objectives

Although several other approaches to reducing NOx and other pollutant emissions exist, none is ideal and there is much room for improvement. The purpose of this research was to develop a novel method of stabilizing lean premixed flames on a conventional burner in order to realize the lower pollutant emissions associated with fuel-lean combustion. It was hoped that the modified burner would be cheap and reliable and could be easily retrofitted into existing appliances. The targeted NOx emissions were below standards legislated by the South Coast Air Quality Management District in California, the most stringent in the world. In addition, CO and HC emissions were not to increase as a result of the combustion modifications. This new type of burner would be ideal for domestic and industrial heating applications or any other process where high combustion gas temperatures are not required.

2. SURVEY OF LEAN FLAME STABILIZATION

Although it is commonly known that lean flames will burn at lower flame temperatures with corresponding low NOx and CO emissions, a narrow flame stability range has prevented this fact from being exploited in industry. Over the years much research has been focused on efforts to stabilize lean premixed flames, some of which will be reviewed here. First however, the stabilization of a traditional rim stabilized "Bunsen type" burner will be examined.

2.1 Classical Rim Stabilization

Figure 2.1 shows streamlines through a Bunsen flame that is stabilized on the rim of a burner.
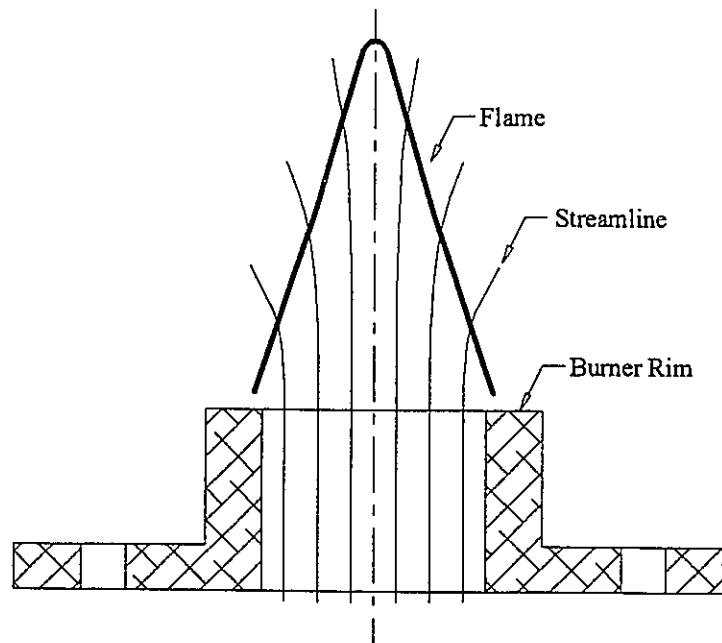
Figure 2.1: Flow Through a Bunsen Flame (after Glassman [7])

Following Lewis and von Elbe [28] and Glassman [7], by assuming Poiseuille flow in the burner and concentrating on a region of the flame very near the wall (of the order of 1 mm), one can assume a linear velocity profile for the reactants. It is also assumed that the flow lines are parallel to the burner walls. Figure 2.2 shows this edge region in detail with three possible positions of the flame.
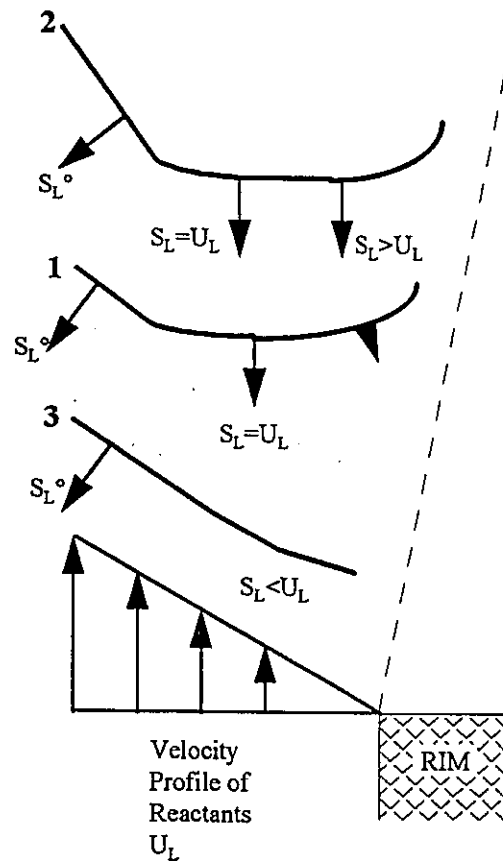
Figure 2.2: Stabilization Region of a Bunsen Flame (after Lewis and von Elbe [28])

Near the edge of the flame, the burning velocity decreases from its maximum S_L° as heat and chain carrying radicals are lost to the burner rim. At position 1, the flame is stable. At some point along the surface of the flame, the local burning velocity (S_L) is equal in magnitude and opposite in direction to the reactant gas velocity (U_L). If the flame is displaced slightly upward to position 2, the heat loss to the burner rim decreases causing

the burning velocity to increase. This increased burning velocity allows the flame to propagate back towards the burner and return to its stable equilibrium position. Conversely, if the flame is displaced to position 3, heat loss to the burner rim increases causing the burning velocity to decrease. The flame is driven back from the burner by the reactant flow and again maintains an equilibrium position.

This stabilizing effect is limited. As the flame moves farther away from the burner rim, outside air is entrained and the reactants are diluted, causing the burning velocity to decrease. If this dilution effect over balances the burning velocity increase associated with the lower heat loss to the burner rim, the flame will become unstable and blowoff. This instability is particularly problematic for lean flames because further air entertainment dramatically reduces the burning velocity. The operating conditions under which this destabilization first occurs are referred to as the blowoff limit. However, as long as the lower heat loss effect dominates, the flame will remain stable.

Alternatively, if the flame moves to position 3 and the increased heat loss to the burner rim is insufficient to prevent the burning velocity from exceeding the reactant gas velocity, the flame can flashback or propagate back inside the burner. The operating conditions under which this first occurs are known as the flashback limit. Again, as long as the increased heat loss effect dominates, the flame will remain stable.

In this fashion a premixed flame is stabilized on a traditional burner. It should be noted that the overall operating range between flashback and blowoff is quite narrow. Furthermore, since lean flames are already partially diluted with excess air, they are very susceptible to blowoff and are almost impossible to stabilize without some modifications to the burner itself.

2.2 Other Modes of Stabilization

Because of the narrow operating range associated with classical rim stabilization (particularly for lean flames), researchers have investigated a variety of 'improved" methods and approaches for flame stabilization. Although all such procedures are too

numerous and varied to be discussed completely, an effort will be made to review the more relevant attempts.

2.2.1 Bluff Body Stabilization

The majority of approaches to stabilizing flames (including this research) fall under the general category of bluff body stabilization. Many researchers have focused on stabilization of flames in high speed flows ([29-32] for example) with applications including ram-jet engines and turbo-jet afterburners. The focus of most of this work was to increase the maximum blowoff velocity, not to stabilize lean flames. Although the present research involves flows with Reynolds numbers that are several orders of magnitude lower, the principles involved in the bluff body stabilization remain the same.

In bluff body stabilization, an obstacle such as a rod, V-gutter, ring, etc. is placed in the flow creating a wake of hot combustion products. The recirculating hot gases interact with the reactant gas and act as a continual ignition source [33,34,28,7]. A simplified representation of a bluff body stabilized flame is shown in Figure 2.3.
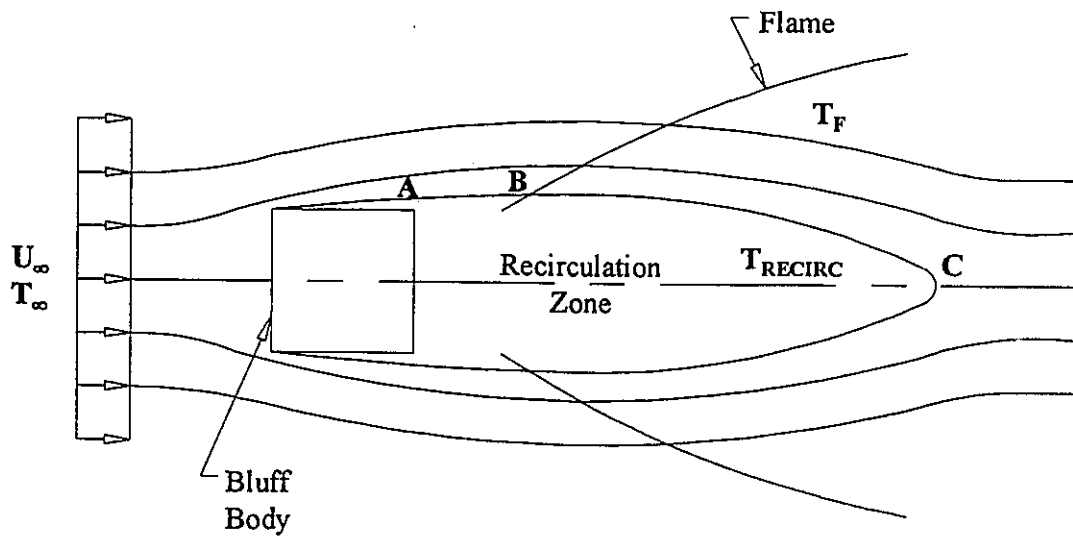
Figure 2.3: Idealized Stabilization by a Bluff Body (after Kundu et al. [33])

Between A and B, the hot gases in the recirculation zone ($T=T_{RECIRC}$) transfer heat to the comparatively cool reactant gas ($T=T_\infty$) and the flow is ignited. From B to C, heat from the flame zone ($T \approx T_F$) is transferred back to the recirculation zone. Thus, in the steady bluff body stabilized flame, an energy balance exists in the recirculation zone [33,34]. If the heat demand by the reactants across AB exceeds the heat transferred to the recirculation zone across BC, the flame blows off [33].

Glassman [7], citing data by Zukowski and Marble, describes the wake behind a rod stabilizer as a function of Re_R, the reactant flow Reynolds number based on the rod diameter. Although a cold flow analysis would suggest a stable fully developed turbulent wake would only exist at $Re_R > 10^5$, when the flow is combusted shedding eddies that would occur for $10^2 < Re_R < 10^5$ are replaced by a well defined, steady vortex. This change in flow is probably due to the increase in kinematic viscosity as a result of the increase in temperature [7]. Thus for $50 < Re_R < 10^5$, which encompasses most of the range of flows in the present research, a stable recirculation zone will occur in the wake of the rod. However, the present research uses rings with square cross-sections instead of rods to stabilize flames and thus, the Reynolds numbers and flow patterns may not correlate directly. No previous data were found that dealt with rods or rings of square cross section in a combusting flow.

Although the Reynolds numbers for the wake flow will vary somewhat, the shape of the bluff body is not critical for flame stability and several different configurations have been tried [28, 33]. Flames stabilized by V-gutters [30], rods [32], and disks [35] have all been investigated by many researchers. In all cases, the most stable flames occur when the temperature in the wake is maximum [28]. Unfortunately a simple independent dimensional dependency between blowoff velocity and bluff body shape and size does not exist [7]. Some success in correlating blowoff data has been achieved using a characteristic ignition time [36,7] but this theory will not be discussed further in this review.

Most researchers have studied blowoff limits with the primary goal of increasing the maximum blowoff velocity (usually at stoichiometric conditions), but a few have included measurements of the lean blowoff limit and more recently emissions. While

Yang et al. [30] were concentrating on high speed stabilization in their investigation of slit V-gutters, they were successful in stabilizing lean premixed petroleum gas and air flames down to equivalence ratios of 0.7. However, they made no attempt to study exhaust emissions.

Cheng [37] investigated a variety of V-flames stabilized by rods, bars, and V-gutters of various sizes. For the optimum rod size, blowoff occurs at an equivalence ratio of about 0.51. By contrast blowoff occurs at $\phi=0.7$ for the optimum V-gutter. However, tests were conducted for only one reactant flow velocity (5 m/s) and exhaust gas emissions were not studied.

Another method of attaching flames, similar in principle to bluff body stabilization, is flame stabilization by wall recesses [38]. Here, recesses in the wall of a burner tube create recirculation zones which stabilize the flame. While this approach appears to have the advantage of lower drag in high speed flows, the stable lean operating range is smaller than for most bluff body stabilized flames.

The current research relies on using an axisymmetric ring placed in a circular burner port to stabilize a flame. The ring stabilized flames are essentially the same as rod stabilized flames except they are axisymmetric and produce conical flames.

2.2.2 Swirl, Electrical, Pilot Flame, and Enhanced Thermal Stabilization

In the past swirl has been used predominantly in fuel rich systems where devices such as turning blades were used to enhance mixing of fuel and air [39]. Recently however, swirl stabilized burners have generated interest as a method of stabilizing lean premixed flames. Cheng et al. [40-42] have developed a "weak-swirl" burner that stabilizes premixed hydrocarbon flames in a divergent flow field. In the weak-swirl burner, air is injected tangentially around a central jet of premixed fuel and air, upstream of the burner exit. As the reactants exit the burner, the centrifugal force due to the swirl flow causes the jet diverge. As the jet diverges radially, it decelerates so that a flame can remain stable over a wide range of burning velocities and hence equivalence ratios.

Stable methane and air flames with equivalence ratios as low as 0.57 have been stabilized on this burner [40]. The weak-swirl burner was recently adapted for a small hot water heater and efficiency and emissions were measured [42]. At an equivalence ratio of 0.7, NO concentrations (corrected to 3% excess oxygen) were less than 10 PPM. However, the authors acknowledge that CO concentrations were not measured and are known to increase at similar equivalence ratios. Furthermore, unburned hydrocarbons were not measured and could possibly increase since the divergent flow field provides a potential path for methane molecules to escape without passing through the flame front.

Berman et al. [43] have tried an entirely different approach to lean flame stabilization. An 3 kV electric field from a ring electrode placed above the burner (which is grounded) is used to stabilize the flame. The electric field imposes a force on the ion particles in the flame zone which acts to stabilize the flame over a wider range of equivalence ratios. Using this approach stable flames down to equivalence ratios of 0.73 have been achieved with corresponding reduced NO emissions. However, the authors have not reported concentrations of other emissions. Although the authors suggest that the electric power requirements are only 0.01% of the combustion power being controlled, the required field strength of 3 kV may make this design difficult to implement.

Pilot flames have also been used to stabilize combustion processes. Although Jensen and Shipman [44] used this method to stabilize high speed flows, the results are applicable to burner design as well. In this approach, small pilot flames are used to continually ignite a lean premixed main flame. The pilot flames are kept stable by either making them stoichiometric or fuel-rich. However in low NOx systems, emissions from the hotter pilot flames can be significant and problematic. Alternatively the pilot flames can be generated by decelerating a small portion of the lean main flow usually along the burner rim. In this case the stability limits are not as broad and large scale reductions in NOx may not be possible.

A final method of stabilization involves trying to enhance the heat transfer process responsible for classical rim stabilization. Alternatively, for the purpose of lowering NOx emissions, one can simply increase the heat loss from the flame to the burner in an attempt to lower peak combustion temperatures. Yuuki and Matsui [45] investigated flames

stabilized on wire meshes with the goal of trying to achieve low NOx emissions. In this type of surface combustion, low flame temperatures result when heat is conducted away in the wire mesh. While low temperature flames were achieved, the occurrence of flashback was problematic when the mesh was heated past some critical point.

3. EXPERIMENTAL APPARATUS

3.1 The Laboratory Burner

Figure 3.1 shows a cross-sectional view of the natural gas burner used in this research and a schematic of the fuel and air flows.
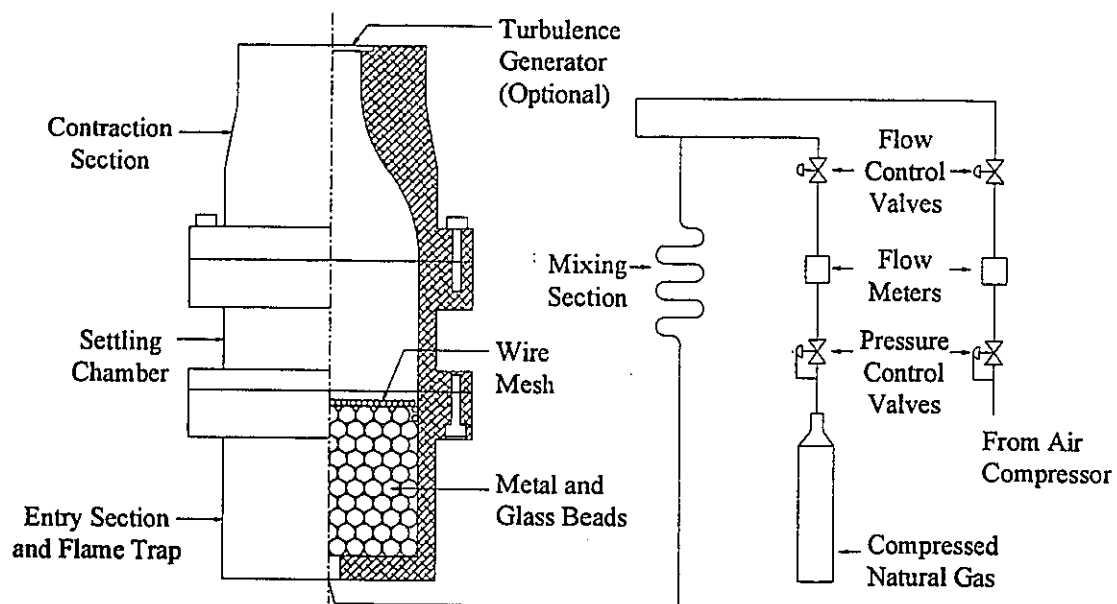
Figure 3.1: Laboratory Burner Cross-section and Flow Schematic

Bottled compressed natural gas and compressed air from building supply lines were separately regulated to approximately 310 kPa (45 psig). The fuel and air were then passed through Matheson hot-wire mass flow transducers which have voltage outputs of 0-5 V and ranges of 0-0.30 g/s and 0-6.83 g/s respectively. The rated accuracy of both flow meters was 1% of full scale. The flow meters were calibrated using nitrogen as a test gas and conversions are applied to permit measurement of flows of gases with different properties. Appendix B contains details of the flow meter calibrations. The natural gas used was City Gas from the City of Edmonton which had an average composition of 94%

methane, 2% ethane, 3% nitrogen, and 1% carbon dioxide by volume. Composition measurements for each tank of fuel used are contained in Appendix C.

The flows of the two reactant streams were controlled by two manually operated valves prior to being mixed and injected into the bottom of the burner. To ensure complete mixing, the combined flow was passed through a 1.4 m length of 1.27 cm diameter tubing containing 10 successive 90 degree bends.

The burner was machined from aluminum on a numerically controlled lathe and consists of 4 main sections: an entry section and flame trap, a settling chamber, a contraction section, and an exit section (not shown in Figure 3.1). The burner is approximately 33 cm (13 inches) long and up to 15 cm (6 inches) in diameter. The metal and glass beads in the entry section act to break up the incoming jet of reactants and disperse it evenly inside the burner. A fine gauge wire mesh on top of the beads eliminates any large scale vortices that might shed from the beads, ensuring quiescent flow. The wire mesh and beads also act as a flame trap. If flashback occurs and the flame propagates back inside the burner, the wire mesh and beads prevent further propagation back into the piping system.

As the flow leaves the entry section of the burner, it becomes laminar in a short settling chamber before being accelerated through the contraction section. The contraction ratio is 9:1 by area and the diameter at the exit is 32 mm. It should be noted that a commercial prototype of this burner would not need to be nearly so complex. The laboratory burner was specifically designed to have precise and repeatable operation characteristics suitable for experimental research.

At the end of the contraction section there is a provision for a turbulence generator. For this research two different perforated plates with either 2 or 3 mm holes and 50% blockage ratios were used. Identical turbulence plates were used previously and turbulence measurements were reported [46,47]. Based on this previous work, the smaller scale, 2 mm turbulence plate can be expected to produce a turbulence intensity at the burner exit which is 8% of the mean flow. The larger scale, 3 mm turbulence plate will produce a turbulence intensity at the burner exit which is 11.5% of the mean flow.

3.2 Stabilization Methods

After leaving the contraction section, the flow enters the exit section of the burner where a variety of different flame stabilization methods can be applied. Figure 3.2 shows the exit section of the burner for traditional rim stabilization. The rim stabilized case formed the basis for comparison in the experiments. The inner diameter of the rim, the flow diameter, is 32 mm (1.25 inches) and the length of the exit section along the flow axis is 25 mm (1 inch). This exit section is fastened to the end of the contraction section shown in Figure 3.1.
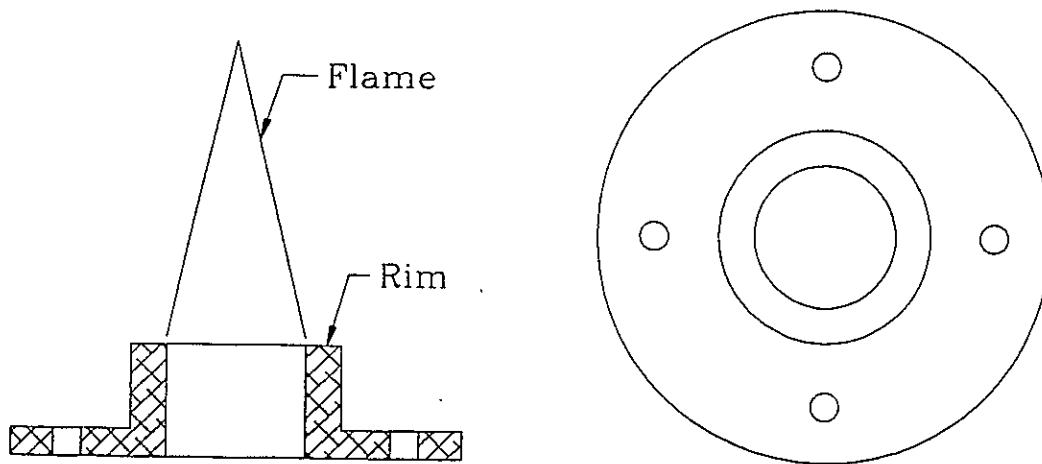
Figure 3.2: Rim Stabilized Burner Exit Section

Figure 3.3 shows the ring stabilized burner exit section. In this configuration rings of different diameters and cross-sections can be placed in the flow to aerodynamically anchor the flame. The rings, which were made of stainless steel or aluminum, are held in place by three small spindles 0.5 mm (0.02 inches) in diameter which are anchored to the burner rim. Several different rings with a variety of diameters and cross sectional areas were investigated as summarized in Table 3.1. The flow obstruction due to the ring stabilizer is termed blockage, β, and is defined as the ring planform area divided by the burner exit area.

Figure 3.3: Single Ring Stabilized Burner Exit Section

Table 3.1: Single Ring Stabilizer Dimensions

Ring Name	Outer Diameter (mm)	(inches)	Gap Size (mm)	(inches)	X-Section (mm)	(inches²)	Blockage, β (%)
G0	32.8	1.250	0	0	2 x 2	0.0787²	23.6
G1	30.2	1.1875	0.8	1/32	2 x 2	0.0787²	22.3
G2	28.6	1.125	1.6	1/16	2 x 2	0.0787²	21.1
G3	27.0	1.0625	2.4	3/32	2 x 2	0.0787²	19.8
G4	25.4	1.000	3.2	1/8	2 x 2	0.0787²	18.6
S1	28.6	1.125	1.6	1/16	1 x 1	0.0394²	10.9
S3	28.6	1.125	1.6	1/16	3 x 3	0.1181²	30.4

A third type of device for flame stabilization was also investigated. These "concentric ring stabilizers" are shown in Figure 3.4. Compared to the single ring, the concentric ring offers the advantage of increased flame area and lower overall flame height. For all of the concentric rings investigated, the outer rings were identical in shape and size. Both the inner and outer rings for all concentric stabilizers had 2 x 2 mm square

cross-sections and were made of stainless steel. Dimensions of the stabilizers that were studied are shown in Table 3.2.
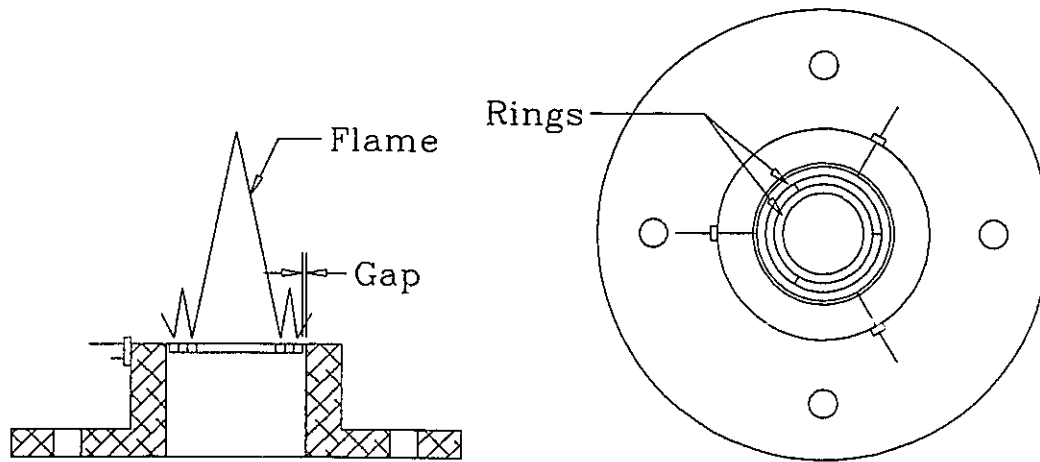
Figure 3.4: Concentric Ring Stabilizer

Table 3.2: Concentric Ring Stabilizer Dimensions

Ring Name	Outer Ring				Inner Ring				Blockage
	Outer Dia.		Gap Size		Outer Dia.		Inner Dia.		β
	(mm)	(inches)	(mm)	(inches)	(mm)	(inches)	(mm)	(inches)	(%)
C0	30.2	1.1875	0.8	1/32	4.0	.157	0(disk)	0	23.9
C2	30.2	1.1875	0.8	1/32	9.5	.375	5.5	.218	28.3
C4	30.2	1.1875	0.8	1/32	15.9	.625	11.9	.468	33.4
C6	30.2	1.1875	0.8	1/32	22.2	.875	18.2	.718	38.4

3.3 Flame Height Measurement

Flame height measurements were an important part of this research. In order to investigate the possibility of retrofitting the modified burner design into existing appliances, the height of the visible flame edge was studied using the device shown in Figure 3.5. The device has a range of 0 - 35 cm with a resolution of 1 mm from 0 - 10 cm and 2 mm from 10 - 35 cm. The sight slides freely up and down the supports and the visible flame height is read from the graduated support.
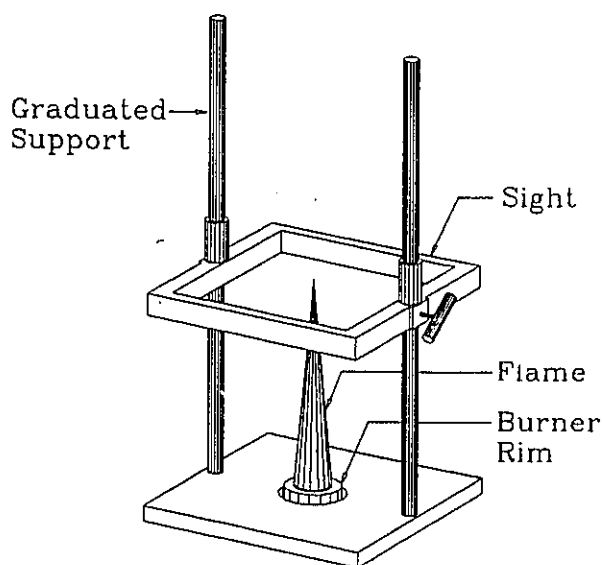
Figure 3.5: Visible Flame Height Measurement Device

3.4 Emissions Measurement

In order to accurately measure pollutant emissions from the burner, a specialized gas collection system was developed. A fully enclosed generic heat exchanger was

designed to sit on top of the burner and collect and cool all of the exhaust emissions. This device, which is welded stainless steel, is shown in Figure 3.6.
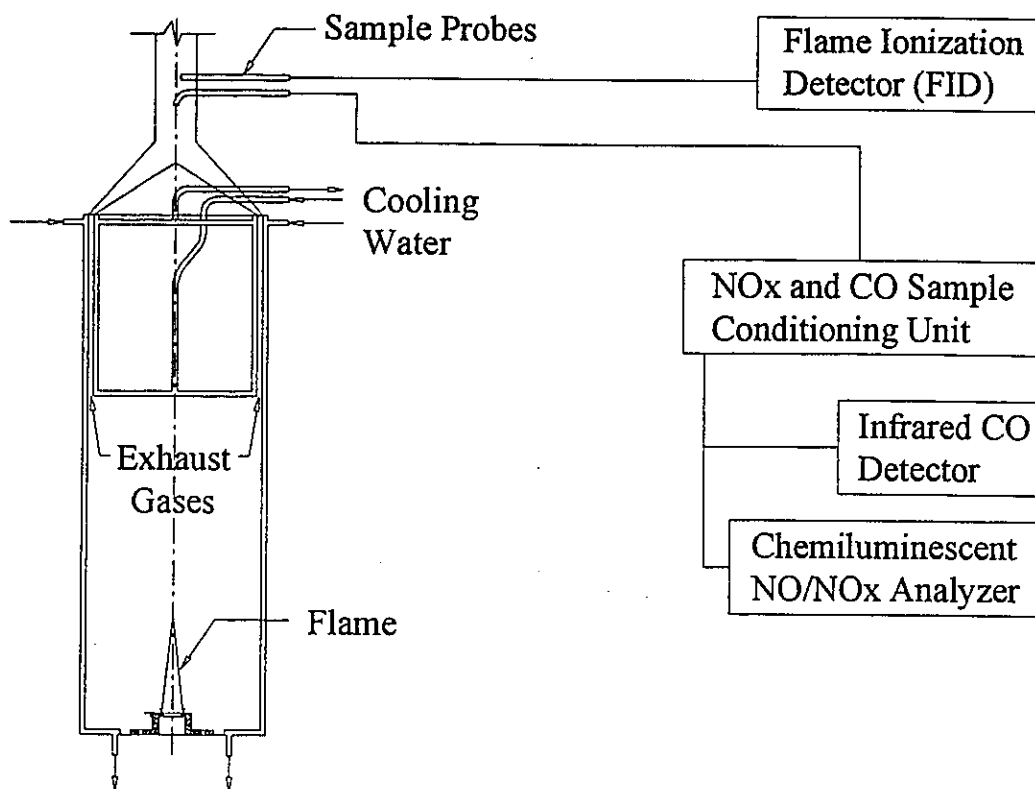
Figure 3.6: Generic Heat Exchanger and Gas Analysis Schematic

As shown, the walls of the heat exchanger are hollow to permit circulation of cooling water. Domestic cold water was used as a coolant . There are two separate water flow paths: one through the outer wall, and one through the inner wall or "boot" at the top of the exchanger. The exhaust gases were forced through a narrow 6.4 mm (1/4 inch) wide and 22.5 cm (9 inch) long annulus between the cooled walls providing the necessary heat transfer coefficient to reduce the exhaust gas temperature to approximately 400 K. Water flow rates for the two paths were individually metered and controlled. A series of type T copper-constantan thermocouples were used to measure the temperature rise of the cooling water through the heat exchanger.

The firing chamber portion of the heat exchanger is approximately 40 cm (16 in.) long and 20 cm (8 in.) in diameter. A single type K chromel-alumel thermocouple was used to measure the firing chamber temperature. There is an 11 cm (4.25 in.) diameter access port at the front of the exchanger near the bottom to provide access to the burner exit for igniting the flame and changing the flame stabilization device. The door to this port bolts to the exchanger to ensure a leak free seal. A small quartz window in the door permits visualization of the flame during the experiments.

The cooled exhaust gases are funneled into a 5 cm (2 in) diameter 45 cm (18 in) long stack from which samples are drawn using two separate probes. Two type T copper-constantan thermocouples were used to measure the exhaust gas temperature at the sampling point. The location of the probes are sufficiently far upstream from the stack exit to ensure accurate results in accordance with SAE guidelines as outlined in [48].
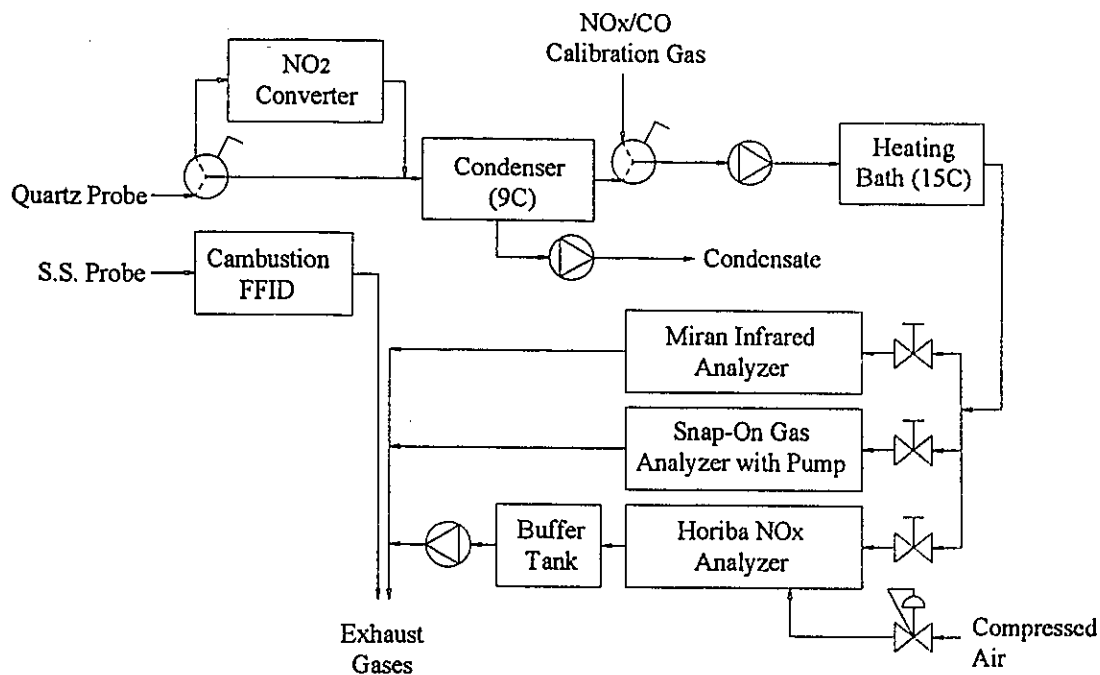
Figure 3.7: Emissions Sampling System Schematic

Sample gas from the probes is fed to a Cambustion HFR 400 fast flame ionization detector (FFID), a Wilks Miran I variable filter infrared analyzer, and a Horiba CLA-510SS NOx analyzer. In addition, a Snap-On MT3500 Emissions Analyzer was used to supplement CO measurements from the Wilks analyzer at concentrations above 600 PPM. The gas sampling system is shown in a detailed schematic in Figure 3.7. For the NOx and CO measurements , the sample is drawn through an un-cooled quartz probe. Evans et al. [49] recommends the use of a quartz probe to prevent conversion of NO_2 to NO which can occur in stainless steel probes. All fittings upstream of the condenser are Teflon (where temperatures might be high and there is a chance that conversion of NO_2 to NO could take place in the presence of stainless steel) and Teflon sample lines are used throughout the system.

Cernansky [50] and Evans et al. [49] describe how NO_2 is readily absorbed in water. For this reason the NO_2/NO converter is placed ahead of the condenser in the sampling system. In addition, the condenser is of small volume and is designed so that sample gas never has to bubble through cold water. Any condensate that is collected is immediately pumped away and drained. The temperature of the cooling water in the condenser is fixed at 9°C using a constant temperature bath with a circulating pump. After leaving the condenser, the sample gas is drawn through a Teflon seat sample pump and pushed through a second constant temperature bath where the temperature is fixed at 15°C. From here the sample is split into three separate streams, one for each analyzer.

The Horiba chemiluminescent NOx analyzer was used to measure NO and NO_2 concentrations. Briefly, the analyzer deduces NO concentrations by measuring the luminescence of reactions 3.1. The incoming sample is reacted with ozone to produce NO_2, some of which exists in a partially excited state. The excited NO_2* molecules emit photons as they return to the ground state. The luminescence quantity is proportional to the original amount of NO in the sample. NOx concentrations in the sample are found by first converting all of the NO and NO_2 to NO via the converter and measuring the total quantity as NO. NO_2 concentrations are then found by subtracting the concentration given by the exclusively NO measurement from that given by the total NOx measurement.

$$NO + O_3 \rightarrow NO_2{}^* + O_2$$
$$NO_2{}^* \rightarrow NO_2 + h\nu$$
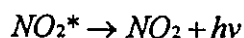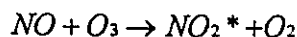
Equations 3.1: Chemiluminescent NO Detection Reactions

The Horiba analyzer has 7 selectable ranges from 0 - 25 PPM to 0 - 2500 PPM. The rated accuracy is ±0.5% of full scale for higher ranges and ±1.0% of full scale for ranges of 0-100 PPM or less. For the ranges encountered in this research this translates to an uncertainty error of no more than 1.25 PPM. The Horiba analyzer provided direct 0-1 V output so that a computer based data acquisition system could be used to record measurements.

To measure concentrations of CO two different analyzers were used. The primary analyzer was the Wilks Miran 1 General Purpose Gas Analyzer. This device measured light adsorption over a range of selectable wavelengths in a sample of gas. The Miran analyzer was calibrated to measure CO concentrations by determining the amount of adsorption from a infrared source at approximately a 4.5 μm wavelength. The voltage output of the device had a square root dependence on concentration. The maximum range was 580 PPM of CO and the uncertainty was estimated at ±15 PPM. For concentrations of CO greater than 580 PPM the Snap-On emissions analyzer was used. Like the Miran analyzer, the Snap-On device measures infrared adsorption to determine CO concentrations. The resolution of the Snap-On analyzer is 0.01% or 100 PPM and uncertainty in measurement was estimated to be ±100 PPM.

Sampling of unburned hydrocarbons was done using a separate sample path. A stainless steel probe was used to draw some exhaust into the Cambustion fast flame ionization detector (FFID). In essence the FFID measures quantities of ions produced when hydrocarbons from the sample gas are passed through a hydrogen flame. The number of ions produced is essentially proportional to the number of carbon atoms burnt in hydrocarbon form.

For this research where small concentrations of hydrocarbons were measured, the FFID was used at its maximum sensitivity of 1 mV/PPM of C_3H_8 equivalent at an STP

sample flow of 50 cc/min. Since it was assumed that methane was the only hydrocarbon present in the exhaust gas, this equates to a sensitivity of 0.33 mV/PPM. The rated accuracy in this range is ±10%. The Cambustion FFID provides direct voltage output of 0-10 V and measurements were recorded using computer based data acquisition.

3.5 Data Acquisition

To record and process the data in these experiments, a computer based data acquisition system was developed. A DOS based 486 DX2/66 MHz computer with 16 Mb memory driving a Kiethly Metrabyte DAS-1602 data acquisition board was used. Four main QuickBasic 4.5 programs were written to collect data from a variety of experiments. The crux of all four programs is the sampling routine that reads the fuel and air flows from the Matheson mass flow meters. Output from these meters was 0-5 Vdc Unipolar. The output signal was multiplied by a gain of two on the DAS-1602 board which was configured for 0-10 Vdc input with 12 bit resolution. The two flow meters were read simultaneously, 750 times each, at a sample rate of 3333.3 Hz. These readings were then averaged and the mass flow rates of the air and fuel, the equivalence ratio, and the energy release were immediately calculated. By continually averaging a large number of samples, data errors due to signal noise were virtually eliminated. Errors during analog to digital conversion are quoted at 0.01% of reading ±1 least significant bit, which are generally negligible compared to the rated 1% accuracy of the flow meters.

For the three programs used in blowoff, flashback, and flame height measurements, calculated data are used to plot equivalence ratio versus reactant mass flow rate on the computer screen in real time. At the command of the operator, operating conditions of the burner are immediately recorded on disk. Thus, reactant flow parameters for blowoff and flashback conditions are easily determined. In the case of flame height measurements, as the computer records the burner operating conditions, the user is prompted for keyboard input of the flame height as read using the device described in Section 3.3.

The fourth program, used for emissions measurement, was considerably more complex. This program makes use of five different data acquisition routines to record data from the fuel and air flow meters, the cooling water flow meters, thermocouples, the thermocouple cold junction, and the gas analysis equipment. The reactant flow meters were read using the same routine as in the other three programs. The NOx and CO analyzers and the FFID were read simultaneously, 500 times each, at a sample rate of 1333.3 Hz. Each of the thermocouples was read in series, 100 times each, at a sample rate of 1000 Hz. The cold junction temperature was read 100 times at a rate of 1000 Hz at 10 second intervals. Finally the cooling water flow meters were connected to a totalizer which was read at measured time intervals to allow flow rates to be determined. Data from the transducers was compiled in real time and updated on the screen. Burner and heat exchanger operating parameters were automatically tabulated and stored on disk.

4. EXPERIMENTAL METHODOLOGY

4.1 Measurement of Blowoff Limits

Quantifying the exact moment at which blowoff occurs is difficult if not impossible. In fact the conditions at which blowoff can be said to occur are somewhat arbitrary. In the laboratory as the flame is made leaner and leaner, signs of instability start to appear. These instabilities appear as "flame jumping" near the burner rim or directly above the ring stabilizer depending on which stabilization method is employed. Small sections of the flame briefly liftoff and then reattach themselves, creating small intermittent "holes" at the base of the flame. This condition will be referred to as stage 1 blowoff.

As the equivalence ratio is lowered further, the initial instabilities become increasingly severe and the holes grow larger. Subsequently, the holes grow to the point where they are no longer closed and entire sections of the burner support no flame. This condition will be referred to as stage 2 blowoff. For a ring stabilized burner at stage 2 blowoff, a section of the ring between the support spindles will support no flame. For the rim stabilized burner, the flame will remain attached to no more than a 180 degree section of the rim. When the flame liftoff is this severe, it is obvious that the pollutant levels and burner efficiency will be adversely affected.

The final stage of blowoff, stage 3 blowoff, occurs when the flame disappears from the burner completely. This stage is more easily defined than stages 1 and 2, but has less relevance to a practical burner. Because of sharply increased pollutant emissions and loss of efficiency, a burner would be essentially inoperable at stage 2 blowoff. Thus, for the purposes of this research blowoff will be defined as stage 2 blowoff.

A different choice of definition for blowoff would not significantly affect results. The entire range of equivalence ratios from stage 1 to stage 3 blowoff is generally less than 0.05. Moreover, even under laboratory conditions the three stages are not always

36

apparent especially for turbulent flow at high flow rates. At high flow rates the flame can sometimes move directly from stage 1 to stage 3 or jump directly to stage 2, making the distinctions in stages less relevant.

The experimental procedure for determining blowoff is quite straightforward. The flame is brought to steady state conditions near an equivalence ratio of unity. Very slowly the fuel flow is decreased making the flame progressively leaner. Eventually stage 1 instabilities start to appear. The fuel flow is then decreased slightly until stage 2 blowoff is reached. At this point flow data is recorded on computer disk as the blowoff limit has been reached. Since the fuel comprises only a small fraction of the total reactant flow, the path taken to blowoff is approximately one of constant flow rate. Alternate paths of fixing the fuel flow and slowly increasing the air flow, as well as adjusting both air and fuel flows simultaneously, were also tested. However, the blowoff limit does not seem to be influenced by the path taken. This procedure is then repeated starting with flames of different flow rates until an entire blowoff limit versus flow rate curve has been generated. The test is conducted in partial darkness to aid visualization of the flame.

This method of determining blowoff has given very consistent results. However, at very low flow rates time lags in the reactant piping system become apparent. This is rectified by allowing a time interval of 5 seconds or more to observe the flame between flow rate adjustments at low flow rates. This ensures that the flame is operating under quasi-steady state conditions.

4.2 Measurement of Flashback Limits

Flashback is much more dramatic and hence more easily defined than blowoff. At low flow rates, if the component of the burning velocity in the direction of the burner exceeds the corresponding component of the reactant velocity leaving the burner, the flame will jump back inside the burner and propagate back into the premixed reactants. In the lab, this usually occurs dramatically with little or no warning. Therefore, flashback will be defined as the point where the flame moves completely into the burner.

Flashback tests are conducted in a similar manner to blowoff tests. The procedure was to start with a flame with an equivalence ratio far away from unity. Slowly the fuel and air are adjusted to produce a flame closer to stoichiometric. As the equivalence ratio approaches unity, the burning velocity increases until suddenly the flame flashes back. Unfortunately, because blowoff occurs at low flow rates, time lag in the piping system is prominent. Therefore it is usually necessary to wait up to 10 seconds between flow adjustments to ensure that quasi-steady state flow is maintained. As soon as flashback occurs, flow data is stored on computer disk. To prevent burner overheating, the fuel flow is immediately cut off by closing a solenoid valve.

For the case of a ring stabilized burner, time lag effects can be even more pronounced. The ring tends to act as a heat sink which can slow the burning velocity and delay flashback. However, care must be taken to ensure that heat transfer through the ring reaches steady state before readjusting the fuel and air flows. This was particularly difficult with early versions of the ring stabilizers which like the burner were made of aluminum. The energy release inside the burner during flashback was often enough to melt the aluminum stabilizers.

A further problem with flashback tests relates to the accuracy of the flow measurement for very low flow rates. As described in section 3.5, the error in analog to digital conversion is 0.01% ± 1 least significant bit. For low flow rates, 1 bit represents a higher percentage of the total flow. As the flow is reduced discretization uncertainty increases. For the lowest flow rates encountered in these experiments the uncertainty in measurement climbs from 1% to 5%.

4.3 Measurement of Flame Height

To aid visualization of the flame edge, flame height measurements were conducted in total darkness. The rim stabilized burner's widest operating range occurred at an input energy of about 6 kW. Hence, to permit direct comparisons, all flame height tests were conducted for flames at that power.

The measurement procedure was straightforward. Using the device described in section 3.3, the sight is lowered until it is aligned with the top of the flame at which point the flame height can be read from the scale on the support post. The design of the sight prevents parallax error. Obviously, since interpretation of the flame edge was done by eye, the resolution of the measurements will be quite coarse. For turbulent flames near unity equivalence ratio, the repeatability of the measurements was estimated to be ±0.5 cm. At very low equivalence ratios ($\phi \approx 0.7$), the transparent nature of the flames made identification of the flame edge very difficult. Under these conditions the repeatability of the measurements was estimated to be ±1 cm or worse. Nevertheless, for the purpose of comparing flame height data for different stabilization mechanisms, the results were sufficient.

By fixing the fuel flow for a heat input of 6 kW and adjusting the air flow, flame height versus equivalence ratio data were generated. Once the height was read from the measurement device, flow parameters were automatically stored on disk and the flame height was typed directly into the computer via the keyboard.

4.4 Emissions Measurement

Emissions measurements could have been conducted in a variety of ways. It was decided that all of the exhaust gas must be collected and cooled before sampling, as the case would be in most potential applications of the burner. Emissions tests were conducted with the burner running with an input power of 6 kW. Ideally, the exhaust gas temperature would be fixed. However, since the limiting component in the heat transfer from the hot exhaust to the cooling water was the convection coefficient between the gases and the exchanger wall, of which there is no control, this was not possible. Varying the cooling water flow rate did not have a sufficient effect on the overall heat transfer to control the exhaust gas exit temperature. Although this temperature varied somewhat, it never exceeded 500 K and thus was more than sufficiently cool to ensure that any reactions with NO, NO_2, and CO were quenched.

Igniting the burner was very difficult. With the access port open, the heat exchanger set up very strong acoustic resonance that destabilized the flame. However, once the port was closed the resonance ceased. Once the burner was ignited, the door to the generic heat exchanger (Figure 3.6) was sealed and the burner was brought to steady state conditions at an input power of 6 kW. Typically, the burner was allowed to run for a minimum of 30 minutes before testing began. The sampling unit required a total of 3 hours of warm-up time to ensure reliable operation.

In equivalence ratio steps of 0.05, over a range of 0.7 to 1.15, the exhaust gases were sampled. To allow for time lag in the heat exchanger and sample lines, sampling took place a minimum of 10 minutes after any adjustments to the equivalence ratio. Since the gas analysis equipment seemed to reach steady state output within 5 minutes of a change in burner operating conditions, 10 minutes was deemed a sufficient delay. Obviously NO and NOx concentrations could not be measured simultaneously. Therefore, once the prescribed 10 minutes had elapsed, NO concentration and all other data were recorded. Subsequently the NO_2/NO converter was engaged and after an additional 5 minutes, NOx concentration was recorded along with repeat measurements of all other data.

During testing 15 different parameters were monitored continually with the data acquisition computer. Inlet and outlet cooling water temperatures for each flow path, the exhaust gas and firing chamber temperatures as well as the thermocouple cold junction temperature, the cooling water flow rates, the air and fuel flows, and the NO, NOx, CO, and HC concentrations were all measured. Data were automatically stored on disk. The computer data acquisition program automatically calculated grams of pollutants per kilogram of fuel. Following rules 1111 and 1121 of the South Coast Air Quality Management District in California [5], NOx was assumed to have the molecular mass of NO_2 in all calculations. Since the natural gas fuel on average consisted of 94% methane and only 2 % ethane (refer to appendix C for detailed analysis), the hydrocarbon emissions detected by the FFID were assumed to be solely methane in all calculations.

5. RESULTS AND ANALYSIS

The primary goal of this research was to investigate a bluff-body stabilized, low emissions, lean premixed burner with the eventual goal of retrofitting the technology into existing appliances. Extensive tests were conducted to quantify the operation limits of the burner with several different stabilizers according to a variety of constraints including flame stability, flame height, and pollutant emissions. Each of these three main areas of testing will be discussed separately.

The experimental burner has a nominal power input of 20 000 BTU/h or 6.0 kW. This rated input power corresponds with a relatively large stable operating range when running as a traditional rim stabilized burner. At this power input, the Reynolds number of the reactant flow based on the burner diameter (Re_D as defined in Equation 5.1) is between 3700 and 5100 depending on the equivalence ratio. When the burner operates with a ring stabilizer, the range of possible equivalence ratios is significantly increased. For the ring stabilized burner at 6 kW input power, Re_D can vary from 4125 up to 9500, depending on both equivalence ratio and flow blockage. Under the same conditions the Reynolds number based on the width of the ring (Re_R as defined in Equation 5.2 where the width of the ring W is the outer radius of the ring minus the inner radius) varies from 130 to 550.

$$Re_D = \frac{\rho_{REACTANTS} \times U_{AVG} \times D_{BURNER}}{\mu_{REACTANTS}} \qquad (5.1)$$

$$Re_R = \frac{\rho_{REACTANTS} \times U_{AVG} \times W_{RING}}{\mu_{REACTANTS}} \qquad (5.2)$$

During testing of stability limits, the input power to the burner was varied. Under these conditions $1395 < Re_D < 10206$ for the rim stabilized burner and for the ring stabilized burner $25 < Re_R < 1400$ and $670 < Re_D < 22300$. Although these Reynolds numbers are

transitional, the flow is laminar at the burner exit. The walls of the contraction section were carefully machined on a computer numeric control milling machine and followed two successive cubic curves which ensured a smooth acceleration of the flow as it moved towards the burner exit.

With the exception of a few data points, $50 < Re_R < 10^5$ which would produce a stable recirculation zone behind a rod stabilizer as discussed in Glassman [7]. However, the present research uses rings with square cross-sections instead of rods to stabilize flames and thus, the Reynolds numbers and flow patterns may not correlate directly. No previous papers were found that discussed wake flows for rods or rings of square cross section in a combusting flow.

5.1 Stability Regimes

5.1.1 The Rim Stabilized Burner

To form a basis for comparison, the stability limits (blowoff and flashback limits) of the burner running with traditional rim stabilization were determined. Blowoff and flashback were defined in sections 4.1 and 4.2. The stability limits for the rim stabilized burner with laminar flow are shown in Figure 5.1.

The upper line in Figure 5.1 represents the blowoff limit as a function of equivalence ratio and burner input power. Stable flames are not possible above this limit. The lower curve defines the flashback limit. The regime of stable operation is defined as the area between the two curves. Ideally the two curves would meet as the equivalence ratio is reduced, but it is essentially impossible to hold a flame near this region since any small disturbance leads to destabilization. It should be noted that the upper curve will extend beyond what is shown and is only limited by the range of the present flow measurement equipment. The stability regime of a rim stabilized burner is well understood and is described in detail in Lewis and von Elbe [28].

The most important aspect of Figure 5.1 is the limit on lean flame combustion. For the best case, with the laboratory burner operating under laminar conditions, stable combustion is only possible down to an equivalence ratio of approximately 0.8 and only then for a very narrow range of input power. Although traditionally blowoff data is presented on plots of equivalence ratio as a function of velocity or flow rate, this is not done here. In Figure 5.1 blowoff and flashback data are plotted so that burner input power appears as a function of equivalence ratio. This choice of axes is more meaningful for burner design purposes, since it is more relevant to compare two burners operating at a single power input than at a single flow velocity. Thus, the range of possible powers can be easily mapped over a range of equivalence ratios.
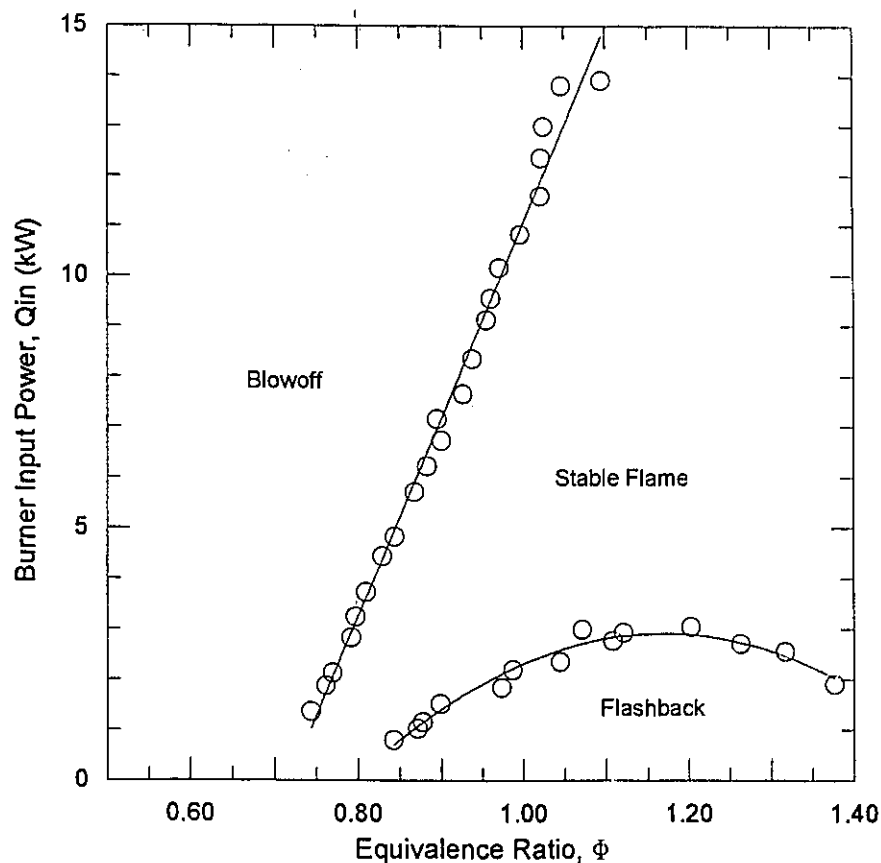
Figure 5.1: Laminar Stability Limits for Rim Stabilized Burner

For a laminar flame at $\phi=1$, the maximum stable input power is about 10.8 kW, above which blowoff occurs. The minimum stable input power is 2.3 kW below which flashback occurs. The ratio of these input power limits defines a burner turndown ratio of 10.8/2.3 or 4.9:1 which is typical of many commercial burners. The turndown ratio is significantly reduced for lean flames.

Figure 5.2 shows how turbulence affects the stability limits of the rim stabilized burner. As the scale and intensity of the turbulence are increased, the stable operating range is significantly reduced.
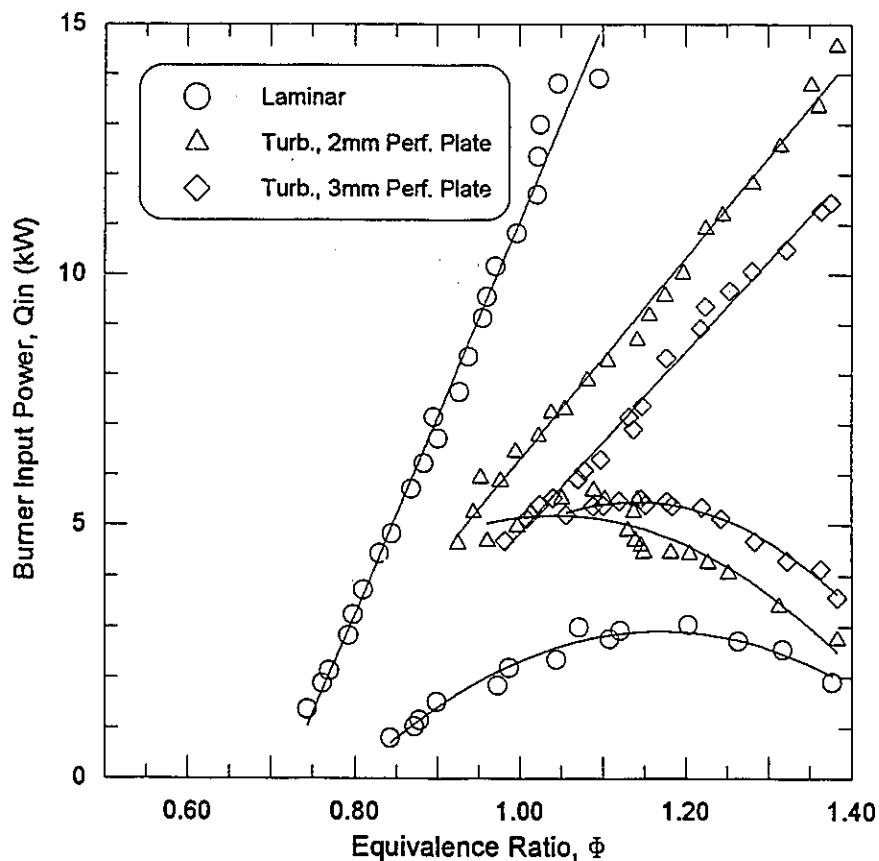
Figure 5.2: Influence of Turbulence on Rim Stabilized Stability Limits

With the 2 mm perforated plate in place (~8% turbulence intensity), the turndown ratio at $\phi=1$ is approximately 1.2:1 and the lean blowoff limit is at best $\phi=0.95$. With the 3 mm plate in place (~11.5% turbulence intensity), the burner can not even be operated at

$\phi=1$ and lean combustion is impossible. This suggests that the rim stabilized burner is very sensitive to disturbances in the flow. Although the turndown for the laminar case was 4.9:1 in the controlled conditions of the laboratory, it would be less in practical situations.

5.1.2 The Single Ring Stabilized Burner

5.1.2.1 Relative Performance of the Single Ring Stabilized Burner

Figure 5.3 shows a comparison between the stability limits of a ring and rim stabilized burner. Data is shown for ring G4 (as summarized in Table 5.1) which has a square 2 x 2 mm cross section and a gap size, δ, of 3.2 mm (0.125 inches).
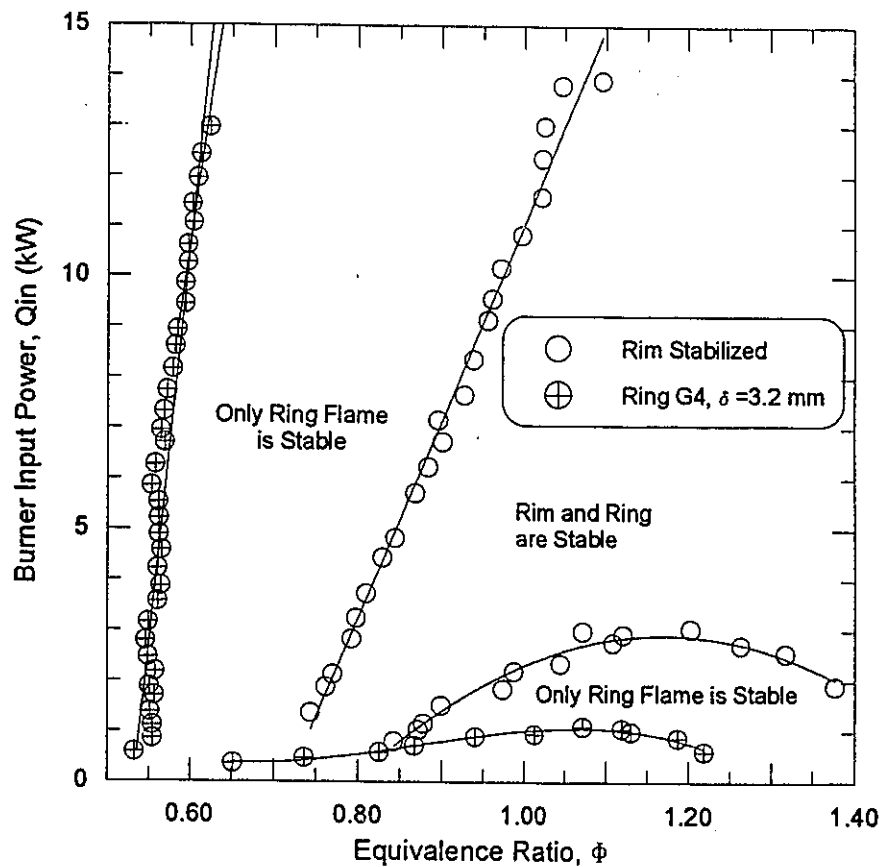
Figure 5.3: Comparison of Rim and Ring Stability Limits for Laminar Flow

With the ring in place, the range of stable operation is significantly increased, into the region of lean flame combustion. The lean blowoff limit with ring G4 in place is as low as φ=0.55 which approaches the flammability limit for a mixture of natural gas and air at 298 K and 1 ATM. Also noteworthy is the increase in the burner turndown ratio. The upper limit of the blowoff line again extends beyond the range of the current measurement equipment, but the turndown ratio at φ=0.8 could be conservatively estimated to be 20:1. The traditional rim stabilizer essentially has no turndown at φ=0.8 and operation is fixed at an input power of 1.5 kW. At φ=1 the turndown for the ring stabilized burner is easily much greater than the 4.9:1 turndown of the traditional burner. This result is significant in terms of commercial application. A burner with a large turndown can adapt to a wide range of heating loads and thus maintain efficient operation without wasting energy due to overcapacity.

Table 5.1: Single Ring Stabilizer Dimensions

Ring Name	Outer Diameter		Gap Size		X-Section		Blockage
	(mm)	(inches)	(mm)	(inches)	(mm)	(inches^2)	β (%)
G0	32.8	1.250	0	0	2 x 2	0.0787^2	23.6
G1	30.2	1.1875	0.8	1/32	2 x 2	0.0787^2	22.3
G2	28.6	1.125	1.6	1/16	2 x 2	0.0787^2	21.1
G3	27.0	1.0625	2.4	3/32	2 x 2	0.0787^2	19.8
G4	25.4	1.000	3.2	1/8	2 x 2	0.0787^2	18.6
S1	28.6	1.125	1.6	1/16	1 x 1	0.0394^2	10.9
S3	28.6	1.125	1.6	1/16	3 x 3	0.1181^2	30.4

While the improvement in the blowoff limit was expected following the theory outlined in section 2.2.1, the change to the flashback limit is serendipitous. There are three possible explanations for this change. First, the ring obstructs the flow and hence,

for an equivalent mass flow rate, the average velocity of the reactant gas will increase. As explained previously, this flow obstruction due to the ring stabilizer is termed blockage, β, and is defined as the ring planform area divided by the burner exit area. The increased reactant flow velocity helps prevent the flame from entering the burner, and thus helps to prevent flashback from occurring.

A second explanation could be that the ring acts as a heat sink and absorbs energy from the flame as the flame approaches the burner. Similar to classical rim stabilization, this increased heat loss slows the burning velocity and hinders flashback. The heating of the ring stabilizers during flashback tests was evident in the lab as several of the original rings (made of aluminum) overheated and deformed.

A final possible reason for the improvement in the flashback limit would be the impedance of flame propagation by an obstacle in the flow path. In order for the flame to propagate back inside the burner, it must first deform and stretch around the ring stabilizer. The increase in flame stretching could again slow the burning velocity and hinder flashback, although this effect is probably secondary compared to the effects of increased gas velocity and heat loss. Most likely a combination of these three processes is responsible for the change in the flashback limit for a ring stabilized burner.

Another advantage of ring stabilized flames is that they are not very sensitive to turbulence in the flow. Figure 5.4 shows how increasing the scale and intensity of turbulence in the reactant flow affects the stability regime of the burner with ring G4 in place. Data for ring G4 and all others (see Appendix D) indicate that the stability limits decrease slightly from the laminar case to the most turbulent case. Cheng [37] observed a similar effect in equivalence ratio at blowoff for V-gutters in increasing levels of turbulence but found a trend towards the opposite for rods and bars. However, Cheng conducted tests at a single flow velocity and the trends in his data are not entirely clear.
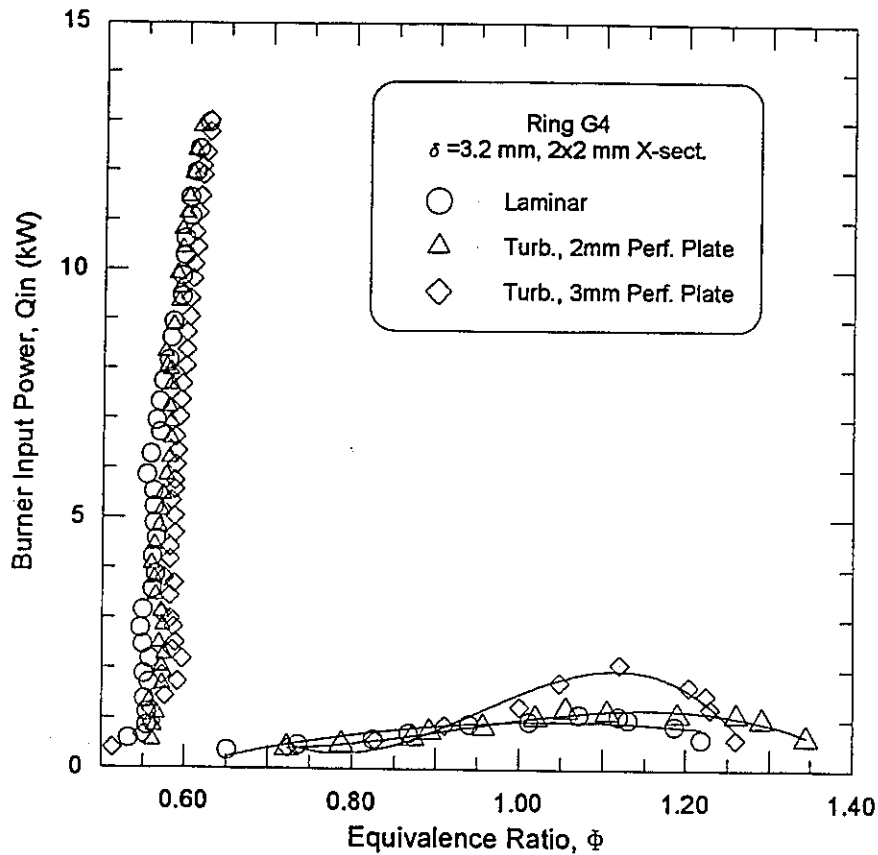
Figure 5.4: Influence of Turbulence on a Ring Stabilized Burner

Nevertheless, compared to the traditional rim stabilized burner, the ring stabilized burner is insensitive to turbulence in the flow. This is significant for two reasons. First, the ring stabilized burner should be less sensitive to disturbances or perturbations in the reactant flow. This permits safe operation at equivalence ratios and power inputs near the blowoff and flashback limits and certainly in the range of lean premixed combustion. Secondly, since turbulence does not significantly alter the stability regime, turbulence plates could be used to lower large flame heights normally associated with lean flames. The problem with lean flame heights will be discussed in detail in section 5.2.

Figure 5.5 shows the comparative stability limits for the rim and ring stabilized burners with the larger scale turbulence plate in place. Here, the differences in the stable operating range are most apparent. While turbulence adversely affected the flame stability on the traditional rim burner, the stable range for the ring stabilized burner is more robust

and remains relatively constant. The ring stabilized burner makes stable lean premixed combustion feasible and raises the potential for lower NOx emissions at lower flame temperatures.
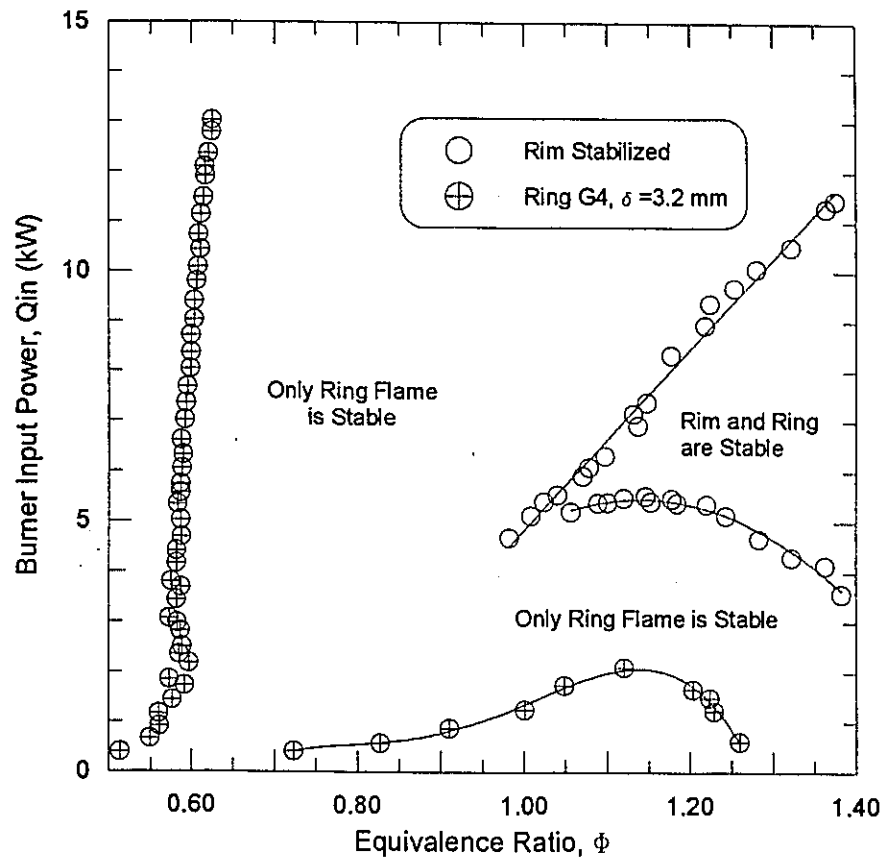
Figure 5.5: Comparison of Rim and Ring Stability Limits in Larger Scale Turbulence

5.1.2.2 Critical Parameters of the Single Ring Stabilizer

The most influential parameter in the performance of a ring stabilizer was found to be the gap size, δ, between the outer edge of the ring and the inner edge of the burner. Figure 5.6 shows the change in blowoff and flashback limits for a ring stabilizer of 2x2 mm

cross-section in laminar flow as the gap size is varied. Figure 5.7 shows the same set of curves but for larger scale turbulent flow (3 mm perforated plate in place). Clearly for both sets of data, the equivalence ratio at blowoff is reduced as the gap size, δ, is increased. This is a logical result since a larger δ would guarantee even flow on both sides of the ring stabilizer and hence stimulate a strong recirculation zone. There is also a secondary effect of blockage, β, on stability. As δ is increased, the ring diameter and planform area shrink and β is reduced. As β is lowered, the reactant gas velocity should also drop, helping to prevent blowoff.
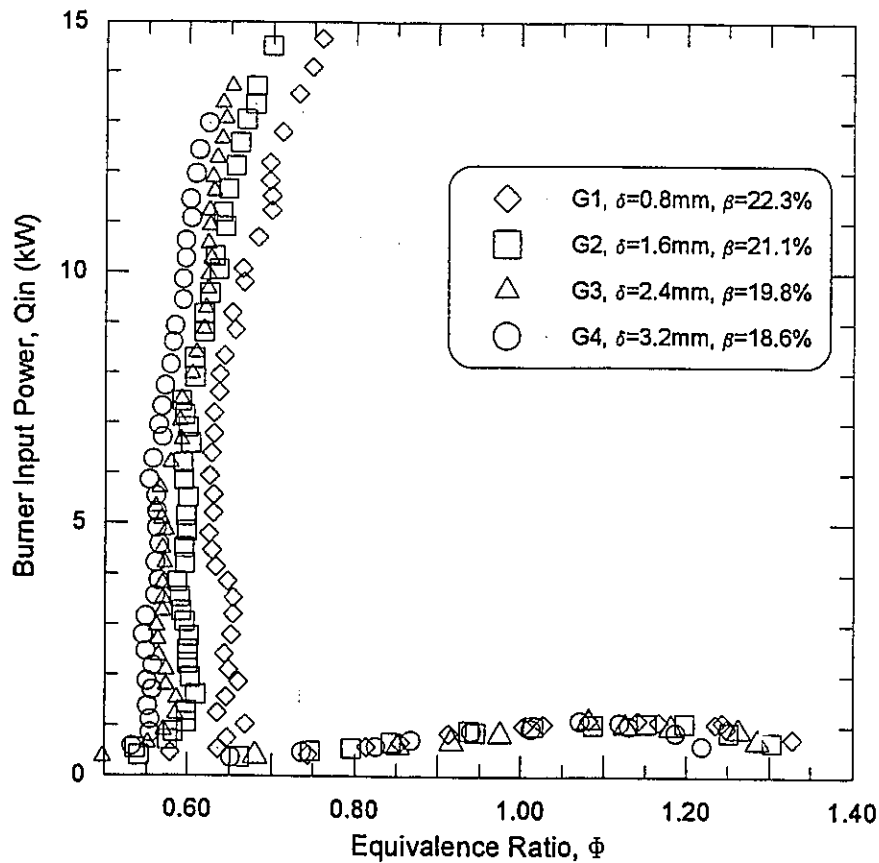
Figure 5.6: Influence of Gap Size of Ring Stabilizer in Laminar Flow

The effect of increased stability with increasing δ is not as significant at larger δ. The difference in ϕ at blowoff for rings G1 and G2 is greater than the difference for rings

G3 and G4, especially in the turbulent case (Figure 5.7). While the stability range might possibly be increased further for a ring with $\delta > 3.2$ mm, the potential for fuel leakage through the gap may become problematic. The influence of gap size on emissions will be discussed in later sections.
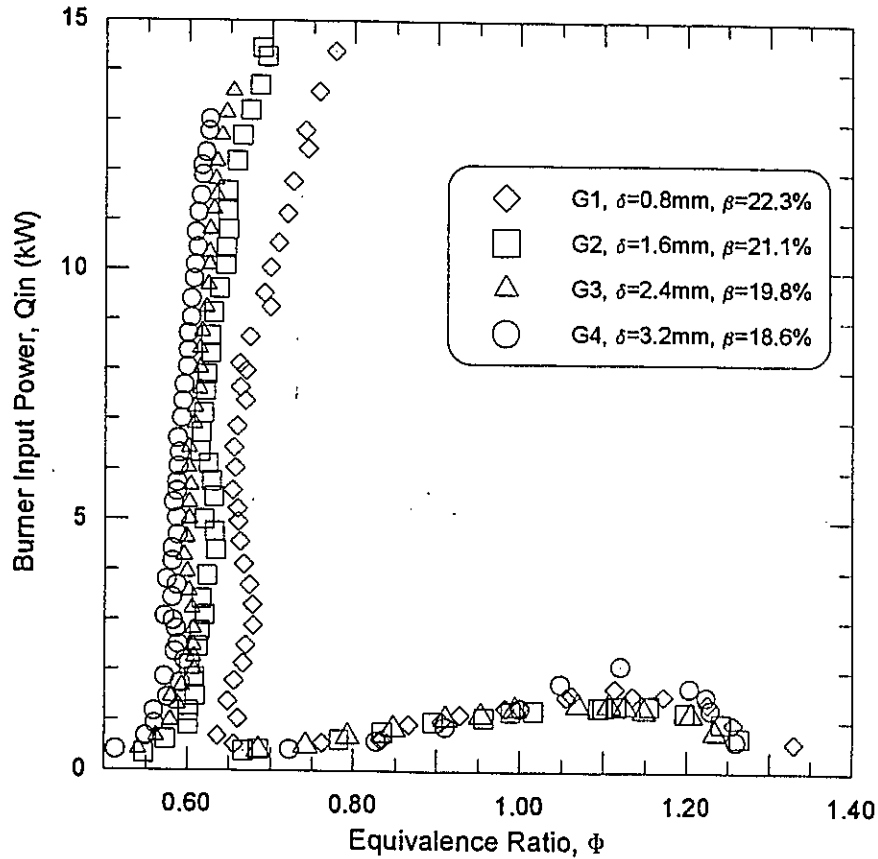
Figure 5.7: Influence of Gap Size in Larger Scale Turbulent Flow

By contrast, the flashback limits are relatively unaffected by the change in gap size. Three possible modes of influence of a ring stabilizer on flashback were previously discussed, but it was impossible to quantify their relative strengths. A smaller gap ring could lead to higher reactant gas velocities (as δ decreases, planform area and thus β increases) which would hinder flashback, but this velocity increase should be small. Also, a larger ring could lead to increased heat transfer from the flame which would again help to prevent flashback from occurring. Conversely, a larger diameter ring could reduce

stretching of the flame front as it starts to propagate back inside the burner, which could augment the tendency towards flashback, possibly negating the other two effects. Which, if any, of these effects dominates is not necessarily important since the gap size does not affect the flashback limit.
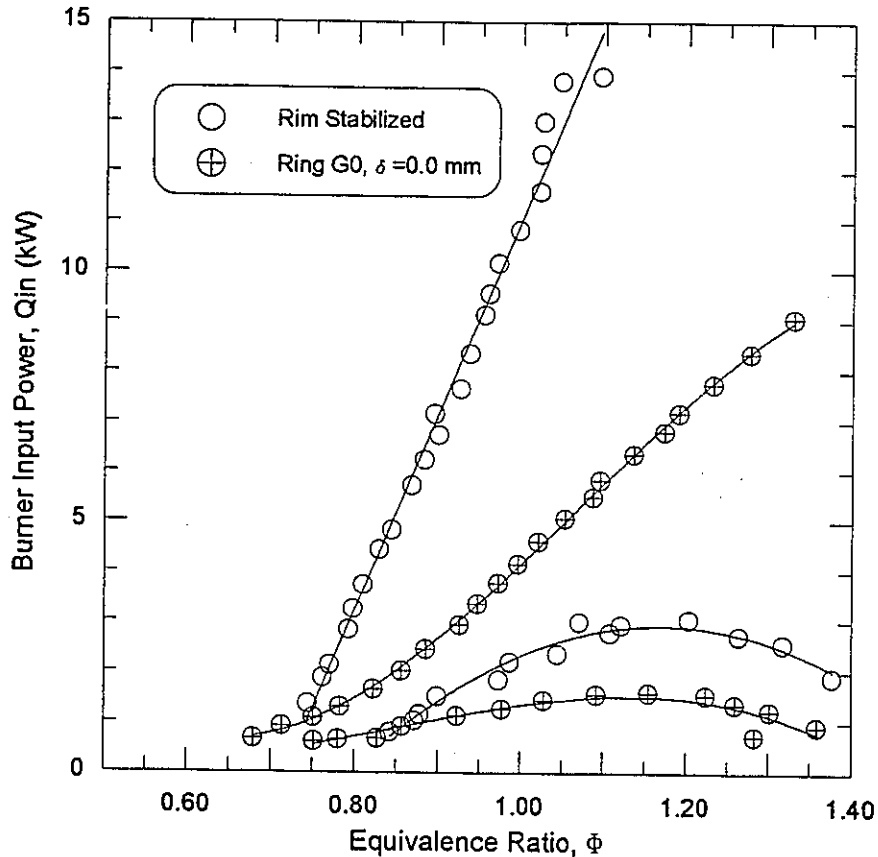
Figure 5.8: Laminar Stability Limits for Rim and Zero-Gap Ring

For completion, a ring stabilizer with zero gap ($\delta=0$) was also tested as shown in Figures 5.8 and 5.9. Ring G0 had the expected effect of shrinking the overall stability limits of the burner. With $\delta=0$, a stable recirculation zone is not generated and the burner essentially reverts to being a rim stabilized burner. The reduced burner exit area causes an increase in the reactant gas velocity which promotes blowoff and hinders flashback. Obviously, there is a minimum gap size required to create a stable recirculation zone but this size is less than 0.8 mm (1/32 inch), the gap size for ring stabilizer G1.
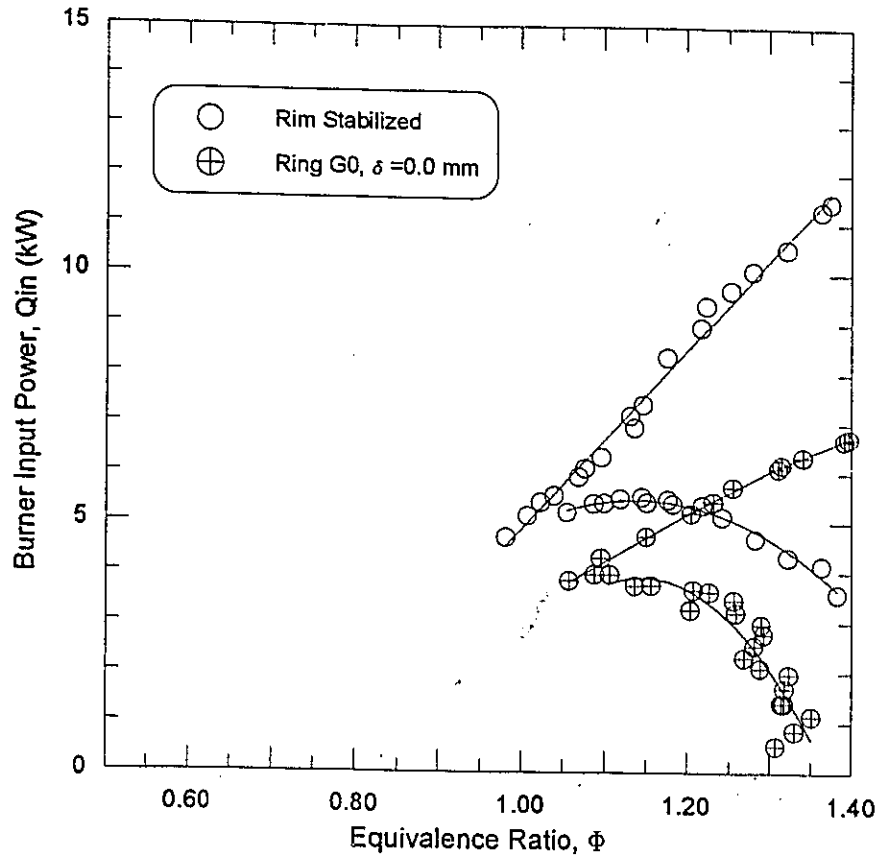
Figure 5.9: Large Scale Turbulent Stability Limits for Rim and Zero-Gap Ring

Finally, the influence of ring cross sectional area on stability limits was investigated. Figure 5.10 shows the laminar stability regime for three rings with constant gap sizes δ=1.6 mm and cross sectional areas of 1x1 mm (β=10.9%), 2x2 mm (β=21.1%), and 3x3 mm (β=30.4%). Figure 5.11 shows the same curves for turbulent flow.

Ring cross sectional area has a modest influence on stability. While increasing the width of the ring increases the Reynolds number of the wake flow and creates a larger wake, the larger ring planform area causes more flow blockage and raises the reactant gas velocity. Thus, there should be an optimum ring width or cross-sectional area for a given burner diameter. This optimum also exists for rod stabilized flames as verified by data from Scurlock (1948) cited in Glassman [7].
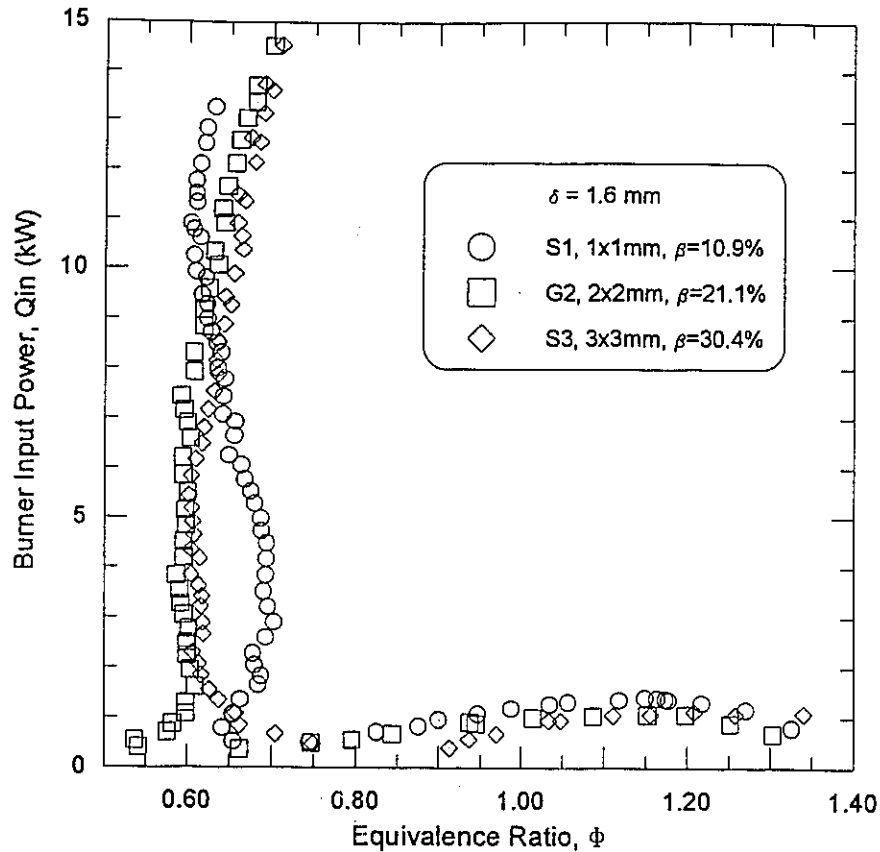
Figure 5.10: Influence of Ring Cross-Sectional Area in Laminar Flow

Ring G2, with a blockage of 21.1%, appears to have the optimum cross-sectional area for the experimental burner. Ring S3 (3x3 mm cross section, β=30.4%) has a slightly shifted blowoff limit although the difference is small. More interesting is ring S1 (1x1mm cross-section, β=10.9%), which has a distinctive S shape in the blowoff curve. At lower input powers, hence lower reactant gas velocities and Reynolds numbers, the blowoff limit for ring S1 is relatively high (up to ϕ=0.7 in laminar flow, ϕ=0.74 in turbulent flow). However, at higher powers and flow velocities the blowoff limit is improved (near ϕ=0.6 laminar and ϕ=0.68 turbulent). This is probably because at lower Re, ring S1 is too small too generate the necessary wake for optimum stability. Conversely at higher Re, the wake is sufficient and the reactant gas velocities are reduced due to lower blockage. This in turn, helps to prevent blowoff. Still, of the rings tested, G2 is optimum. Moreover, the

differences between rings S1, G2, and S3 are small when compared to the rim stabilized case, and all three rings improve stability substantially.
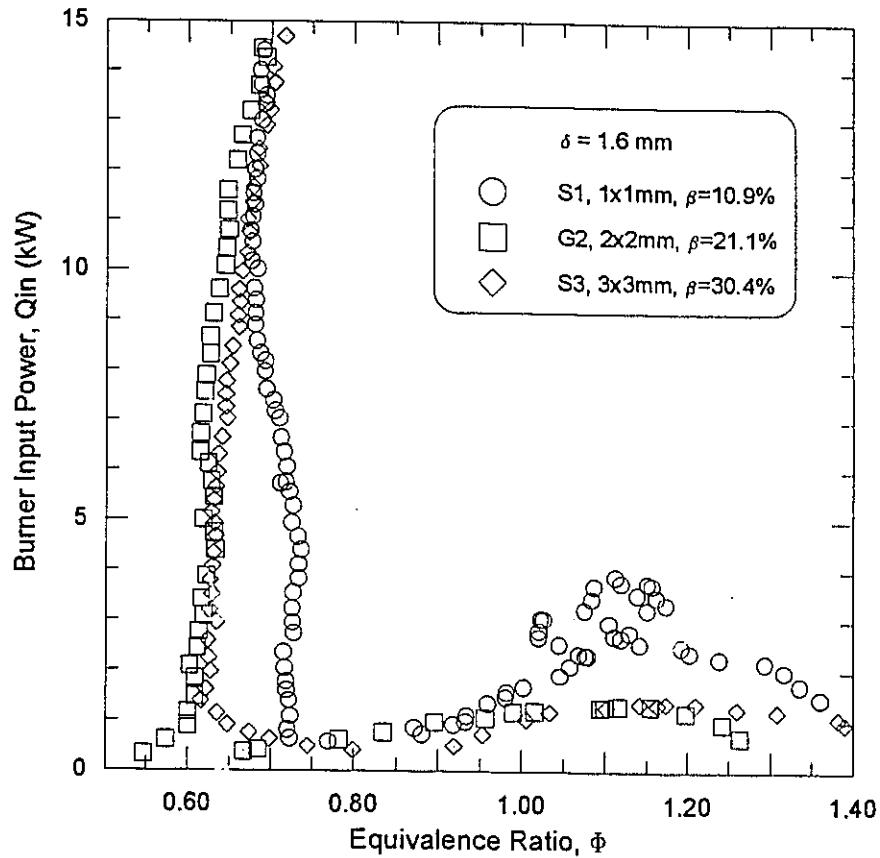
Figure 5.11: Influence of Ring Cross-Sectional Area in Larger Scale Turbulent Flow

Differences in flashback limits for the three rings were less clear. There may be a slight improvement in the flashback limit with increased ring planform area and blockage, but the observed differences are within experimental error. The flashback curve for the smallest ring, S1, in large scale turbulent flow is particularly interesting. A similar set of points was generated on three separate occasions. Possibly, the reduced ring size diminished the effects of heat transfer and velocity increase which act against flashback. During testing, the occurrence of flashback seemed to be chaotic as evidenced by the shape of the flashback curve.

5.1.3 The Concentric-Ring Stabilized Burner

Four different concentric ring stabilizers were examined in this research as summarized in Table 5.2. These four stabilizers have identical outer rings with different inner rings or a disk mounted concentrically. The outer ring is the same as single ring G1 which has a 2x2 mm cross-section and overall the smallest gap size, $\delta=0.8$ mm. The main purpose of this design was to create flames with lower overall heights, as will be discussed in section 5.2.

Table 5.2: Concentric Ring Stabilizer Dimensions

Ring Name	Outer Ring		Inner Ring		Blockage
	Outer Dia. (mm) (inches)	Gap Size (mm) (inches)	Outer Dia. (mm) (inches)	Inner Dia. (mm) (inches)	β (%)
C0	30.2 1.1875	0.8 1/32	4.0 .157	0(disk) 0	23.9
C2	30.2 1.1875	0.8 1/32	9.5 .375	5.5 .218	28.3
C4	30.2 1.1875	0.8 1/32	15.9 .625	11.9 .468	33.4
C6	30.2 1.1875	0.8 1/32	22.2 .875	18.2 .718	38.4

Blowoff for a concentric ring stabilizer occurs in a slightly different manner than for a single ring stabilizer. Almost invariably the flame lifts off the outer ring before it lifts off the inner ring or disk. Once this initial separation occurs the blowoff limit is said to be reached even though a stable flame still exists on the inner ring. Because this initial lift off likely would be accompanied by a sharp increase in pollutant emissions (primarily unburned hydrocarbons and CO), it would not be desirable to operate in this range. However, since a stable flame exists over a slightly wider range than for the single ring stabilizer, the concentric ring stabilizer has an added measure of safety. Figure 5.12 shows the laminar blowoff limits of concentric ring C2 and single ring G1 plotted together. Figure 5.13 shows blowoff and flashback curves for the same stabilizers but large scale turbulent flow.
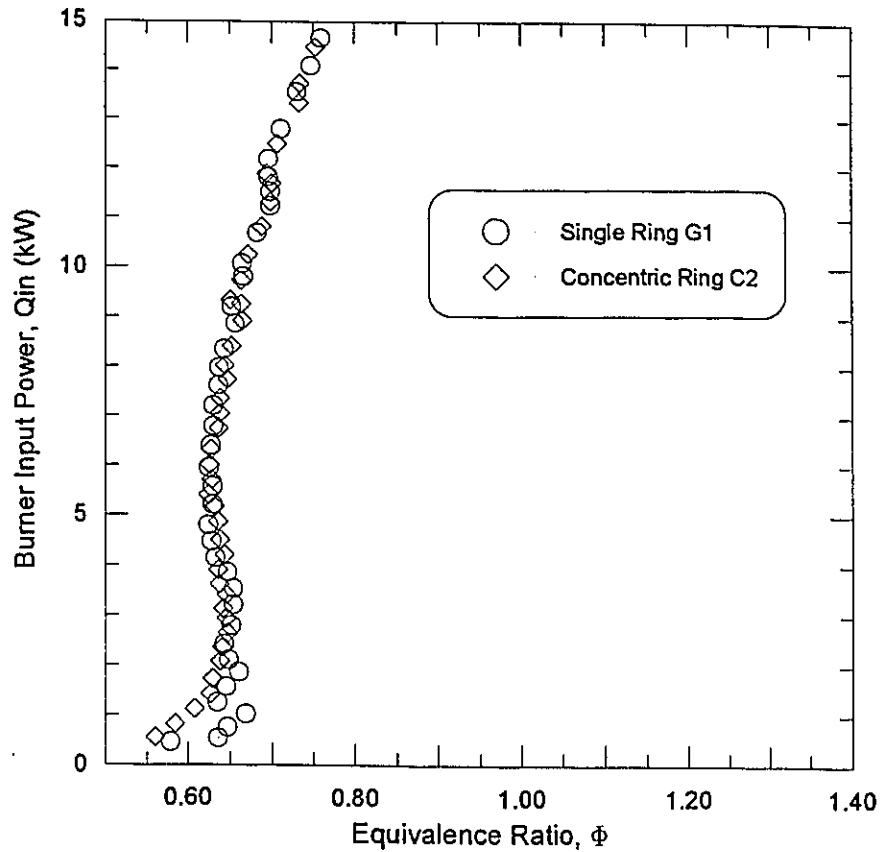
Figure 5.12: Laminar Blowoff Limits for Concentric Ring C2 and Single Ring G1

Although the blockage is increased to 28.3 % from 22.3 %, there is no detectable change in the blowoff limit. There are two reasons for this insensitivity. First a blockage increase of 6 % is small. Previously, in Figures 5.10 and 5.11, it was shown that increasing β by 9.3 % for a single ring stabilizer with constant δ had only a modest effect on the blowoff limit. Secondly, since the flame on the inner ring does not separate until well after the flame has blown off the outer ring, the inner flame acts as a pilot flame and helps stabilize the outer flame. Thus, the negative effect of increased blockage is somewhat countered by the inner flame acting as a pilot. The entire range of concentric ring stabilizers blowoff at almost identical equivalence ratios as single ring G1; ring G1 has the same dimensions as the outer ring in each of the concentric ring stabilizers. Plots of blowoff limits for the other concentric ring stabilizers can be found in Appendix E.
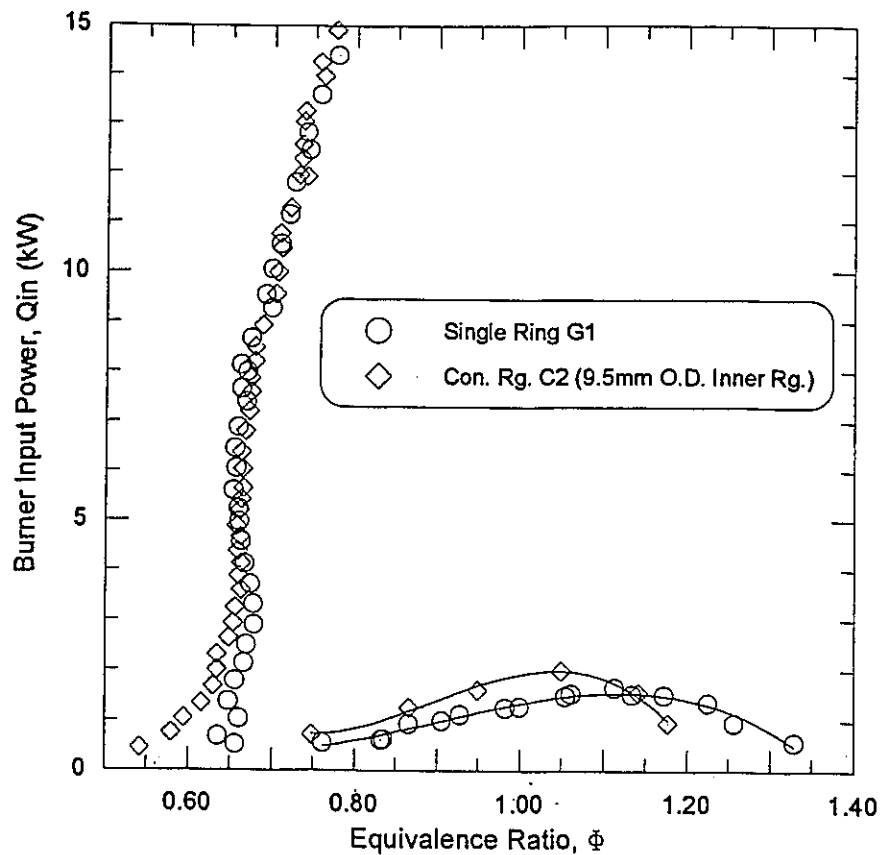
Figure 5.13: Turbulent Stability Limits for Concentric Ring C2 and Single Ring G1

5.2 Flame Height

There is a second problem with lean flame combustion besides stability -- excessive flame heights. As the combustion equivalence ratio is reduced, the burning velocity decreases and the flame angle is reduced. Lower flame angles lead to much taller flames and the increase in flame height with lower equivalence ratios is quite dramatic. Most current commercial burners operate at or near stoichiometric conditions. If the ring stabilized burner is to be considered for retrofitting, the flame heights at lean conditions would most likely need to be comparable to flame heights of a rim stabilized burner operating at $\phi=1$.

5.2.1 Flames Stabilized with a Single Ring

Figure 5.14 shows laminar flame height as a function of equivalence ratio for a rim stabilized flame and four different single-ring stabilized flames. For all data points, the burner input power was fixed at 6.0 kW. Clearly as the equivalence ratio is reduced the flames grow dramatically by as much as 500%. Also, as the gap size is reduced and the blockage increases accordingly, the flame height grows further. If retrofitting is to be considered for this type of burner, this overall problem of excessive lean flame heights needs to be addressed.
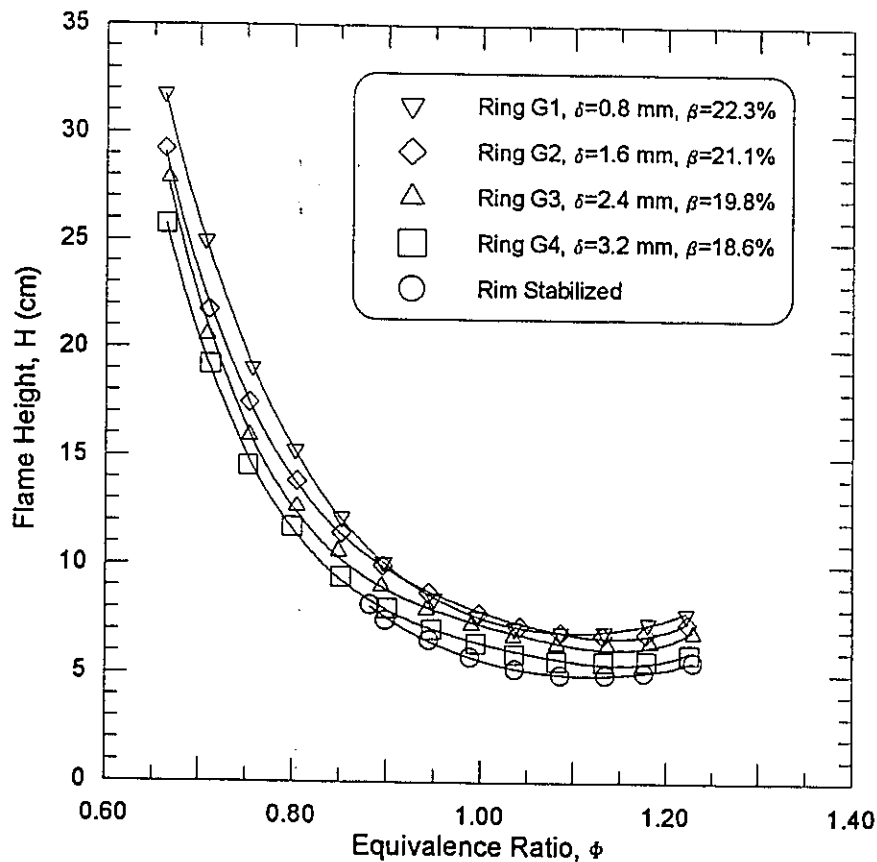
Figure 5.14: Laminar Flame Heights for Rim Stabilized Flame at 6.0 kW

Consider a hypothetical 6.0 kW natural gas appliance designed to operate at or near φ=1. This would be typical of a small gas powered hot water heater or a home furnace with a series of 6.0 kW flames in multiple burner ports. For stability, the flames would most likely be laminar with an expected flame height at φ=1 of about 6 cm. If this appliance was retrofitted with a ring stabilized burner and operated near φ=0.7, the heat exchanger would have to accommodate flames as tall as 25 cm. In many cases this would not be possible without modifications to prevent the flame from impinging on surfaces of the heat exchanger.
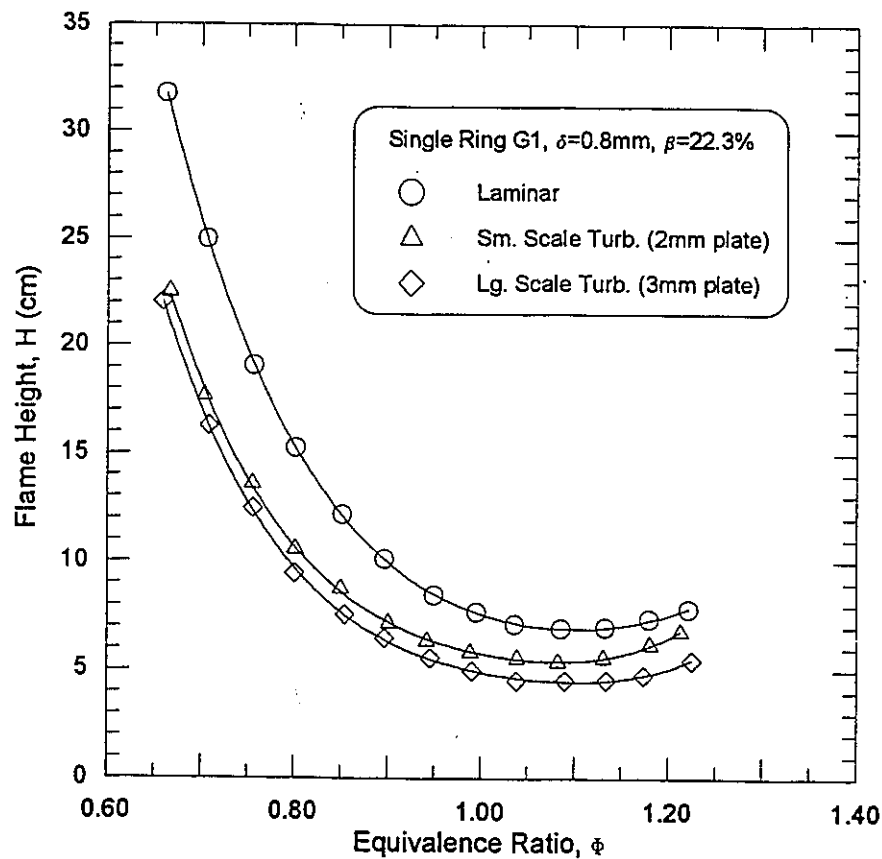
Figure 5.15: Influence of Turbulence on Flame Height for Single-Ring G1

Since flame stability limits are relatively unaffected by turbulence, one approach would be to further modify the burner for turbulent operation. Figure 5.15 shows how flame height is affected by turbulence in the flow. Flame heights for stabilizer ring G1

(δ=0.8mm, β=22.3%) are plotted for laminar, smaller scale (2 mm perforated plate), and larger scale (3 mm perforated plate) turbulent flow. As the turbulence intensity and scale are increased, the burning velocity increases and the flames are reduced in height. At ϕ=0.7, the flame height is reduced by 10 cm from the laminar to the large scale turbulent case. However, the dramatic increase in flame height with decreasing equivalence ratio remains unchanged.
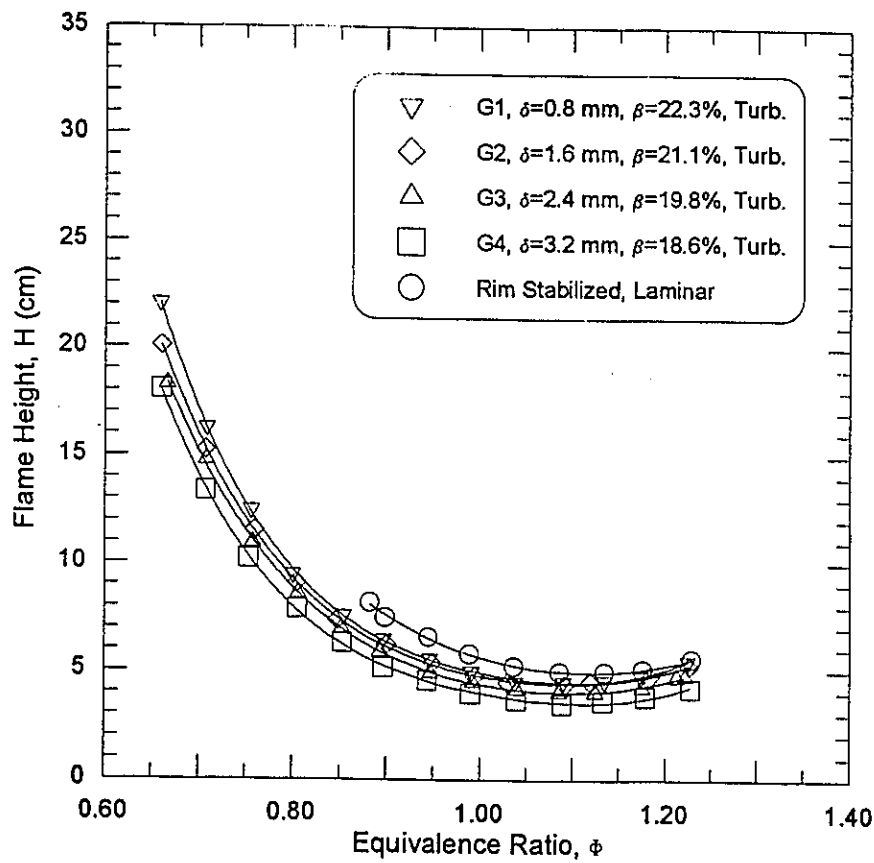
Figure 5.16: Single-Ring Turbulent Flame Heights at 6.0 kW Input Power

Figure 5.16 shows flame height curves for the four ring stabilizers for the larger scale turbulent flow and the flame height curve for the laminar rim stabilized flame. Although the increased turbulence lowers the flame height, at ϕ=0.7 the flames may be as tall as 16 cm -- still a 267 % increase over the laminar rim stabilized case. In some applications an increase in height of 10 cm for a 6.0 kW flame may be manageable, but in

many situations further modifications to the burner or heat exchanger would be required. With lower temperature lean flames it may be necessary to bring the flames slightly closer to the heat exchanger to maintain high rates of heat transfer, but an increase in height of 267 % would likely be much more than necessary.
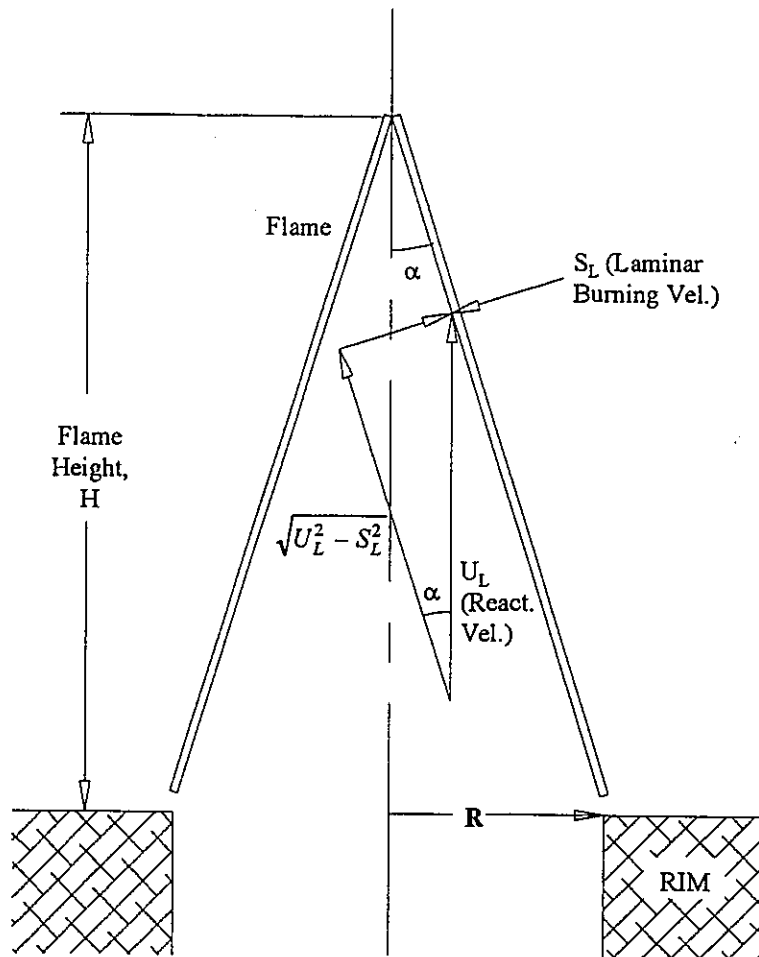
Figure 5.17: Velocity Vectors in an Idealized Conical Flame

Despite the inherent inaccuracies in measuring flame heights by eye, especially in the turbulent case, the data are very consistent. Figures 5.14 and 5.16 show virtually identical trends for all four sizes of the single-ring stabilizer. It was theorized that the

offsets in these curves were primarily a result of a change in ring radius and blockage. If one assumes a uniform reactant velocity profile at the burner exit, and a perfect conical flame, a simplified velocity polygon can be generated as shown in Figure 5.17.

By similar triangles:
$$\frac{H}{R} = \frac{\sqrt{U_L^2 - S_L^2}}{S_L} \qquad (5.3)$$

Assuming that $U_L \gg S_L$ (this is certainly true for lean flames and less accurate for stoichiometric flames), 5.3 can be simplified to:

$$\frac{H}{R} \approx \frac{U_L}{S_L} \qquad (5.4)$$

This relation should be sufficiently accurate for a laminar rim stabilized flame. However, when a stabilizer ring is inserted into the flow, it may no longer be reasonable to assume a uniform velocity profile. Nevertheless, by assuming ring stabilized flames can be modeled in a similar fashion to conical rim stabilized flames, some insight may be gained. For a ring stabilizer, R in Equation 5.4 would refer to the outer radius of the ring above which an approximately conical flame exists. Rewriting Equation 5.4 as the ratio of the height of a ring stabilized flame to the height of a rim stabilized flame at an identical equivalence ratio and input power, Equation 5.5 can be written:

$$\frac{H}{H^\circ} = \frac{UR}{U^\circ R^\circ} \qquad (5.5)$$

where $^\circ$ means the variable is for the rim stabilized case.

Using continuity:
$$\frac{U^\circ}{U} = 1 - Blockage = 1 - \beta \qquad (5.6)$$

63

Finally: $$\frac{H}{H^\circ} = \frac{1}{(1-\beta)} * \frac{R_{RING}}{R_{BURNER}} \qquad \text{or} \qquad H^\circ = H * (1-\beta) * \frac{R_{BURNER}}{R_{RING}} \quad (5.7)$$

H° in Equation 5.7 defines the adjusted flame height for a ring stabilized burner which should factor out height increases due to change in flow blockage and effective cone radius. Figure 5.18 shows the adjusted flame height as a function of equivalence ratio for the four single-ring stabilizers and the rim stabilized burner. (According to Equation 5.7 the adjusted height and the actual height for the rim stabilized burner are identical.)
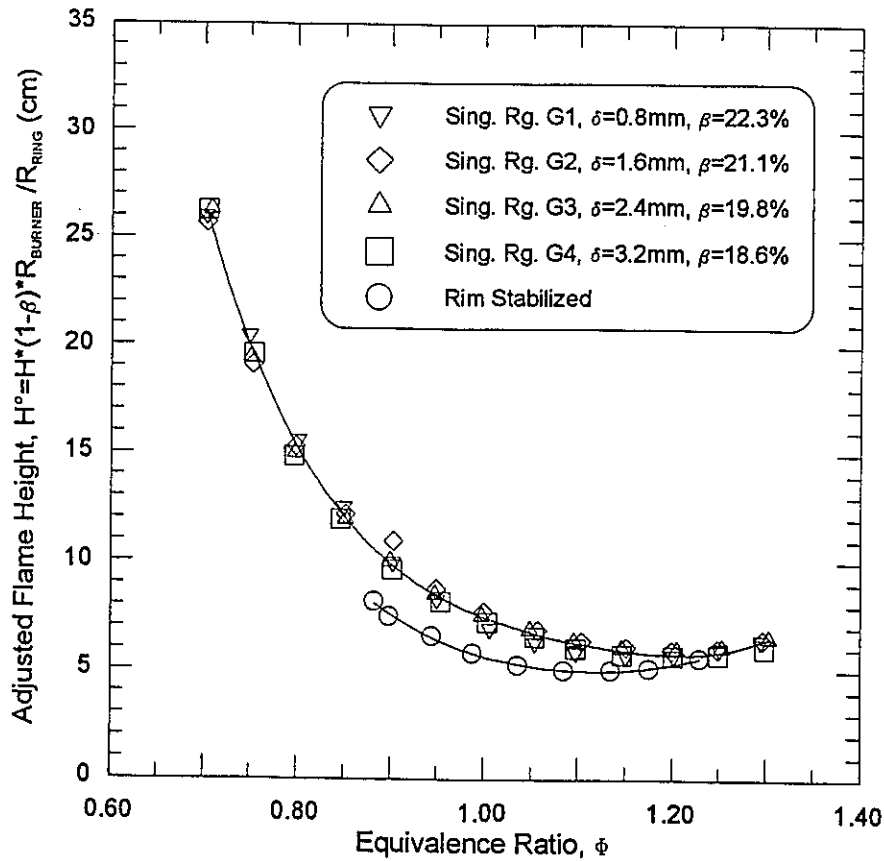
Figure 5.18: Adjusted Laminar Single-Ring Flame Heights at 6.0 kW Input Power

Remarkably, although Equation 5.7 is crude, data for the four ring stabilizers correlate very well; the correlation coefficient, R^2, for the fourth order polynomial fit (Equation 5.8) is 0.997. The choice of a fourth order polynomial fit is arbitrary.

$$H^\circ = 735.9 - 2562.1*\phi + 3422.6*\phi^2 - 2056.5*\phi^3 + 467.4*\phi^4 \qquad (5.8)$$

However, the flame height curve for the rim stabilized burner is noticeably different. This discrepancy can only be explained by the assumptions used to develop Equation 5.7. Nevertheless, the adjusted flame height relation could be useful in comparing and predicting performance of different single-ring stabilizers.

Although the adjusted flame height relation was developed for laminar flow, it is surprisingly accurate with turbulent flame heights as well. Figure 5.19 shows the adjusted flame heights for the four single-ring stabilized flames in large scale turbulent flow. Flame heights for the turbulent rim stabilized case are also plotted but, because of stability limitations, only four data points ($\phi > 1.1$) could be generated. While data for the four ring stabilizers collapse neatly onto a single curve, the rim stabilized flame heights still do not conform. The correlation coefficient for the fourth order curve fit (Equation 5.9) of the adjusted ring stabilizer flame height data is 0.999. Again, the choice of a fourth order polynomial fit is arbitrary.

$$H^\circ = 431.3 - 1541.3*\phi + 2121.5*\phi^2 - 1320.9*\phi^3 + 313.4*\phi^4 \qquad (5.9)$$

The discrepancy between the rim and ring stabilized data is again most likely due to the assumption of a uniform reactant velocity profile with the ring stabilizer in place. However, even though Equation 5.7 was developed for laminar flow, it is useful as a tool for design and comparison in turbulent flow as well.
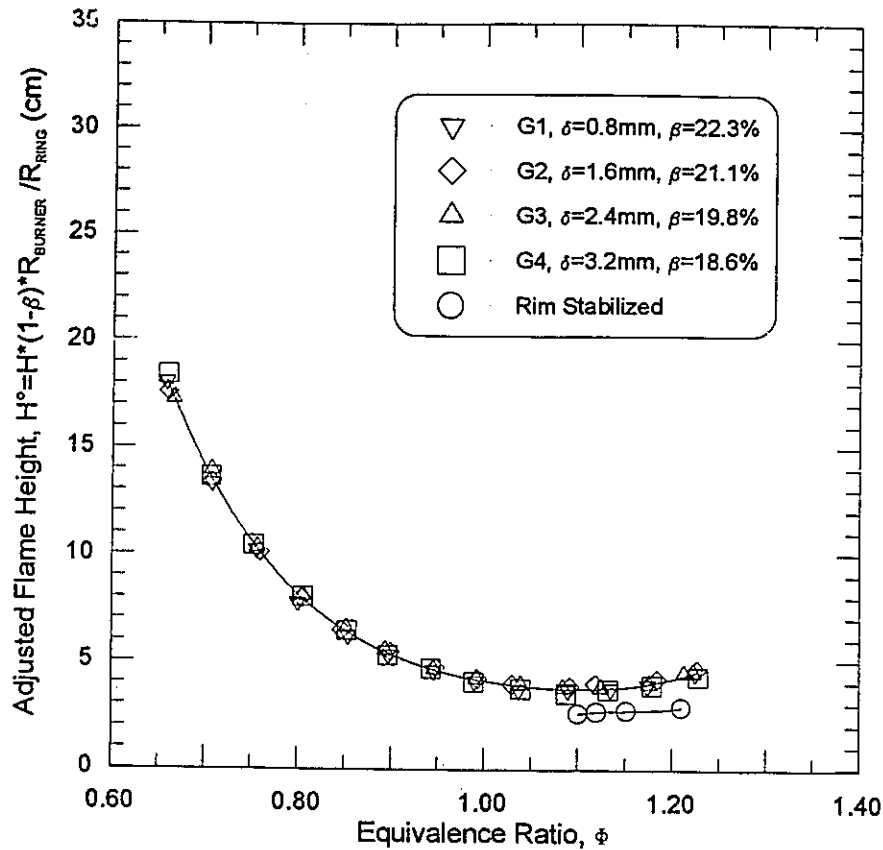
Figure 5.19: Adjusted Turbulent Single-Ring Flame Heights at 6.0 kW Input Power

5.2.2 Flames Stabilized with Concentric Rings

A second technique for lowering flame heights would be to increase the cone area of the flame, which is a slightly different approach than increasing flame area through turbulence induced wrinkling. The concentric ring stabilizer was designed to augment flame area by having two concentric recirculating zones which generate differently shaped flames with large surface areas. For stabilizers C2, C4, and C6, a conical flame sits above the inner ring and an annular flame sits concentrically around this inner flame, attached to both the inner and outer rings. Figure 3.4 shows an idealized representation of this type of flame. For stabilizer C0, the inner ring is actually a solid disk so that only an annular flame

(still with an increased area compared to a single conical flame) sits attached to both the inner disk and outer ring. Figure 5.20 shows a cross-sectional view of this annular flame.
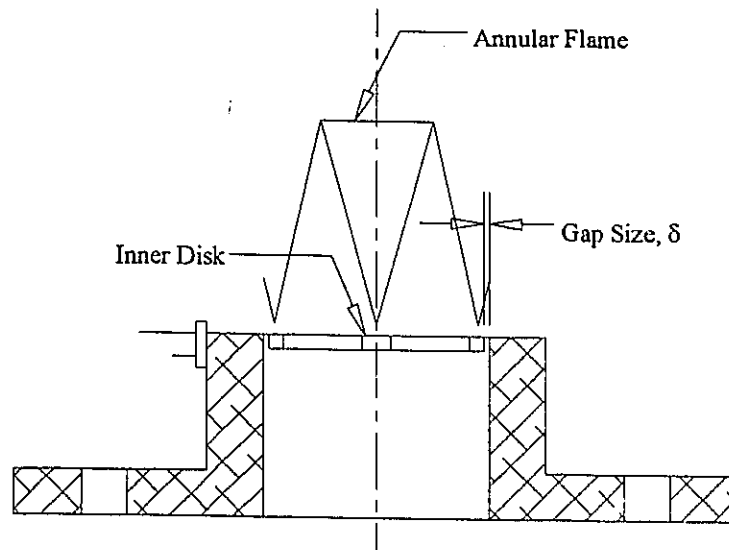
Figure 5.20: Idealized Annular Flame (Concentric Ring C0)

In Figure 5.21, the laminar flame heights for the four concentric ring stabilizers are compared with laminar rim stabilized flame heights. The burner input power is again fixed at 6.0 kW. Although there is still a marked increase in flame height at lower equivalence ratios, the curves are flatter than those of the single ring laminar case. More importantly, at $\phi=1$ the flame heights for stabilizers C0, C2, and C4 are all lower than those of the rim stabilized base case. Thus, with the proper choice of stabilizer, lean flame heights could be manipulated to match the stoichiometric flame height of the rim stabilized burner. At $\phi=1$, the rim stabilized flame has a height of approximately 6 cm. This height could be matched with either stabilizer C4 operating at $\phi=0.85$, or C0 at $\phi=0.77$, or C2 at $\phi=0.74$.
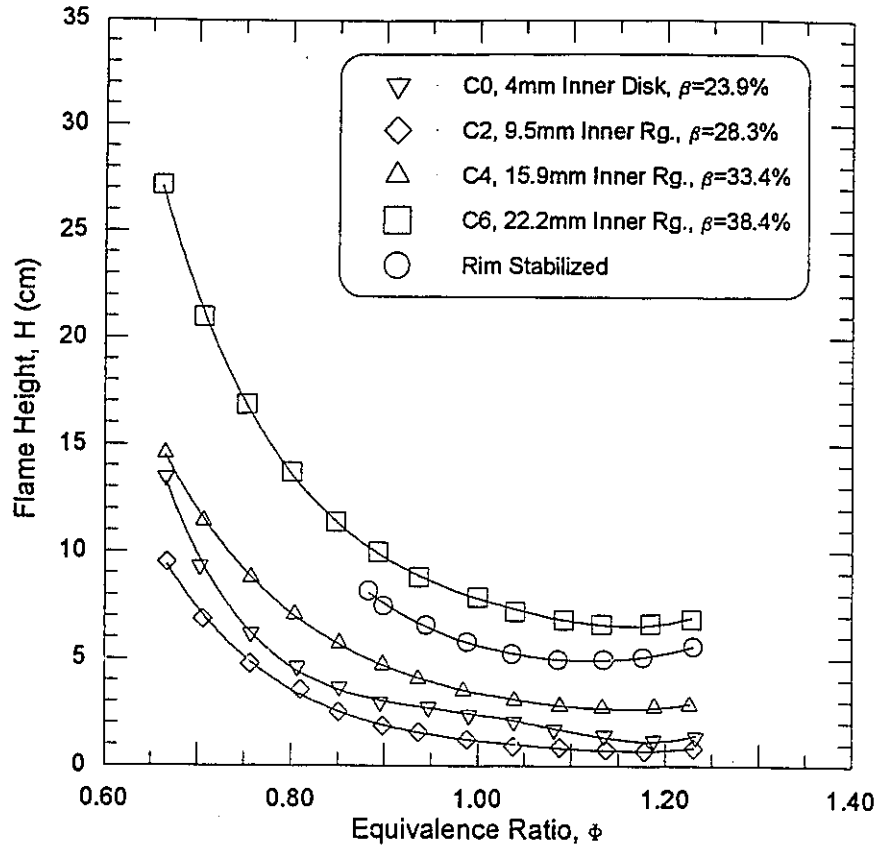
Figure 5.21: Concentric-Ring Laminar Flame Heights at 6.0 kW Input Power

Turbulence remains as an additional method of control. Figure 5.22 shows flame heights for the four concentric ring stabilizers in large scale turbulent flow. In this configuration, the laminar rim stabilized stoichiometric flame height could be matched by using either stabilizer C6 operating at ϕ=0.95, C4 at ϕ=0.8, C0 at ϕ=0.77, or C2 at ϕ=0.73. Thus, the potential problems with lean flame heights in retrofit should be avoidable with the proper choice of stabilizer.

It is interesting to note that turbulence has less of an effect on flame heights of the concentric-ring stabilizers than on flame heights of the single-ring stabilizers. This is because the flame angles for the concentric-ring flames are smaller and the flames are flatter so that changing the burning velocity and hence flame angle through increased turbulence has less of an effect on the overall flame height.
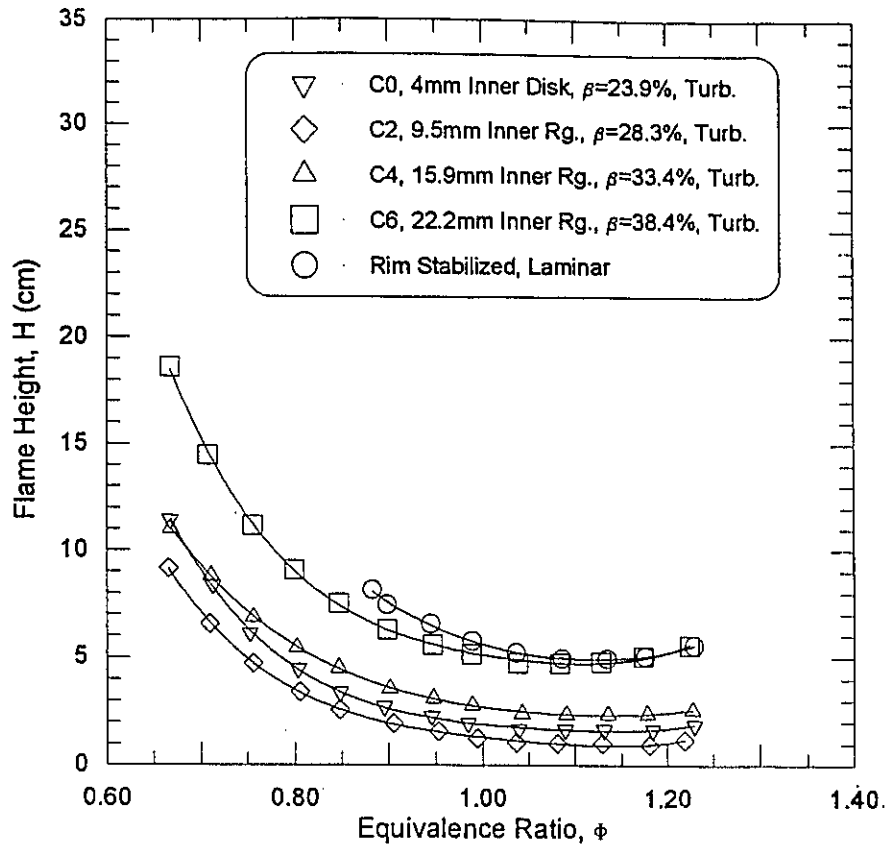
Figure 5.22: Concentric-Ring Larger Scale Turbulent Flame Heights at 6.0 kW Input Power

Differences in flame heights among the four stabilizers should be primarily a function of blockage and ring radius. For stabilizer C6 in Figure 5.21, although the flame area has increased significantly over the rim stabilized case, the large increase in flow blockage (β=38.4%) actually causes the flame height to grow. Attempts to correlate data for the concentric-ring stabilizers using a similar form of Equation 5.7 failed. Presumably the assumption of a uniform reactant velocity profile fails completely with the concentric-ring stabilizer in place.
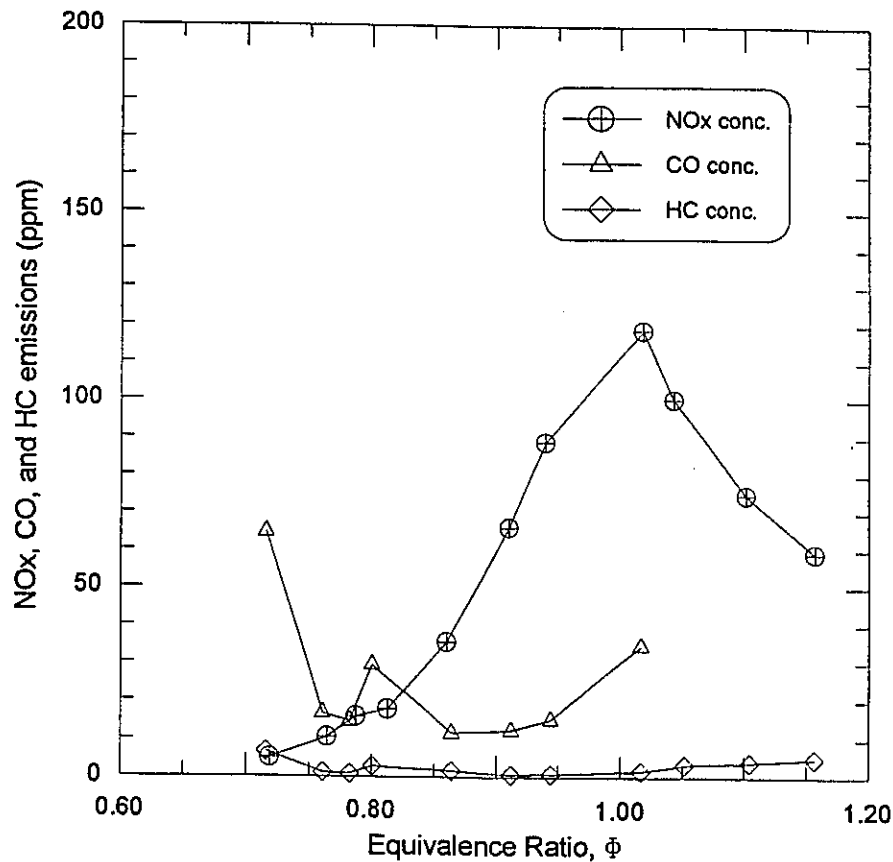
5.3 Pollutant Emissions

The most important aspect of this research is the emissions testing. Although the previous results show that stable lean premixed combustion is achievable, even in retrofitting applications, the predicted reductions in pollutant emissions remain to be seen. Since leakage of unburned hydrocarbons through the gap in the ring stabilizers was identified as a primary mode of failure, emissions tests were focused on understanding the influence of gap size on emissions. Due to problems with the CO analyzer, tests were conducted only for two single-ring stabilizers, G1 and G4, which represent the extremes in gap size for all of the ring stabilizers. It is predicted that results for the four concentric ring stabilizers would be comparable to those of single-ring G1, since the gap size (δ) is identical. This is left for future verification.

5.3.1 The 0.8 mm Gap, Single-Ring Stabilizer, G1

Figure 5.23 shows measured NOx, CO, and HC emissions, measured in PPM, for the burner with single-ring G1 in place. The energy input to the burner was 6.1 kW and the flow was turbulent. As predicted by thermal NOx theory, there is a dramatic reduction in NOx emissions as the equivalence ratio is reduced. The peak value of 119 PPM of NOx coincides with $\phi=1.02$, where the flame temperature should be near its maximum. As the equivalence ratio is reduced to $\phi=0.72$, the concentration drops to 5 PPM. Because of the stability limitations of stabilizer G1, emissions measurements were not conducted at equivalence ratios less than 0.72.

As expected, there is a similar drop in NOx emissions when the mixture is made fuel rich, but this is accompanied by a corresponding increase in CO emissions of several orders of magnitude due to incomplete combustion (not shown in Figure 5.23). The rapid increase in CO saturated the range of the Miran infrared analyzer at equivalence ratios greater than $\phi=1.03$. Using the SNAP-ON emissions analyzer which has a resolution of 100 PPM for CO measurements, CO concentrations of 3.1 % (31000 PPM) were found at

ϕ=1.16. For equivalence ratios between 0.76 and 1.02, the CO concentration remains relatively low, but as the equivalence ratio was reduced to 0.72 the concentration rose to 65 PPM. This rise in CO emissions at very low equivalence ratios was expected [15-17] and will be discussed later. The increase in CO concentrations for very lean reactant mixtures is much less severe than the increase for fuel rich mixtures.

Figure 5.23: Measured Pollutant Emissions for Stabilizer G1 in Turbulent Flow

Emissions of unburned hydrocarbons were essentially insignificant over the entire testing range. Although there was a very slight increase in emissions for very lean and moderately rich mixtures, the maximum concentration was less than 7 PPM. Fuel leakage with a gap size δ=0.8 mm was not an issue. Overall the results are very encouraging. It is also apparent that an optimum operating point will exist which will represent a

compromise between NOx and CO emissions, and efficiency, as well as a number of other factors.

Rule 1121 of the South Coast Air Quality Management District (State of California) [5], states that for a natural gas burner similar to the one used in this research, NOx emissions should be less than 40 ng of NOx (calculated as NO_2) per joule of useful energy delivered. Assuming a heating value for natural gas of 52 057 000 J/kg and a heating efficiency of 80%:

$$40 \times 10^{-9} \frac{g\,NO_2}{J\,useful\,energy} * 0.8 \frac{J\,useful}{J\,input} * 52057000 \frac{J\,input}{kg\,fuel} = 1.666 \frac{g\,NOx\,as\,NO_2}{kg\,fuel} \quad (5.10)$$

Thus, for the current burner NOx emissions must be less than 1.666 g NOx as NO_2 per kg of fuel to meet the strict SCAQMD standard.

CO emissions legislation taken from the joint ANSI/CGA standard [6] dictates that "a furnace shall not produce a concentration of carbon monoxide in excess of 0.04 percent in an air-free sample of the flue gases." This is interpreted to mean that CO emissions must be less than 400 PPM in the combustion products (which have normal air supply) before dilution with atmospheric air, which would normally take place in the stack. For lean mixtures, modeling natural gas as methane and ignoring dissociation:

$$\phi CH_4 + 2(O_2 + 3.76N_2) \rightarrow \phi CO_2 + 2\phi H_2O + 7.52N_2 + 2(1-\phi)O_2 \ \{+xCO\} \quad (5.11)$$
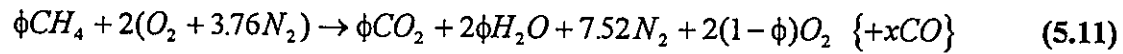
Neglecting the minute quantities of CO, at $\phi=0.6$, the total number moles in the products is 10.12. Thus, to get a concentration of 400 PPM of CO in the products, there must be 0.00405 moles of CO as shown in Equation 5.12.

$$\frac{x\,moles\,of\,CO}{10.12} = 400PPM = 4 \times 10^{-4} \quad (5.12)$$
$$x = 4.05 \times 10^{-3} moles$$

At $\phi=0.6$, using 17.0 as the molecular weight of natural gas, this means there can be no more than 11.1 grams of CO per kilogram of fuel burned. At $\phi=1$, similar calculations show that the limit on CO emissions is 6.93 g CO/kgfuel.
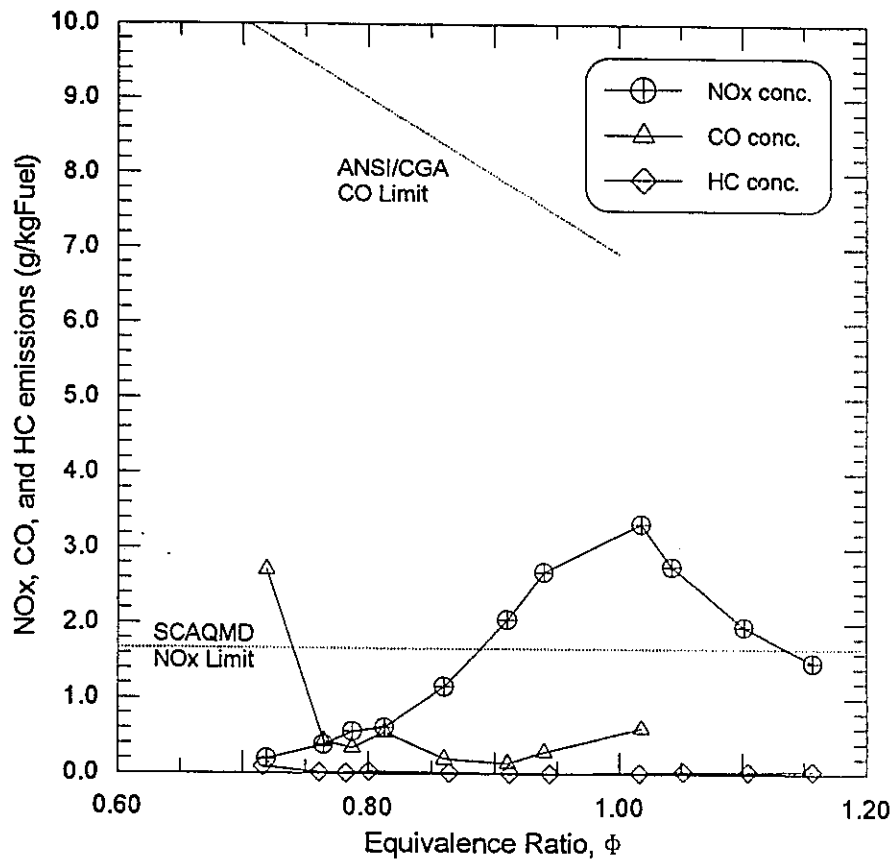
Figure 5.24: Pollutant Emissions by Mass for Stabilizer G1

Figure 5.24 shows the emissions for stabilizer G1 plotted on a g/kgfuel basis. The relevant CO and NOx emissions limits (as calculated above) are plotted as dashed lines. For equivalence ratios between 0.72 and 1.02, CO emissions are well below legislated standards. Even more encouraging is the fact that for $\phi<0.88$, NOx concentrations are below the legislated limits of the SCAQMD -- the most strict in the world. Many current appliances can not meet this standard. Thus, for an equivalence ratio range of 0.72 to 0.88, the ring stabilized burner simultaneously meets and beats legislated standards for CO and NOx emissions with virtually no HC emissions. Depending on the constraints of

individual applications, the desired operating point could lie anywhere within this range depending on parameters such as turndown, efficiency, and relative harm of CO and NOx emissions.

5.3.2 The 3.2 mm Gap, Single-Ring Stabilizer, G4
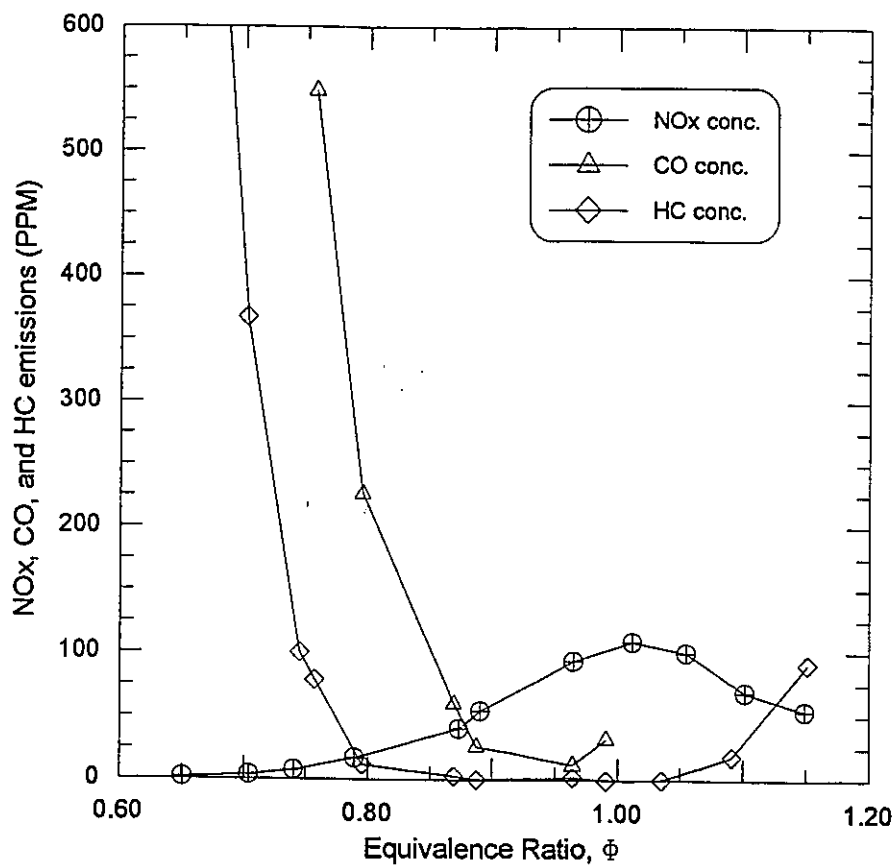
Figure 5.25: Emissions for Stabilizer G4 in Lg. Scale Turbulence at 6.1 kW

Emissions for single-ring G4, plotted as measured in PPM, are shown in Figure 5.25. Above ϕ=0.75, the NOx emissions are comparable to those for stabilizer G1 (109 PPM @ ϕ=1.01, 8 PPM @ ϕ=0.75). However, since ring G4 has a slightly wider stability range, stable combustion is possible down to ϕ=0.65. For this very lean condition, NOx concentrations in the exhaust gas were only 1.7 PPM. Unfortunately, this

near elimination of NOx emissions comes with a penalty -- HC and CO emissions are dramatically increased. At an equivalence ratio of 0.75, HC emissions climb to 100 PPM and as the equivalence ratio is lowered to $\phi=0.65$, the HC concentration inflates to 1088 PPM. This increase in HC emissions, particularly at low equivalence ratios, is evidence that leakage of unburned natural gas is occurring through the 3.2 mm gap of stabilizer G4.

As the flame is made leaner, the flame angle decreases so that the annulus of "flamelets" that attach to the ring and lean out over the gap, become more vertical as shown in Figure 5.26. When the flamelets stand more upright there is an easier path of escape for unburned fuel molecules. While this was not a problem with ring G1 ($\delta=0.8$ mm), the larger gap of stabilizer G4 ($\delta=3.2$ mm) significantly increases the possibility of fuel leakage. Although ring stability improves with increasing gap size, CO and HC emissions deteriorate.
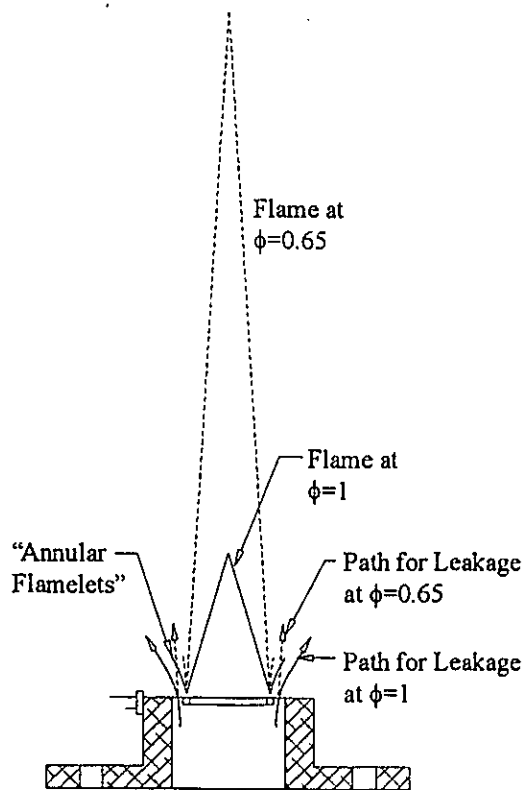

Figure 5.26: Idealization of Fuel Leakage for Stabilizer G4

Closely coupled with the increase in HC emissions at low equivalence ratios is a dramatic increase in CO emissions. At an equivalence ratio of 0.76, CO emissions rise to 548 PPM. For leaner mixtures the range of the primary CO detector was saturated, but the coarser SNAP-ON detector measured a CO concentration of 1700 PPM at ϕ=0.65. While this extreme rise in CO emissions can be partially accounted for with the processes described by Fenimore and Moore [15], Roesler et al. [16], and Glassman et al. [17], it is hypothesized that CO emissions due to combustion of leaked unburned fuel, outside of the primary flame zone, are also significant. This secondary combustion would take place at temperatures much below those of the primary flame zone since significant dilution with cooler combustion products could be expected to occur. If the secondary combustion temperature falls below 1270 K, quenched carbon monoxide would be produced according to Fenimore and Moore [15]. This proposed coupling of increased CO emissions with increased hydrocarbon emissions would explain the difference in CO concentrations for ring G1 and G4 at ϕ=0.72. For ring G1, at ϕ=0.72 hydrocarbon emissions are less than 10 PPM (indicating minimal fuel leakage), and CO emissions are 65 PPM. At the same equivalence ratio, HC emissions for ring G4 are approximately 368 PPM (indicating significant leakage) and CO emissions were greater than the range of the primary CO detector and were approximately 740 PPM as measured with the coarser Snap-On detector.

NOx, CO, and HC emissions per unit mass of fuel are shown in Figure 5.27. Again, the legislated standards for NOx and CO emissions are shown as dashed lines. Whereas ring G1 met or beat NOx and CO limits for 0.72<ϕ<0.88, ring G4 is only viable for 0.78<ϕ<0.88. Not only is the possible range narrower, the level of emissions within this range is much higher than for ring G1. Once again, a larger gap size leads to improved stability and slightly lower flame heights, but increasing the gap size of the ring stabilizer is detrimental to pollutant emissions.
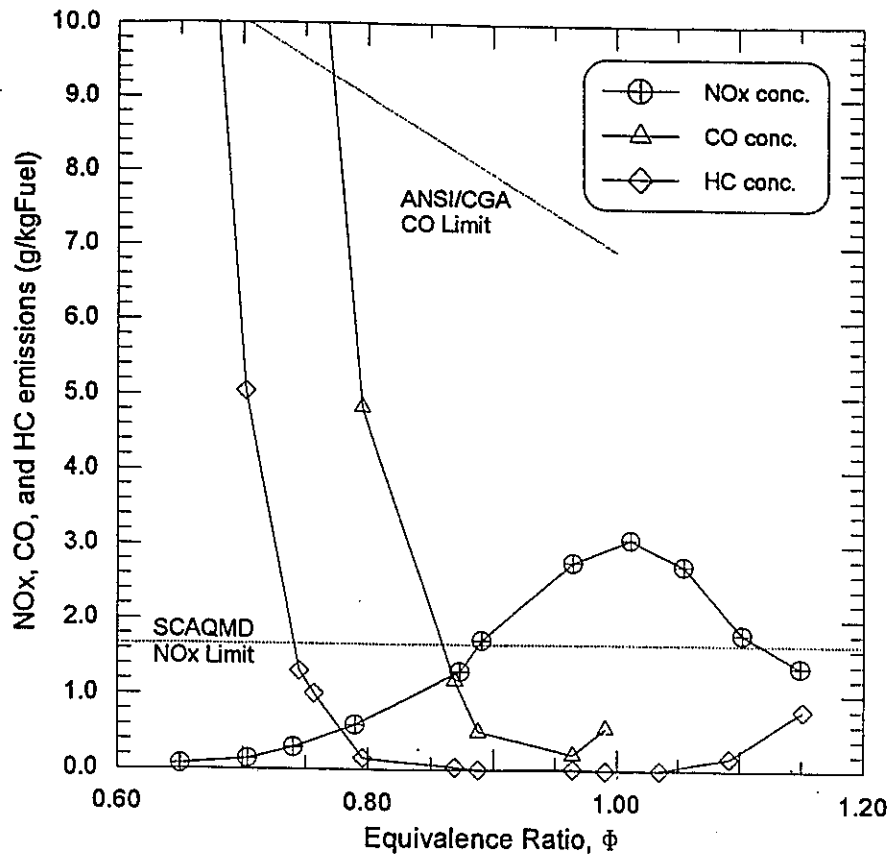
Figure 5.27: Pollutant Emissions by Mass for Stabilizer G4

Although legislated limits for NOx do not differentiate between NO and NO_2, NO_2 is probably the more harmful component [3]. Figure 5.28 show NOx and NO emissions (as measured in PPM) for ring stabilizer G4 in turbulent flow. NO_2 emissions can be inferred from the difference between the two curves. Clearly NO is the dominant component of NOx in the exhaust gas. This is consistent with typical natural gas burners where NO generally accounts for more than 90 % of total NOx [1,3]. Only at very low equivalence ratios does NO_2 become a significant portion of the total concentration. For ring G4, at $\phi=0.75$ the NO concentration drops to 0 PPM while NO_2 is still present at 8 PPM. However, as the equivalence ratio is reduced to 0.65, NO_2 concentrations also drop, to less than 2 PPM.
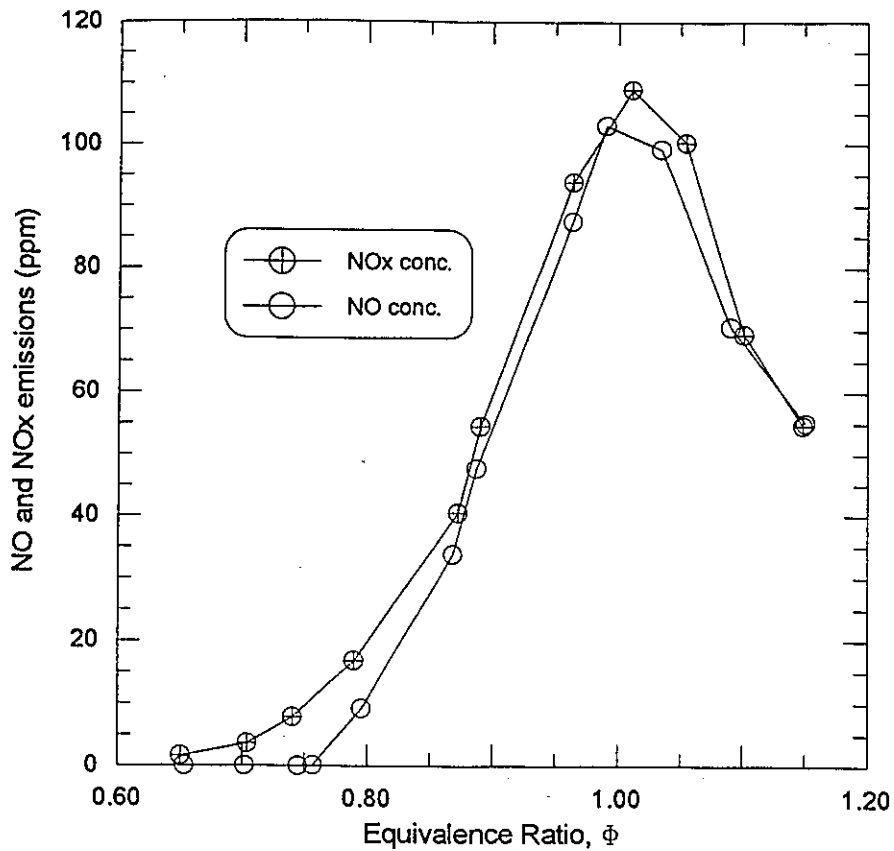
Figure 5.28: NO/NOx Emissions for Stabilizer G4

5.3.3 Other Issues Regarding Emissions

As previously mentioned, emissions tests were not conducted for the concentric ring stabilizers. However, since the gap size for all four concentric ring stabilizers is identical to that of single-ring G1 (δ=0.8 mm), it is predicted that emissions would be similar. If this is true, then the concentric-ring stabilizer would be the logical choice for retrofitting applications, offering flame heights equal to those of rim stabilized flames as well as slightly improved stability over the comparable single-ring stabilizer. Data from more extensive emissions testing will be discussed in future papers.

The influence of turbulence on emissions was also not investigated. It is possible that the increased mixing in turbulent flow could rapidly cool the exhaust products which could cause a slight increase in CO emissions due to quenching. Whether or not this effect is real, the current tests were conducted in large scale turbulent flow which would represent a worst case scenario. Even in large scale turbulence, the ring stabilized burner showed dramatic reductions in pollutant emissions, particularly NOx, to levels well below legislated standards.

5.4 Issues of Efficiency

Efficiency measurements were beyond the scope of this research. However, the importance of such testing cannot be ignored. Because of the lower flame temperatures associated with lean premixed combustion, there is the possibility that heat transfer rates between the exhaust gas and any relevant heat exchangers could be reduced. In applications that depend on radiant heat transfer, lower flame temperatures would be especially problematic since radiation heat transfer has a fourth order dependence on temperature.

While losses in radiant heat transfer may be difficult to recover, it may be possible to counteract this effect by boosting the convective heat transfer. One possible approach would include moving heat exchangers closer to the flame zone to shorten heat transfer distances and hopefully increase the rate of convective heat transfer. In lean premixed combustion for an equivalent input power (hence mass flow rate of fuel), the Reynolds number is significantly higher than for stoichiometric combustion due to the large increase in the amount of inerts present in the reactants. Higher Reynolds numbers would guarantee increased Nusselt numbers which could in turn boost the heat transfer rate and counter the effect of a lower overall temperature difference between a heat exchanger and the flame zone.

Efficiency measurements for a lean premixed hot water heater where weak swirl was used to stabilize the flame have been reported by Yegian and Cheng [42]. They found

only a very slight decrease in efficiency as the equivalence ratio was lowered from ϕ=1 to ϕ=0.65 (in the order of 1 % which was probably within their experimental uncertainty) and they concluded that 'thermal efficiency was independent of ϕ (and thus combustion temperature)." This result is very encouraging in terms of the present research. Currently, a second project is underway to retrofit the ring-stabilized burner into an existing furnace and experiments will include efficiency testing.

6. CONCLUSIONS

6.1 The Low Emissions, Lean-Premixed Natural Gas Burner

As worldwide concern for the environment increases, researchers are being forced to look for new ways to reduce and control pollutant emissions. Lean combustion is a well known approach to reducing NOx, HC, and even CO emissions (for slightly to moderately lean mixtures), but lean flame stability has been problematic in the past. In this research a novel method of stabilizing lean premixed natural gas flames was investigated. A nominal 6 kW Bunsen type burner with a 32 mm (1.25 inch) diameter exit was constructed for use in the laboratory. Various "ring stabilizers" were placed in the exit nozzle of the burner to aerodynamically anchor a flame. The recirculation zone of hot combustion products in the wake of the stabilizer continually ignites the reactants so that stable lean premixed flames are produced.

The ring stabilizers were tested over a wide range of conditions and comparisons were drawn to the base case of a traditional rim stabilized flame. Both "single-ring" and "concentric-ring" stabilizers were investigated. Blowoff and flashback limits were determined for all stabilizers in three different levels of reactant flow turbulence. Flow rates of the reactants were measured to determine equivalence ratio, power input, and nozzle exit velocity. Stability limits were ascertained by slowly varying the equivalence ratio until blowoff or flashback occurred. In this manner the entire operating range for the burner could be mapped for each different stabilizer in various levels of turbulence.

Flame heights were also measured to investigate the potential problems of excessive height at low equivalence ratios. Heights were determined visually by lining up a sight with the peak of the visible flame edge. Measurements were read from graduations on the support posts for the sight. Although it was sometimes difficult to accurately identify the flame edge, measured results were very consistent.

Finally, emissions tests were conducted. A generic heat exchanger was built to collect and cool exhaust gases from the burner. Samples were drawn from the exhaust stack of the exchanger and concentrations of NOx, CO, and HC were determined. NOx was measured using a chemiluminescent NO analyzer, CO was measured using an infrared gas analyzer, and HC was measured using a fast flame ionization detector.

6.2 Results and Optimization

All of the ring stabilizers significantly improved lean flame stability when compared to the base case of a rim stabilized burner. With the rings in place, the blowoff limit of the burner was shifted well into the regime of lean premixed combustion. For the most stable single-ring (G4, δ=3.2 mm), blowoff occurred at equivalence ratios as low as ϕ=0.55 which is near the flammability limit for a natural gas / air flame. The turndown ratio at ϕ=0.8 for this ring exceeded the measurement range of the flow meters but was estimated to be 20:1 or greater. For the laminar rim stabilized case there was no turndown at ϕ=0.8 since the burner was only stable for one input power. Turbulent rim stabilized flames were not stable in the lean combustion regime. By contrast, the stability limits of ring stabilized flames were found to be relatively insensitive to turbulence in the reactant flow.

Although lean flame combustion is made possible by the single ring stabilizer, a new problem of excessive flame heights at low equivalence ratios is potentially troublesome. As the equivalence ratio is reduced from ϕ=1 to ϕ=0.65, flame heights can increase by as much as 500 %. A partial solution to this dilemma is to increase the level of turbulence in the reactant flow which increases the burning velocity and in turn lowers the flame height. However, even with the larger scale turbulence plate in place, height increases of 267% were observed when the equivalence ratio was dropped from ϕ=1 to ϕ=0.65. This dramatic height increase could hinder attempts to retrofit existing appliances for lean combustion with ring stabilizers.

The concentric ring stabilizer can be used to avoid the flame height dilemma altogether. By significantly increasing the flame area, concentric ring stabilizers can

produce lean flames which have approximately equal heights to rim stabilized stoichiometric flames. Moreover, the stability range of the concentric-ring stabilizer is essentially identical to that of the single ring stabilizer. Thus, retrofitting of existing appliances with concentric ring stabilizers should not be problematic.

The major development in this research was the success in simultaneously reducing NOx and CO emissions to well below legislated standards. The SCAQMD NOx standard is currently the most strict in the world and many current appliances can not meet this limit. The reduction in NOx is achieved by lowering the flame temperatures by burning fuel lean. The higher concentration of inerts in the flame zone absorbs some of the combustion energy and lowers the peak temperature in the flame. Since NOx formation is exponentially dependent on temperature (according to the Zeldovich mechanism), lower temperature fuel-lean flames produce significantly reduced levels of NOx. Moreover, the operating range of the burner at low equivalence ratios (where pollutant emissions are low) has actually been enhanced. For the ring stabilized flame, at $\phi=0.8$ NOx emissions were measured at approximately 20 PPM or 0.59 g/kgfuel and the turndown was estimated to be 20:1 or greater. For the laminar rim stabilized burner at $\phi=0.8$ there was no turndown since the flame was only stable at a single input power. At $\phi=1$ the rim stabilized turndown was 4.9:1 but the corresponding NOx concentration was in excess of 100 PPM or 3.0 g/kgfuel.

As the ring gap size (δ, defined as the distance between the outer edge of the ring and the inner edge of the burner) is increased from $\delta=0.8$ mm to $\delta=3.2$ mm, flame stability improves. Unfortunately, with increased stability come increased CO and HC emissions due to leakage of unburned fuel through the larger gap. However, even for the worst case of ring G4 ($\delta=3.2$ mm) in large scale turbulent flow, the NOx and CO emissions were beneath legislated standards for the range $0.78<\phi<0.88$ at a burner input power of 6.1 kW.

Increased gap size also had a slightly negative effect on flame height. However, the height increase with increased gap size is essentially insignificant when compared to the height increase with lower equivalence ratios. For single ring stabilizers, the effect of ring blockage (planform area of ring stabilizer divided by burner exit area) and radius on flame height was quantified. Plots of flame height normalized according to Equation 6.1

as a function of equivalence ratio showed strong correlations. Although agreement with the base case of a rim stabilized flame was not perfect, the concept of a normalized flame height would be a useful design tool in predicting the performance of different single ring stabilizers.

$$H^\circ = H * (1 - \beta) * \frac{R_{BURNER}}{R_{RING}} \qquad (6.1)$$

where β is blockage

While the overall success in reducing pollutant emissions is very encouraging, it is evident that there will be an optimum ring stabilizer and an optimum operational equivalence ratio for each different situation. Although Cheng [42] found that efficiency was only slightly affected by lower equivalence ratios, this may be a constraint in some systems. Tradeoffs between reduced NOx and increased CO emissions will also need to be addressed for each potential application. Other constraints such as the relative importance of turndown and low emissions as well as manufacturing costs and ease of production may need to be considered. Nonetheless, the fact that all of these parameters are controllable for optimization bodes well for successful commercialization.

6.3 Future Work

Since the primary question of whether or not the ring stabilizer will work has been conclusively answered, the focus now shifts to problems associated with commercialization. A project is underway to convert an existing furnace from stoichiometric to lean premixed combustion by retrofitting it with ring stabilizers. More extensive pollutant emissions testing will be conducted and efficiencies at various equivalence ratios and powers will be simultaneously measured. Optimization of efficiency, NOx and CO emissions, turndown, design simplicity, etc. will be considered.

Since the furnace to be modified contains five "in-shot" burners with nominal input powers of approximately 6 kW, problems associated with scaling need not be addressed.

To aid in other possible retrofitting applications, more fundamental questions such as scaling and the effect of burner orientation on stability should be investigated. Since most furnaces contain burners mounted horizontally, the influence of buoyant forces on stability needs to be studied. In addition, potential problems with scaling, ignition, mixing at low pressures, and reactant flow control will need to be addressed.

The ring stabilizer has also been identified for possible exploitation in natural gas flaring. If natural gas flares could be converted for lean premixed combustion a significant source of NOx pollution would be eliminated. Before this can be realized, the ring stabilizer will have to be tested in cross-flow. Modifications may be necessary to prevent blowoff induced by wind shear over flaring stacks.

The single-ring and the concentric-ring stabilizer hold a great deal of promise in a variety of commercial applications. Several avenues for new research have been opened for investigation. The potential to significantly reduce NOx and CO emissions from stationary combustion sources should be exploited as much as possible.

REFERENCES

[1]   Robert F. Sawyer, "The Formation and Destruction of Pollutants in Combustion Processes: Clearing the Air on the Role of Combustion Research", *Eighteenth Symposium (International) on Combustion*, The Combustion Institute, 1981, pp. 1-21.

[2]   'Canadian Energy Supply and Demand 1990-2010", *National Energy Board*, June 1991.

[3]   John H. Seinfeld, <u>Atmospheric Chemistry and Physics of Air Pollution</u>, *A Wiley-Interscience publication*, John Wiley & Sons, 1986.

[4]   Craig T. Bowman, "Control of Combustion-Generated Nitrogen Oxide Emissions: Technology Driven by Regulation", *Twenty-Fourth Symposium (International) on Combustion*, The Combustion Institute, 1992, pp. 859-878

[5]   South Coast Air Quality Management District, 'Rules 1111 & 1121 NOx Emissions for Non-Mobile Residential Forced Air Furnace and Water Heaters", State of California, 1993, pp.1111-1.

[6]   American Gas Association and Canadian Gas Association, "American National Standard/National Standard of Canada for Gas-Fired Central Furnaces", ANSI Z21.47-1993, CAN/CGA-2.3-M93, 1993, pp. 59.

[7]   Irvin Glassman, <u>Combustion</u>, 2nd. Ed., Academic Press Inc., 1987.

[8]   A.A. Westenberg, 'Kinetics of NO and CO in Lean, Premixed Hydrocarbon-Air Flames", *Combustion Science and Technology*, 1971, Vol. 4, pp. 59-64.

[9]   Craig T. Bowman, 'Kinetics of Nitric Oxide Formation in Combustion Processes", *Fourteenth Symposium (International) on Combustion*, The Combustion Institute, 1973, pp. 729-738.

[10]   Peter Glarborg, James A. Miller, and Robert J. Lee, 'Kinetic Modeling and Sensitivity Analysis of Nitrogen Oxide Formation in Well-Stirred Reactors", *Combustion and Flame*, Vol. 65, 1986, pp. 177-202.

[11]   H. Semerjian and A. Vranos, 'NOx Formation in Premixed Turbulent Flames", *Sixteenth Symposium (International) on Combustion*, The Combustion Institute, 1973, pp. 169-179.

[12] C.P. Fenimore, "Formation of Nitric Oxide in Premixed Hydrocarbon Flames", *Thirteenth Symposium (International) on Combustion*, The Combustion Institute, 1971, pp. 373-380.

[13] A.N. Hayurst and I.M. Vince, "The Origin and Nature of 'Prompt' Nitric-Oxide in Flames", *Combustion and Flame*, Vol. 50, 1983, pp. 41-57.

[14] Jean Duterque, Nicole Avezard, and Roland Borghi, "Further Results on Nitrogen Oxides Production in Combustion Zones", *Combustion Science and Technology*, Vol. 25, 1981, pp. 85-95.

[15] C.P. Fenimore and John Moore, "Quenched Carbon Monoxide in Fuel-Lean Flame Gas", *Combustion and Flame*, Vol. 22, 1974, pp. 343-351.

[16] J.F. Roesler, R.A. Yetter, and F.L. Dryer, "On the Dependence of the Rate of Moist CO Oxidation on O_2 Concentration at Atmospheric Pressure", *Combustion Science and Technology*, 1994, Vol. 95, pp. 161-171.

[17] I. Glassman, K. Brezinsky, and F. Frigerio, "The Lean Combustion CO Emissions Problem", *Presented to the Central States Section of the Combustion Institute*, Madison, Wisconsin, June 1994.

[18] STANJAN Chemical Equilibrium Solver, v. 3.80s IBM-PC, (c) Stanford University. 1981, 1984, 1985, 1986, 1987.

[19] Kenneth K. Kuo, Principles of Combustion, *A Wiley-Interscience Publication*, John Wiley & Sons, 1986.

[20] F.N. Egolfopoulos, P. Cho, and C.K. Law, "Laminar Flame Speeds of Methane-Air Mixtures Under Reduced and Elevated Pressures", *Combustion and Flame*, Vol. 76, 1989, pp. 375-391.

[21] Jembu Raghavan, Jim Reuther, and Paul George, "Emissions-Reduction Technology for Gas-Fired Appliances", *presented at seminar O2: Reducing NOx and Carbon Monoxide Emissions from Heating Equipment*, 1995 Annual Meeting of American Society of Heating, Refrigerating, and Air-Conditioning Engineers, San Diego, CA, June, 1995.

[22] Miyauchi, Y. Mori, and T. Yamaguchi, "Effect of Steam Addition on NO Formation", *Eighteenth Symposium (International) on Combustion*, The Combustion Institute, 1981, pp. 43-51.

[23]   S.L. Chen, J.M. McCarthy, W.D. Clark, M.P. Heap, W.R. Seeker, and D.W. Pershing, 'Bench and Pilot Scale Process Evaluation of Reburning for In-Furnace NOx Reduction", *Twenty-First Symposium (International) on Combustion*, The Combustion Institute, 1986, pp. 1159-1169.

[24]   T. Kolb, P. Jansohn, and W. Leuckel, 'Reduction of NOx Emission in Turbulent Combustion by Fuel-Staging/Effects of Mixing and Stoichiometry in the Reduction Zone", *Twenty-Second Symposium (International) on Combustion*, The Combustion Institute, 1988, pp. 1193-1203.

[25]   J.O. Keller and I. Hongo, 'Pulse Combustion: The Mechanisms of NOx Production", *Combustion and Flame*, Vol. 80, 1990, pp. 219-237.

[26]   Ben T. Zinn, 'Pulse Combustion: Recent Applications and Research Issues", *Twenty-Fourth Symposium (International) on Combustion*, The Combustion Institute, 1992, pp. 1297-1305.

[27]   J.O. Keller, T.T. Bromlette, P.K. Barr, and J.R. Alvarez, 'NOx and CO Emissions from a Pulse Combustor Operating in a Lean Premixed Mode", *Combustion and Flame*, Vol. 99, 1994, pp. 460-466.

[28]   Bernard Lewis and Guenther von Elbe, Combustion, Flames and Explosions of Gases, 3rd. Ed., Academic Press Inc., 1987.

[29]   G.C. Williams, P.T. Woo, and C.W. Shipman, 'Boundary Layer Effects on Stability Characteristics of Bluff-Body Flameholders", *Sixth Symposium (International) on Combustion*, The Combustion Institute, 1956, pp. 427-438.

[30]   Jing-Tang Yang, Chang-Wu Yen, and Go-Long Tsai, 'Flame Stabilization in the Wake Flow Behind a Slit V-Gutter", *Combustion and Flame*, Vol. 99, 1994, pp. 288-294.

[31]   G.C. Williams, H.C. Hottel, and A.C. Scurlock, 'Flame Stabilization and Propagation in High Velocity Gas Streams", *Third Symposium (International) on Combustion*, The Combustion Institute, 1949, pp. 21-40.

[32]   Shigeki Yamaguchi, Norio Ohiwa, and Tatsuya Hasegawa, 'Structure and Blow-off Mechanism of Rod-Stabilized Premixed Flame", *Combustion and Flame*, Vol. 62, 1985, pp. 31-41.

[33]   K.M. Kundu, D. Banerjee, D. Bhaduri, 'Theoretical Analysis on Flame Stabilization by a Bluff-Body", *Combustion Science and Technology*, Vol. 17, 1977, pp. 153-162.

[34] S.I. Cheng, and A.A. Kovitz, "Theory of Flame Stabilization by a Bluff Body", *Seventh Symposium (International) on Combustion*, The Combustion Institute, 1959, pp. 681-691.

[35] S. Sivasegaram and J.H. Whitelaw, "Oscillations in Confined Disk-Stabilized Flames", *Combustion and Flame*, Vol. 68, 1987, pp. 121-129.

[36] S.L. Plee and A.M. Mellor, "Characteristic Time Correlation for Lean-Blowoff of Bluff-Body-Stabilized Flames", *Combustion and Flame*, Vol. 35, 1979, pp. 61-80.

[37] R.K. Cheng, "A Tomographic Study of V-flames Interacting with Shear Turbulence", *Proceedings of the Combustion Institute Joint Technical Meeting*, San Antonio, Texas, April 23-26, 1995, pp. 185-190.

[38] Roy Choudhury and Ali Bulent Cambel, "Flame Stabilization by Wall Recesses", *Eighth Symposium (International) on Combustion*, The Combustion Institute, 1962, pp. 963-970.

[39] R-H. Chen, J.F. Driscoll, J. Kelly, M. Namazian, and R.W. Schefer, "A Comparison of Bluff-Body and Swirl-Stabilized Flames", *Combustion Science and Technology*, Vol. 71, 1990, pp. 197-217.

[40] C.K. Chan, K.S. Lau, W.K. Chin, and R.K. Cheng, "Freely Propagating Open Premixed Turbulent Flames Stabilized by Swirl", *Twenty-Fourth Symposium (International) on Combustion*, The Combustion Institute, 1992, pp. 511-518.

[41] R.K. Cheng, "Velocity and Scalar Characteristics of Premixed Turbulent Flames Stabilized by Weak Swirl", *Combustion and Flame*, Vol. 101, 1995, pp. 1-14.

[42] D.T. Yegian and R.K. Cheng, "Laboratory Study of a Low NOx Hot Water Heater with a Weak-Swirl Burner", *Proceedings of the Combustion Institute Joint Technical Meeting*, San Antonio, Texas, April 23-26, 1995, pp. 14-19.

[43] C.H. Berman, R.J. Gill, and H.F. Calcote, "Enhanced Flame Stability Using Electric Fields", *Semi-Annual Report (May 1990-September 1990) for the Gas Research Institute*, Contract No. 5089-260-1884, January, 1991.

[44] W.P. Jensen and C.W. Shipman, "Stabilization of Flame in High Speed Flow by Pilot Flames", *Seventh Symposium (International)) on Combustion*, The Combustion Institute, 1959, pp. 674-680.

[45] Akimasa Yuuki and Yasuji Matsui, "An Experimental Study on Flame Stability on Wire Meshes", *Combustion Science and Technology*, Vol. 43, 1985, pp. 301-314.

[46]   L.W. Kostiuk, 'Premixed Turbulent Combustion in Counterflowing Streams",
Ph.D. Thesis, Cambridge University, 1991.

[47]   L.W. Kostiuk, K.N.C. Bray, and R.K. Cheng, 'Experimental Study of Premixed
Turbulent Combustion in Opposed Streams. Part I--Nonreacting Flow Field",
Combustion and Flame, Vol. 92, 1993, pp. 377-395.

[48]   SAE Handbook, <u>Volume 3   Engines, Fuels, Lubricants, Emissions, & Noise</u>,
Society of Automotive Engineers, Inc., 1991, pp. 25.98.

[49]   A.B. Evans, J.N. Pont, D.K. Moyeds, and G.C. England, 'Emissions Sampling
Protocol for Measuring NO/NOx in the Presence of High Concentrations of NO_2",
*Presented at the Fall Meeting of the Western States Section of the Combustion
Institute*, 1993.

[50]   N.P. Cernansky, 'Sampling and Measuring for NO and NO_2 in Combustion
Systems", *AIAA 14th Aerospace Sciences Meeting*, 1976, pp. 83-101.

Appendix A: Rate Calculation for Zeldovich NO Formation

The formation of thermal or Zeldovich NO in combustion products is governed by the following equations.

$$O + N_2 \Leftrightarrow NO + N \quad (1)$$
$$N + O_2 \Leftrightarrow NO + O \quad (2)$$
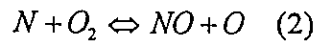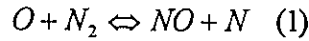
The law of mass action gives the rate of formation of NO as a function of O atom, N atom, Nitrogen, Oxygen, and NO concentrations as:

$$\frac{d[NO]}{dt} = k_{f1}[O][N_2] - k_{b1}[NO][N] + k_{f2}[N][O_2] - k_{b2}[NO][O] \quad (3)$$

Noting that N atoms are highly unstable, one can assume that the concentration of N atoms is constant.

$$\frac{d[N]}{dt} = 0 = k_{f1}[O][N_2] - k_{b1}[NO][N] - k_{f2}[N][O_2] + k_{b2}[NO][O] \quad (4)$$

Rearranging (4) gives (5).

$$[N] = \frac{k_{f1}[O][N_2] + k_{b2}[NO][O]}{k_{b1}[NO] + k_{f2}[O_2]} \quad (5)$$

Adding (3) and (4) and substituting with (5) gives (6).

$$\frac{d[NO]}{dt} = 2k_{f1}[O][N_2] - 2k_{b1}[NO]\left(\frac{k_{f1}[O][N_2] + k_{b2}[NO][O]}{k_{b1}[NO] + k_{f2}[O_2]}\right) \quad (6)$$

Rearranging (6) gives (7).

$$\frac{d[NO]}{dt} = 2k_{f1}[O][N_2] \left(\frac{k_{b1}[NO] + k_{f2}[O_2] - k_{b1}[NO] - \dfrac{k_{b1}k_{b2}[NO]^2}{k_{f1}[N_2]}}{k_{b1}[NO] + k_{f2}[O_2]} \right) \quad (7)$$

Rearranging again gives (8).

$$\frac{d[NO]}{dt} = 2k_{f1}[O][N_2] \left(\frac{1 - \dfrac{k_{b1}k_{b2}[NO]^2}{k_{f1}k_{f2}[N_2][O_2]}}{1 + \dfrac{k_{b1}[NO]}{k_{f2}[O_2]}} \right) \quad (8)$$

Noting that,

$$\frac{k_{f1}}{k_{b1}} = \frac{[NO]_{eq}[N_2]_{eq}}{[O]_{eq}[N_2]_{eq}} \quad (9) \quad \text{and} \quad \frac{k_{f2}}{k_{b2}} = \frac{[NO]_{eq}[O]_{eq}}{[N]_{eq}[O_2]_{eq}} \quad (10)$$

and realizing that $[N_2] \gg [NO]$ and for lean flames $[O_2] \gg [NO]$ so $[N_2]$ and $[NO]$ can therefore be approximated as equilibrium concentrations, substituting (9) and (10) into (8) gives (11).

$$\frac{d[NO]}{dt} = \frac{2k_{f1}[O][N_2] \left(1 - \dfrac{[NO]^2}{[NO]_{eq}^2} \right)}{1 + \dfrac{k_{f1}[NO]}{k_{f2}[O_2]}} \quad (11)$$

Generally in practice, $[NO] \ll [NO]_{eq}$. Again for fuel lean flames, $[O_2] \gg [NO]$. Thus (12) can be derived.

$$\frac{d[NO]}{dt} \approx 2k_{f1}[O][N_2] \quad (12)$$

Finally, one can assume that atomic and molecular oxygen are in equilibrium according to:

$$\tfrac{1}{2}O_2 + M \Leftrightarrow O + M \quad (13)$$
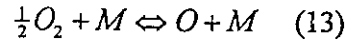
Since,

$$\frac{k_{f13}}{k_{b13}} = \frac{[O]_{eq}}{[O_2]_{eq}^{0.5}} \quad (14)$$

substituting (14) into (12) gives (15).

$$\frac{d[NO]}{dt} \approx 2k_{f1} \frac{k_{f13}}{k_{b13}} [O_2]^{\frac{1}{2}}[N_2] \quad (15)$$

Relevant reaction rates can be taken from standard kinetic data sources and are as follows:

$$k_{f1} = 1.36 * 10^{14} \exp\left(\frac{-76500}{RT}\right) \frac{cm^3}{mol*s}$$

$$k_{f13} = 1.38 * 10^{13} T^{-1} \exp\left(\frac{-339.8}{RT}\right) \frac{(cm^3)^2}{mol*s}$$

$$k_{b13} = 2.75 * 10^{19} T^{-1} \exp\left(\frac{-118687.5}{RT}\right) \frac{(cm^3)^2}{mol*s}$$

Finally, substituting these values into (15) gives (16), the simplified reaction rate equation for the formation of thermal or Zeldovich NO in combustion products.

$$\frac{d[NO]}{dt} = 1.214 * 10^{15} \exp\left(\frac{-68280.8}{T}\right)[O_2]^{\frac{1}{2}}[N_2] \quad (16)$$

Thus, the formation of thermal or Zeldovich NO has a strong exponential dependence on temperature.

Appendix B: Reactant Mass Flow Meter Calibrations

The two mass flow meters were calibrated using nitrogen. One at a time small tanks of 99.95% pure nitrogen were placed on a electronic scale with voltage output readable with a computer data acquisition system. Each tank was fitted with a two-stage regulator which was connected in series with a flow control needle valve and one of the flow meters. The tanks were slowly emptied through the regulator and flow meter and the tank weight as a function of time and the flow meter signal were simultaneously recorded using the computer data acquisition system. The nitrogen flow rate then could be easily calculated from the tank weight versus time data and correlated with the measured flow meter signal.
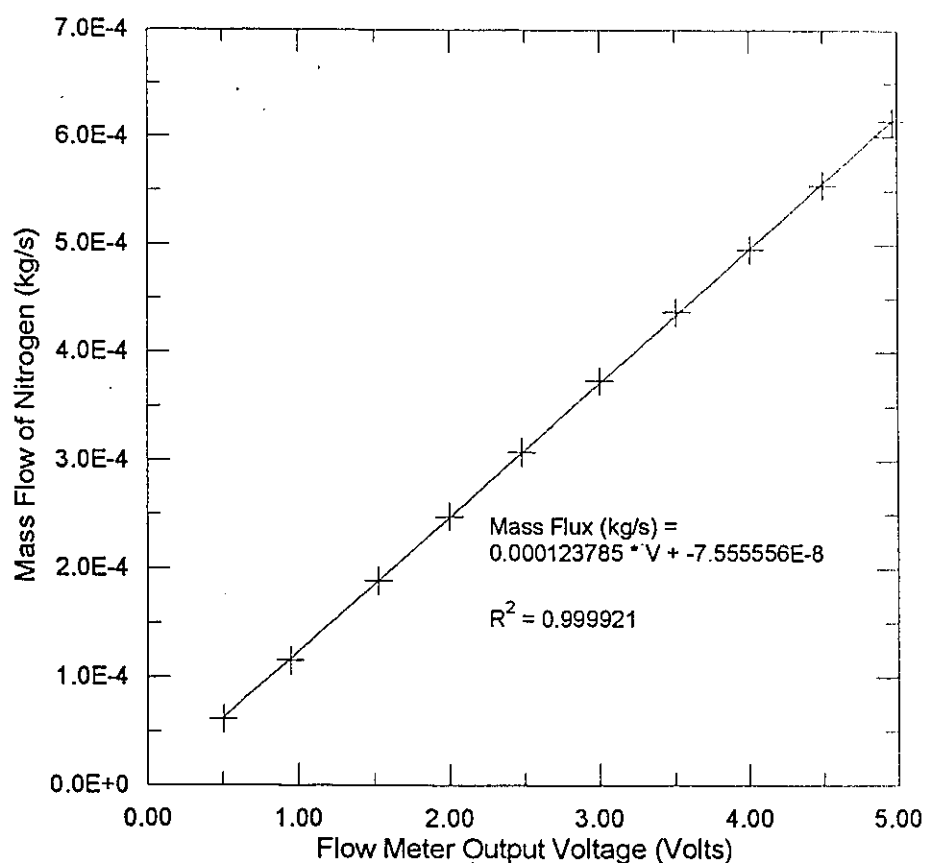
Figure B.1: Nitrogen Calibration Curve for Natural Gas Flow Meter

In this manner, calibration curves were generated for each flow meter. In order to measure natural gas and air flows, respective corrections for heat capacity differences between nitrogen and natural gas and nitrogen and air were applied. Figures B.1 and B.2 show the resulting calibration curves for the two flow meters. Theses curves were incorporated into the data acquisition programs used in the various experiments. Heat capacity corrections were applied in the program and varied with each new tank of natural gas that was used.
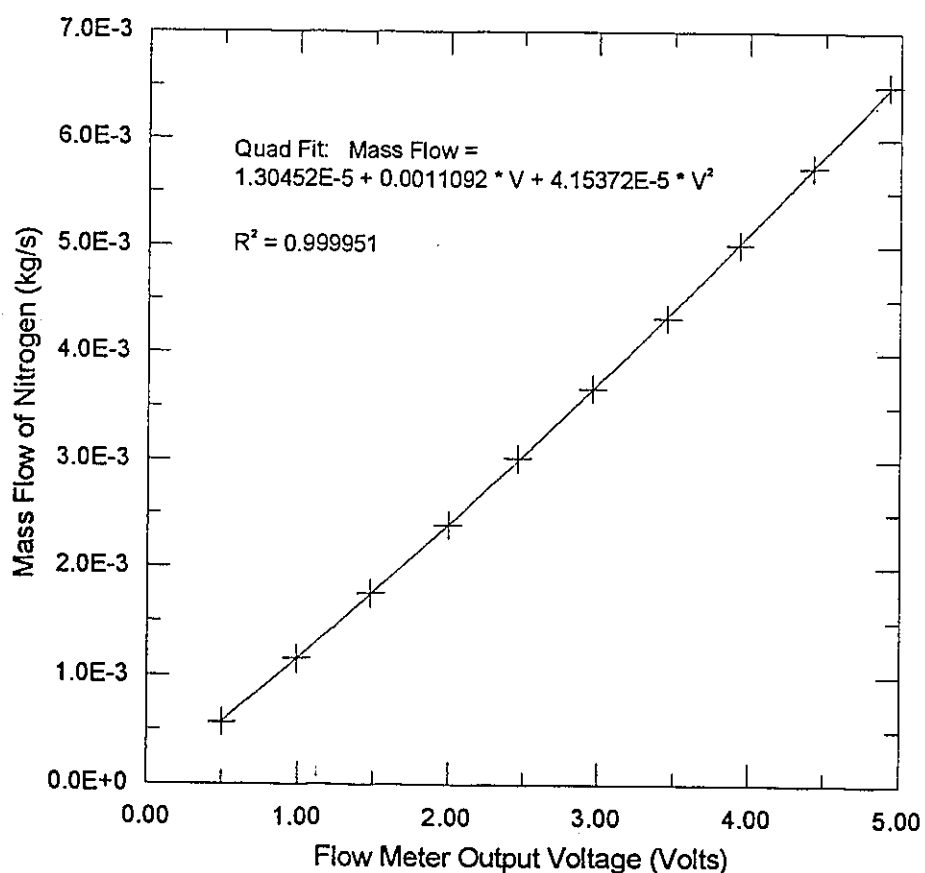
Figure B.2: Nitrogen Calibration Curve for Air Flow Meter

Appendix C: Measured Natural Gas Composition

Natural gas from the city of Edmonton, which was used throughout this research, was periodically collected from city lines and compressed into a gas cylinder. The composition of each new tank of gas was measured using a Microsensor Technology Inc. Model P200 gas chromatograph. The natural gas was analyzed using the 'Relative Volume Method" with the assumption that the gas consisted only of methane, ethane, nitrogen, and carbon-dioxide. No other components were detected with the GC in any of the tanks of fuel. The uncertainty using this method is approximately ±0.2 % with a repeatability uncertainty of ±0.1 %. Table C.1 summarizes the compositions of the 6 tanks of fuel used in this research as well as the overall average composition.

Table C.6.1: Measured Natural Gas Composition

Tank #	Date	CH_4 % vol.	C_2H_6 % vol.	N_2 % vol.	CO_2 % vol.	Mol. Mass	Cp kJ/kgK
1	94/07/10	94.13	2.78	2.45	0.64	16.902	2.135
2	94/09/09	93.12	2.92	3.17	0.80	17.052	2.115
3	94/11/19	93.58	2.45	3.03	0.94	17.009	2.116
4	95/02/01	93.68	2.46	2.87	0.99	17.005	2.117
5	95/03/08	93.88	2.28	2.85	0.98	16.977	2.119
6	95/04/17	93.96	2.07	3.01	0.96	16.960	2.119
Avg.		93.73	2.49	2.90	0.89	16.984	2.120

Appendix D: Influence of Turbulence on Stability Limits of Single Ring Stabilizers

Blowoff and flashback tests were conducted for the four different single ring stabilizers for three levels of reactant flow turbulence: laminar, small-scale turbulence, and large-scale turbulence. For the laminar case the reactant flow exits the burner unobstructed. Plates perforated with 2 mm and 3 mm holes (both with 50% blockage) were inserted into the flow to create smaller and larger scale turbulence respectively. Complete measurement results are shown in the following graphs.
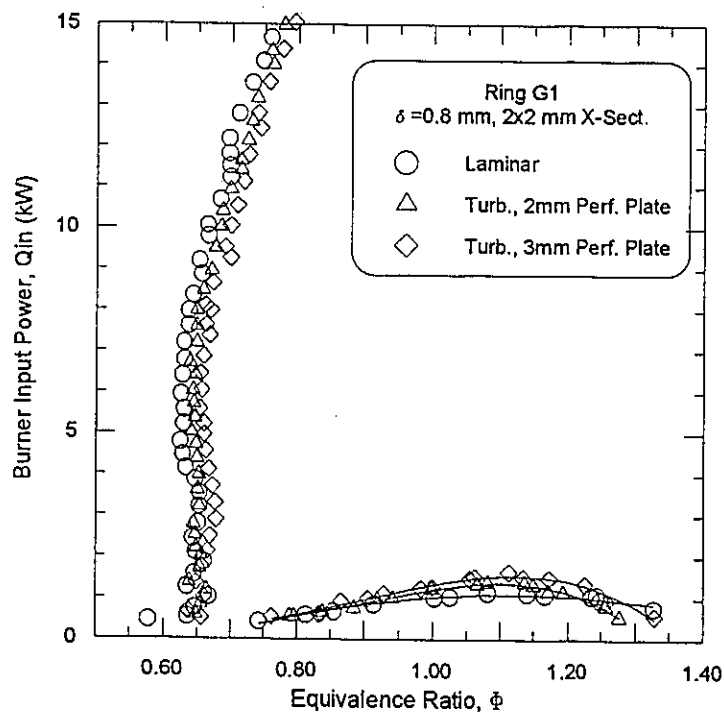
Figure D.1: Influence of Turbulence on Stability Limits of Single-Ring G1
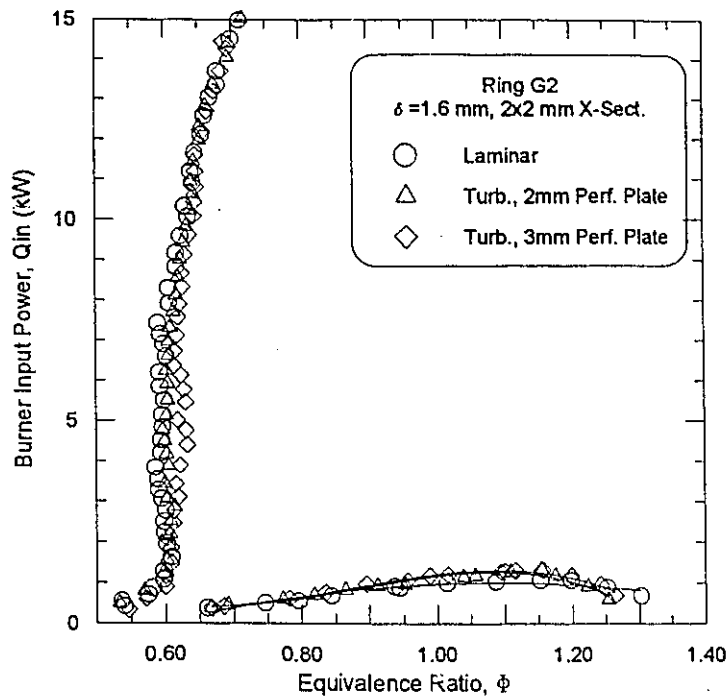
Figure D.2: Influence of Turbulence on Stability Limits of Single Ring G2
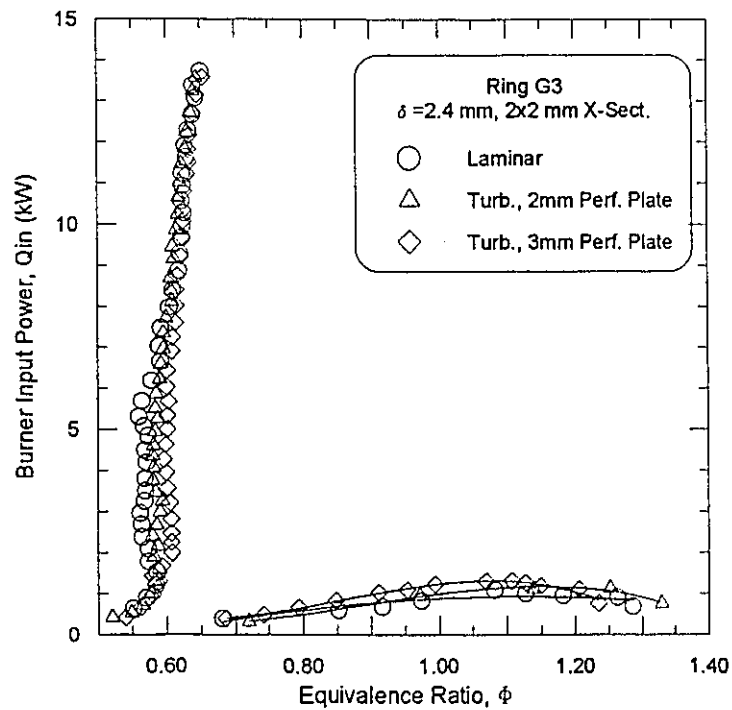
Figure D.3: Influence of Turbulence on Stability Limits of Single Ring G3
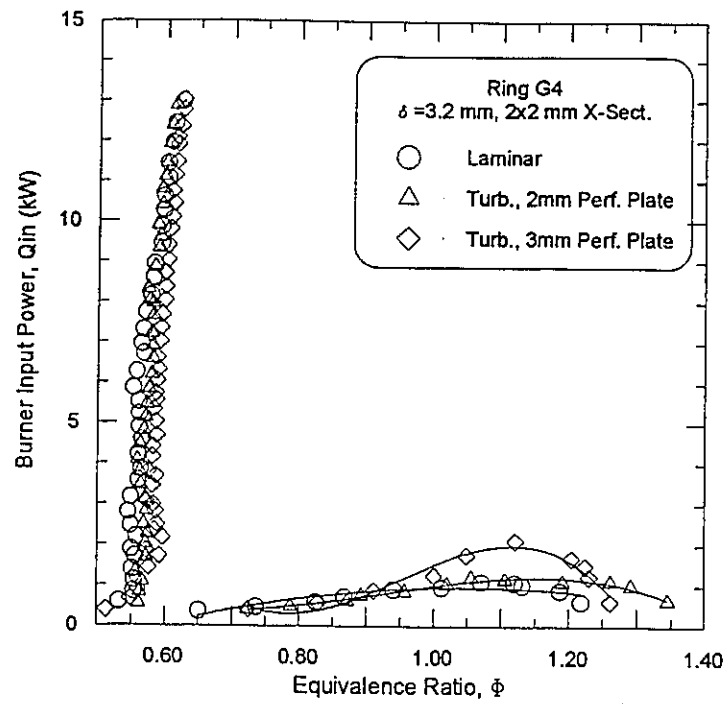
Figure D.4: Influence of Turbulence on Stability Limits for Single Ring G4
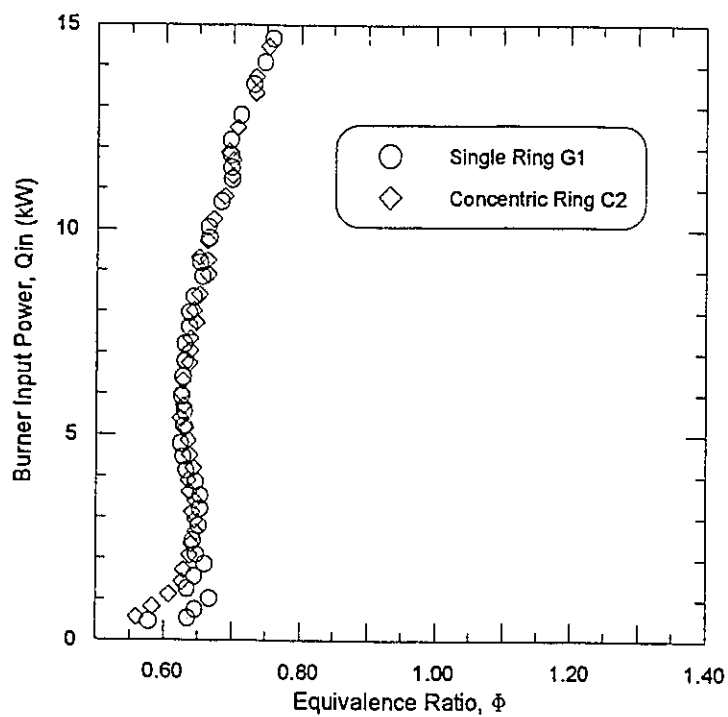
Appendix E: Blowoff Limits for Concentric Ring Stabilizers

Blowoff measurements were completed for all four concentric ring stabilizers in laminar and larger scale turbulent flow with the 3 mm perforated plate placed in the burner nozzle. The outer ring for all of the concentric ring stabilizers was identical: 30.2 mm (1-3/16 inch) O.D., δ=0.8 mm, 2x2 mm cross-section. The inner rings were varied in size as summarized in Table 3.2 shown previously. The stability limits were virtually identical for the four concentric rings and were essentially the same as those of single ring G1 (also 30.2 mm O.D., δ=0.8 mm, and 2x2 mm cross-section). However, it should be noted that flashback in for the concentric ring stabilizers was said to occur when the flame lifted off the outer ring even though it is usually still stable on the inner ring.
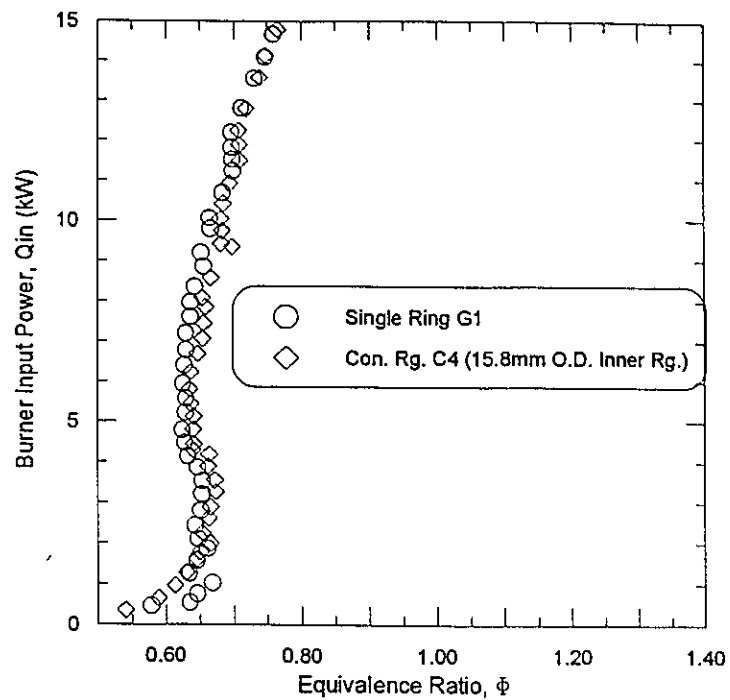
Flashback tests were conducted only for the turbulent case. A larger inner ring results in a slightly reduced flashback limit.
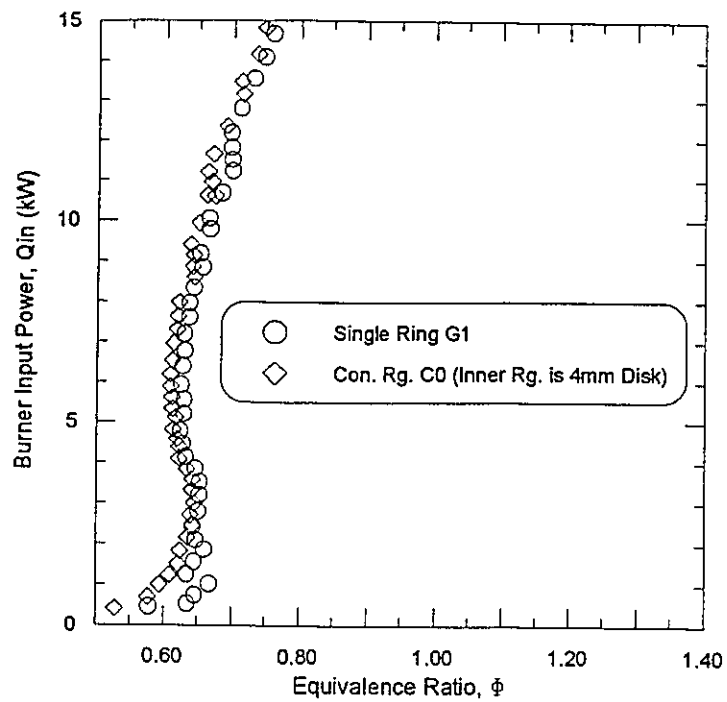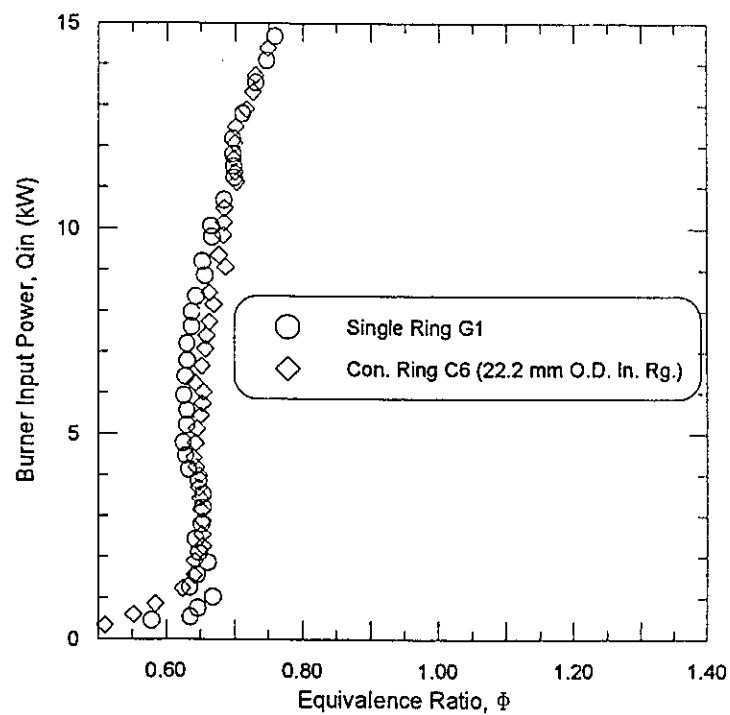
Figure E.1: Laminar Blowoff Limits for Single Ring G1 and Concentric Ring C0
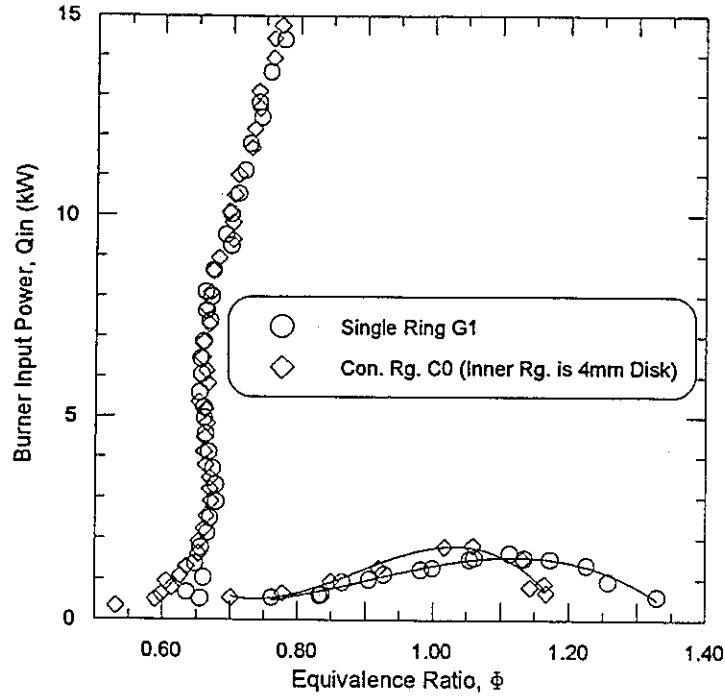

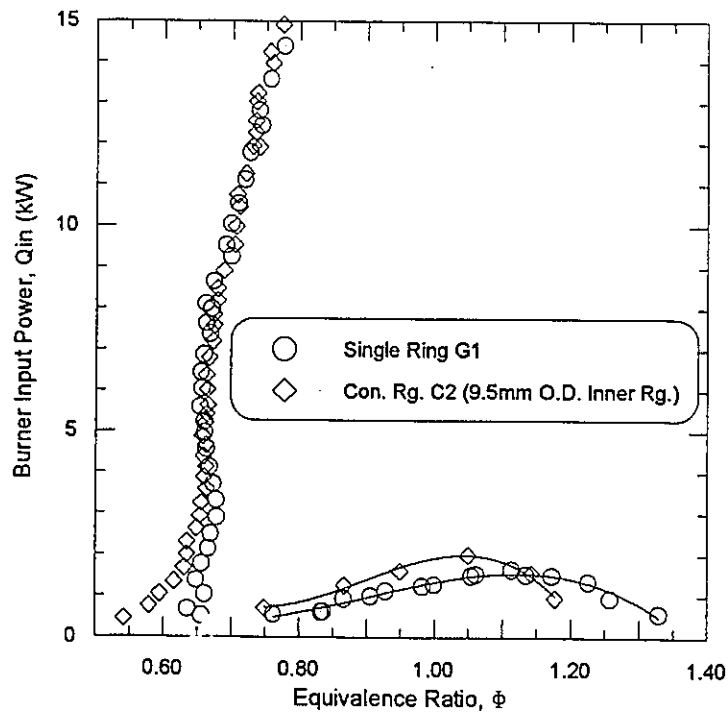**Figure E.2: Laminar Blowoff Limits for Single Ring G1 and Concentric Ring C2**

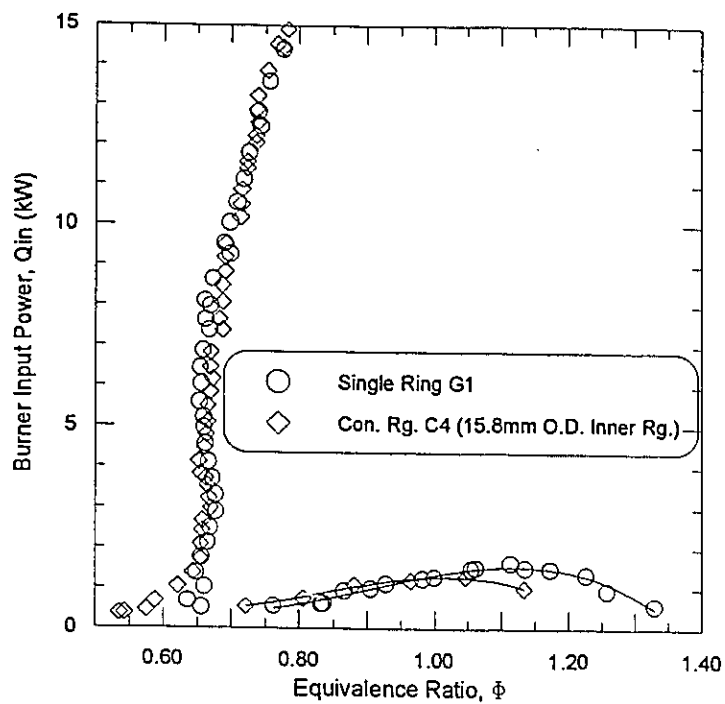**Figure E.3: Laminar Blowoff Limits for Single Ring G1 and Concentric Ring C4**

Figure E.4: Laminar Blowoff Limits for Single Ring G1 and Concentric Ring C6
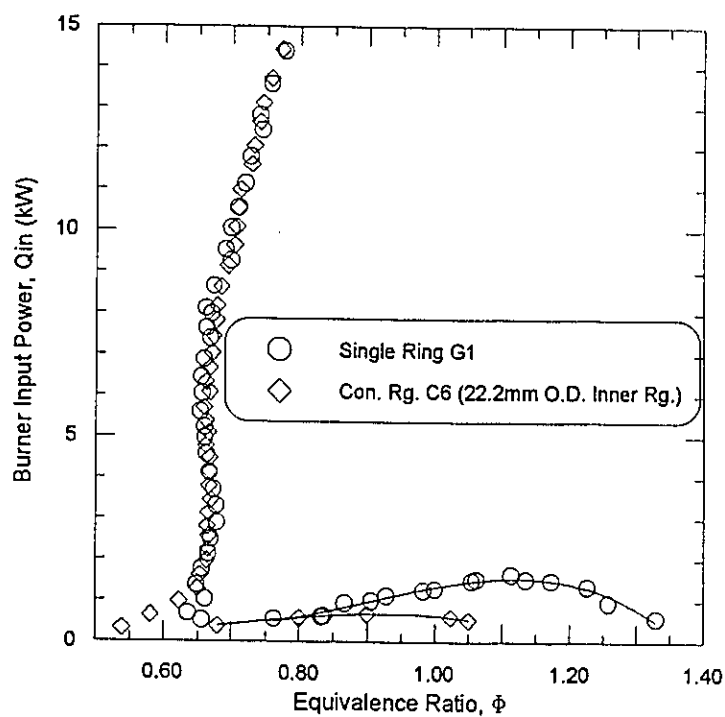
Figure E.5: Turbulent Stability Limits for Single Ring G1 and Concentric Ring C0

Figure E.6: Turbulent Stability Limits for Single Ring G1 and Concentric Ring C2

Figure E.7: Turbulent Stability Limits for Single Ring G1 and Concentric Ring C4

Figure E.8: Turbulent Stability Limits for Single Ring G1 and Concentric Ring C6